NASA Contractor Report 201709

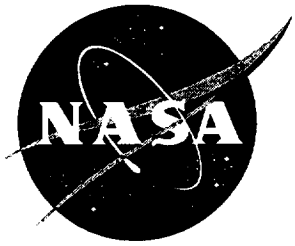

Lightweight Ceramics for Aeroacoustic Applications

H. W. Kwan, G. T. Spamer, and J. Yu
Rohr, Inc., Chula Vista, California

B. Yasukawa
Lockheed Martin Missiles and Space, Sunnyvale, California

Contract NAS1-20102

July 1997

National Aeronautics and
Space Administration
Langley Research Center
Hampton, Virginia 23681-0001

ABSTRACT

Rohr, Inc., in cooperation with Lockheed Martin Missiles & Space (LMMS) Division, has investigated the use of a HTP (High Temperature Performance) ceramic foam for aeroacoustic applications under NASA Contract NAS1-20102, Task 4. HTP ceramic foam is a composition of silica and alumina fibers developed by LMMS. This foam is a lightweight high temperature fibrous bulk material with small pore size, ultra high porosity, and good strength. It can be used as a broadband noise absorber at both room and high temperature (up to 1800 °F). The investigation included an acoustic assessment as well as material development, and environmental & structural evaluations. The results show that the HTP ceramic foams provide good broadband noise absorbing capability and adequate strength when incorporating the HTP ceramic foam system into honeycomb sandwich structure. On the other hand, the material is sensitive to Skydrol and requires further improvements. Good progress has been made in the impedance model development. A relationship between HTP foam density, flow resistance, and tortuosity will be established in the near future. Additional effort is needed to investigate the coupling effects between face sheet and HTP foam material.

TABLE OF CONTENTS

TABLE OF CONTENTS

LIST OF ILLUSTRATIONS

LIST OF ILLUSTRATIONS

LIST OF ILLUSTRATIONS

LIST OF ILLUSTRATIONS

LIST OF ILLUSTRATIONS

LIST OF ILLUSTRATIONS

LIST OF TABLES

1.0 BACKGROUND AND PROGRAM OBJECTIVE

1.1 Background

There is a growing need to develop more effective aircraft engine noise attenuation technology for both subsonic and supersonic aircraft. Over the next ten - fifteen years a large market will exist for new commercial aircraft. This market will be fueled by the need to replace an aging fleet with new, more economical airplanes, a large expansion in Pacific Rim air travel requiring added capacity and new demand for Western aircraft/engines by Eastern bloc countries. There will be intense global competition to produce the needed aircraft and engines. U.S. companies will compete with European manufacturers enjoying the advantage of government subsidization. Better technology as well as lower costs are needed for the United States to be successful in this competition.

One area that could provide the U.S. with a competitive advantage is aircraft engine noise reduction technology. The need for advanced engine nacelle acoustic treatment that can provide noise attenuation over a broad frequency band and operate at high temperatures results from increasingly stringent regulations being proposed by authorities and from projected acoustic attenuation requirements for supersonic commercial transports. Improved noise attenuation is necessary to allow unrestricted airport and fleet growth as well as the introduction of ultra-large aircraft into the fleet. The types of acoustic structures that are currently used in areas of jet engines where the temperature exceeds 350 ^{0}F are primarily constructed of perforated metals bonded or braised to honeycomb support structure. While these structures are capable of operating at temperatures of up to 1000 ^{0}F, their acoustic performance is effective over a relatively narrow bandwidth. Integration of advanced materials such as low density ceramics into the acoustic structure could potentially enhance the acoustic performance and provide a means for the current generation of high-bypass turbofan engines as well as the new generation of ultra-high-bypass engines to meet increasingly strict noise regulations.

In addition to increased acoustic performance, new generation engines designed for supersonic commercial transports require far greater temperature capability for nozzle, ejector and plug area acoustic treatment. These

temperatures are projected to reach or exceed 2000 ^{0}F and must rely on new material concepts since current metallic liners are not capable of operating in such an environment.

A summary of the requirements for subsonic and supersonic commercial transport engines is provided in Table 1.1-1. These figures are based on current FAA requirements and proposed NASA requirements for the High Speed Civil Transport (HSCT). The current subsonic commercial aircraft fleet as well as new supersonic transport aircraft will, as a minimum, have to meet Stage 3 noise criteria. Both the FAA and NASA expect that before the end of this decade, there will be a doubling of the noise stringency rules imposed for new subsonic aircraft. Accordingly, they have outlined a rigorous long range program aimed at developing technology to enable the U.S. aviation industry to meet future noise requirements with an adequate margin. The goal is to maintain a minimum community noise impact even as commercial aircraft numbers increase in size. The U.S. currently possesses a competitive advantage in subsonic Aeroacoustics technology. Continued development of new advanced nacelle acoustic treatment will be necessary if we are to maintain that edge.

1.2 Program Objective

The objective of the program is to develop high temperature, lightweight ceramic acoustic structures that can serve as broad band noise absorbers to reduce aircraft propulsion system noise. Ceramic systems have been selected for evaluation because they offer significant weight savings over metallics, especially at high temperatures and can be produced in forms (foam, etc.) that provide for effective sound suppression. These systems will be targeted to meet the performance requirements of future subsonic applications. An added objective of this effort is to investigate the potential use of these ceramic materials for supersonic propulsion systems applications.

1.3 Program Approach And Report Organization

The approach used to pursue the objective noted above is outlined in the schedule shown in Figure 1.3-1. Potential acoustic structures applications for which bulk absorbers might be suited are identified in Section 2. Ceramic bulk absorber development activities are provided in Section 3. Acoustic property

and environmental structural tests and evaluation are described in Section 4 & 5 respectively. Model development activities are discussed in Section 6 while conclusions and recommendations are detailed in Section 7.

2.0 IDENTIFICATION OF POTENTIAL ACOUSTIC STRUCTURES APPLICATIONS

Applications for which the ceramic foam bulk absorber materials/structures offer potential include inlet, after fan and exhaust region acoustic hardware. These areas are shown pictorially in Figure 2-1. For the inlet region, ceramics would be incorporated for turbofan applications only if a weight saving could be demonstrated since this is not a high temperature area. Inlet treatment as well as aft end acoustic structure, which is provided on the fan cowl, core cowl and thrust reverser are presently characterized by either Helmholtz resonators or perforate plate type liners. A liner using a porous ceramic bulk absorber would offer advantages of being lightweight and providing effective acoustic performance in high temperature environments.

The exhaust system also offers opportunities for weight savings and noise reduction through the use of ceramic foam materials. Presently some engines employ exhaust systems with mixer nozzles to increase the effectiveness of mixing the hot core exhaust with the fan stream and thus reducing exhaust noise. Another method for noise reduction is to include a perforate plate liner in the exhaust nozzle. Because of the high temperatures involved, the nozzles and acoustic treatment are typically constructed from Inconel and are quite heavy. Use of a porous ceramic foam coupled with some of the newer high temperature titaniums (e. g. TI 1100, titanium aluminides, etc.) or a ceramic matrix composite sandwich construction instead of the current approaches offers potential noise and weight benefits.

3.0 MATERIAL DEVELOPMENT

3.1 HTP Ceramic Foams

The performance requirements described in Section 1 provide the basis for modifying and improving manufacturing processes for low density ceramic foams to achieve high porosity and tortuosity that enchance efficient broad band acoustic absorption. The material used in this study is a composition of silica and alumina fibers called "High Thermal Performance" (HTP) that was developed by Lockheed Martin Missiles and Space (LMMS). Integrated acoustic treatment panel structures using this material must pay particular attention to microstructure variability effects, material sonic fatigue survivability and acoustic property retention from operational effects such as fluid wicking and structural flexing.

LMMS has produced standard HTP foams that range in density from 6 to 16 lbs/ft^3 (pcf) or 96 to 256 kg/m^3 to support various high temperature applications (themal insulation for F-117, B-2 bomber; antennas; radomes; lens; and acoustics). Recently, lower density foams ranging from 3 to 4 pcf (48 to 64 kg/m^3)were also developed (LMMS internal funding) to provide lightweight and broad band acoustic liner applications for the AST and HSCT programs. Candidate systems (Table 3-1) investigated to date cover the array of rayl values of interest for the AST inlet and after fan as well as hypersonic nozzle liner applications. It should be noted that these low density (3 to 4 pcf) foams have much lower structural strength than previously developed HTP foams which may limit their utility for certain applications.

The goal in producing the lower density foams was to concentrate on tailoring the pore size and increasing porosity of current foams to maximize acoustic performance. The decrease in structural strength in the lower density foams is the result of expanding pore size and increasing foam porosity to greater than 96%. A number of processing parameters can be varied such as fiber type and composition, blending ratios, casting pressures and as-fabricated density for increasing the mechanical strength of the ceramic foams while retaining nearly the same acoustic performance; rayl ranges, pore size, and porosity. Optimization of the ceramic foam for successful assembly into an

acoustic structural panel must be defined to meet minimum compression strength requirements.

3.2 HTP Ceramic Foam Optimization

An assembly threshold for pressing the ceramic foam into the titanium honeycomb sandwich panel was observed. Ceramic foams of less than 4 pcf density, having compression moduli of less than 400 psi, have shown a propensity to crush rather than be cut by the honeycomb core during panel assembly. This is contrary to higher density (greater than 4 pcf) and higher flow resistance ceramic foams where the honeycomb edges easily sliced the foam allowing successful core compression and panel assembly integration. When hand squeezing these (< 4 pcf) foams; the material exhibited a spongy feel, springing back as it was released rather than retaining the rigid feel exhibited in higher (> 4 pcf) density foams.

Based on a limited experience base, the spongy characteristic occurs when the ceramic foam is less than 4 pcf and the acoustic properties are less than 60 rayls/cm. Under these conditions the foam median pore sizes range from about 95 to 120 microns, porosity is greater than 96%, and the fiber volume concentration is estimated to be 2 to 4 times less than for densities greater than 4 pcf (with high rayl values). The number of fibers and distance between fused fiber joints is greater, hence the larger equivalent pore sizes. The total spectrum of pore sizes for any foam varies from around 300 microns down to 0.1 microns with the median pore size reported in Table 3-1 for a given density. Pore size is determined using a mercury porosimeter which measures the amount of mercury infilrated in a 3-D porous structure under a given pressure. The instrument calculates the equalivent pore size and pore size distribution in the material using a cylinder shape as the standard geometric volume. The non uniformity of the ceramic foam microstructure and torturous path within the bulk contributes to the materials excellent broad band sound absorption characteristics.

Continued development is required at the lower foam densities (less than 4 pcf), especially where flow resistance properties of less than 60 rayls/cm are required for the inlet applications. Two approaches have been identified for enhancing the foams structural strength and rigidity to survive the assembly operations: 1) the density can be raised to increase the number of fused fiber

joints and larger fiber diameters are used to retain the large pore size and low rayl values, and 2) alter the current fiber composition and processing parameters to maintain density while enhancing more uniform fiber fusion. The goal is to achieve a narrower range of pore sizes to enhance bulk foam uniformity and strength. In addition, other reinforcing thin loose weave ceramic cloths can be impregnated during foam fabrication to enhance structural integrity and extend sonic fatigue survivability.

3.3 HTP Fluid Contamination Performance

Environmental contamination from various fluids (discussed in Section 5.1), is a major concern for use of ceramic foams as a bulk absorber in acoustic structural applications. The fluid contamination problem can be addressed at two levels; 1) from a material resistance standpoint, and 2) during acoustic panel design. Fluid resistance materials or coatings can be applied into the foam or as a surface coating to alter the foam's surface wetting characteristics to minimize fluid absorption. In addition, thin surface layers that repel both water and organic liquids can be integrated over the foam to prevent liquid penetration into the foam. Excess fluid absorption must be evaluated to determine whether the any absorbed fluid will create an operational problem. Since the ceramic foam pore structure is open cell with a greater than 96% porosity, the ability of fluids to evaporate or be wicked from the bulk to the surface should easily be accomplished during warm ups.

Further studies are required to investigate the heat of vaporization temperatures for the liquids of concern and the ability of these materials to escape the ceramic foam during engine warm ups or operation. Studies to evaluate ceramic foam heating and depth of heating are required to understand the liquid evaporation effects. In addition, studies to assess the effects of temperature cycling of the ceramic foam with both water and organic liquids must be performed. Approaches to prevent liquid absorption into the foam must be addressed by the methods described above. To that end, any acoustical panel designs that minimize the amount of fluids absorbed into the ceramic foam filled honeycomb must be investigated. Implementation of a combination of metal screens and a foam surface treatment may be sufficient protection against fluids absorption.

3.4 Conclusions and Recommendations

Based on the test results to date, the data indicate that further material optimization is required to allow for ease of ceramic foam integration into the titanium core. Approaches designed to improve the structural strength in low flow resistance materials are listed section 3.2. It is recommended that a fluids environmental contamination program be initiated immediately to address concerns and issues with fluid absorption for inlet applications. The approaches for tailoring the ceramic foams to improve their survivability in the fluid environment are listed in section 3.3. Since there is a good possibility that the acoustic properties will be altered with the application of fluid resistant coatings, it is also recommended that the fluids environment task be initiated prior to the foam material optimization work. Based on the modifications necessary to solve the fluids problem, a new assessment to optimize the foam structural properties can be performed at that time.

4.0 ACOUSTIC PROPERTIES TESTING AND EVALUATION

4.1 Acoustic Impedance Measurement

A two-microphone impedance measuring system was used to conduct all acoustic impedance measurements. The apparatus and methods used are in compliance with the ASTM E1050-90 measurement standards (Reference 8). A block diagram of the Rohr acoustic impedance measuring system standard is shown in Figure 4.1-1.

The sensitivities of the pressure transducers for the acoustic impedance measuring system was calibrated in accordance with Rohr Report No. RHR 89-191 (Reference 9). The amplitude and phase calibration for the two-microphone impedance system transducers were performed in accordance with the method described in the ASTM E1050-90 impedance measurement standard (Reference 8). The performance of the acoustic impedance measuring system was checked prior to any testing by evaluating known reference samples. The reference samples included a 5% POA perforate plate and an empty cavity termination. The root mean square (rms) deviation of the acoustic impedance of the reference samples over the measurement frequency range was evaluated before each series of tests.

A test sample is installed at one end of the impedance tube as a termination as shown in Figure 4.1-2 (a) and (b). Using a random noise excitation, the normal specific acoustic impedance of the test sample is determined from two pressure measurements along the wall of the impedance tube. The frequency for this test ranges from 800 to 6000 Hz. Overall sound pressure levels (OASPL) of up to 160 dB can be achieved at the face of the test sample. The characteristics of this pressure spectrum will be documented for use in the corresponding acoustic impedance predictions. For each test sample, three sound pressure levels were used. The measured acoustic impedance data is presented in 120 Hz bandwidth narrow band form. Data files containing this information presented in 120 Hz bandwidth narrow band form are available on 3.5" diskette in ASCII format.

As part of a previous Rohr - LMMS Joint Program effort, the acoustic impedance of several HTP systems (HTP-4, HTP-6, HTP-10, HTP-12, and HTP-

16), that spanned a wide range of densities (3-16 pcf), were assessed (see Table 3-1). Figures 4.1-3 through 4.1-12 show acoustic impedance test results for HTP materials with various densities and thicknesses. For current fan and nozzle acoustic treatment applications under NASA AST and HSCT programs (i.e., NASA Contract NAS3-26618 - Task 49 – ADP liner design, and NASA Contract NASA-1-20102 Task 13 – HSCT nozzle treatment), the optimum liner impedance ranges from 1 to 2.5 ρc (characteristic impedance - air density times sound speed) for acoustic resistance and -1.5 to 0 ρc for acoustic reactance at design frequencies. The data shows that HTP materials with densities less than 6 pcf fall within the optimum impedance window for these applications over a very broad band frequency range.

Nineteen (19) more material samples (6" by 6") (ID.: 14360B, 14360D, 14360F, 14360G, 14360J, 11093T, 11093B, 11095T, 11095B, 11097T, 11097B, 11105T, 11105B, 11107T, 11107B, 13031T, 13031B, 1438, and 1433A) were received from LMMS to support impedance testing used for material down selection. These materials have a density less than 6 pcf with a wide range of DC flow resistance properties (as shown in Table 3-1). Acoustic impedance measurements were performed on all of the 6" x 6" samples (in-tube test). Single, double, triple, and four layer thick (0.5, 0.75, 1.0, 1.5, and 2.0 inch) test specimens were assembled for each material sample. Figures 4.1-13 through 4.1-25 show test results of averaged acoustic impedance values for all test specimens. Some test samples were assessed at a single sound pressure level, since early test results showed an insignificant effect of this parameter. Based on these impedance test results, the HTP-5 system (such as the 1438 and 1433A samples in Figures 4.1-24 and 4.1-25) is the most promising material for inlet applications whereas the 11095, 11097, and 11105 samples (Figures 4.1-19, 4.1-20, and 4.1-21) have desirable characteristics for bypass duct treatment. For supersonic vehicle and subsonic nozzle applications, additional noise signature information is required for down selection, however, it is anticipated that one of the 8-10 pcf systems would be satisfactory. Table 4.1-1 lists down selected HTP systems for future program evaluation.

4.2 Acoustic Testing of Downselected Material Systems

As discussed in Section 4.1, three systems were down selected for a scale-up validation. Material and acoustic properties of these three systems are

shown in Table 4.1-1. Panels were fabricated in support of panel impedance, flow duct insertion loss measurement, and high cycle fatigue testing to evaluate the three down selected material were conducted. The 4 pcf system was initially identified for use in the inlet region, with a lower density system (3 pcf) to be used for the bypass duct (see Table 4.1-1). However, insertion of the lower system (3 pcf) into the titanium sandwich panels was extremely difficult (the material was very spongy). Thus, only the 4 pcf system was used to fabricate an acoustic panel for the inlet and the bypass duct application.

4.2.1 Acoustic Impedance Measurements

The panel configuration is shown in Figure 5.2-2. The POA of the Ti perforate face sheet was 37%. Acoustic impedance panel testing was conducted on two (2) 5.5" x 24" flow duct panels. Also, acoustic impedance in-tube testing was performed on a 1" ceramic foam sample (LMMS ID 1437). Figures 4.2-1 through 4.2-6 show test results of averaged acoustic impedance values for the panel test and in-tube test (1" foam only). The test results indicate that acoustic impedance of bulk material structures are affected by the face sheet parameters and the differences in panel test and in-tube test boundary conditions (i.e. sound energy through the in-tube test is constrained whereas sound energy through the panel test is not). In the future, a correlation between acoustic impedance and face sheet parameters (such as POA, hole diameter, and plate thickness) needs to be investigated in order to produce an optimum acoustic liner design (References 5 & 6).

4.2.2 Acoustic Insertion Loss Measurements

The Rohr air/noise flow duct facility was used to measure the acoustic insertion loss of the test samples. Figure 4.2-7 shows a schematic of the flow duct facility. The test section of the duct is rectangular, with a cross section of 5 by 6 inches, and is connected by aerodynamic transition ducts to two reverberant rooms on either end of the duct. The method used for measuring the acoustic insertion loss compares the sound pressure levels (SPL) in the upstream and downstream reverberate rooms at different air flow velocities. First, hard walls are mounted at the test section, and the SPL differences (i.e., attenuation IL(H), between the upstream and downstream rooms) is measured at different air flow velocities. This set of data is used as a baseline. After

replacing the hard walls with the test samples, the same procedure is followed, and the attenuation, IL(S), is measured. Finally, the acoustic insertion loss of the test samples is calculated by taking the difference of the two readings: IL(S) - IL(H).

Measurement frequencies range from 1000 to 6000 Hz. Overall sound pressure levels of up to 152 dB can be achieved at the upstream reverberant room. For each test sample, five different air flow velocities between 0.2 and 0.6 Mach number were used. The measured acoustic insertion loss data is presented in one-third octave bandwidth form. Data files containing this information presented in one-third octave frequency form are available on 3.5" diskette in ASCII format.

The Rohr air/noise flow duct facility is operated in the 'exhaust' mode, i.e., the air flow direction is the same as the noise propagated direction, not in the 'inlet' mode (the air flow direction is opposite to the noise propagated direction). It is also noted that this facility is optimally designed for an acoustic liner with 1 ρc acoustic resistance and -0.5 ρc acoustic reactance.

Figures 4.2-8 through 4.2-13 show acoustic insertion loss test results for a 4.78 pcf ceramic foam (LMMS HTP ID. 1437) filled sandwich structure. A single degree of freedom (SDOF) DynaRohr liner is a common acoustic liner used in aircraft; and an 80 rayl single layer DynaRohr panel (0.95" core depth) was used as a reference to evaluate the acoustic performance of the foam filled sandwich structure. Comparison of the acoustic insertion loss of the ceramic foam filled sandwich structure and the 80-rayl SDOF DynaRohr structure at Mach numbers 0.4, 0.5, and 0.6 is shown in Figures 4.2-14 through 4.2-16.

The test results indicate that the acoustic insertion loss of the 80-rayl SDOF DynaRohr is better than the ceramic foam filled sandwich structure in the frequency range from 1,250 Hz to 3,150 Hz. The measured acoustic impedance (panel test) of the 80-rayl SDOF DynaRohr at different SPLs is shown in Figures 4.2-17 through 4.2-19. Comparing Figures 4.2-1 and 4.2-17 show that the acoustic reactance of the 80-rayl SDOF DynaRohr reaches an optimal value (-0.5 ρc) between 2,000 Hz and 3,000 Hz and the ceramic foam (LMMS HTP-1437) filled sandwich structure reaches its optimal value (-0.5 ρc) between 5,000 Hz and 6,000 Hz. This may be the cause of the decrease in the acoustic

insertion loss for LMMS HTP-1437 system. Also, as mentioned in Section 4.2, the lower density system (~3 pcf) was chosen to be used for the bypass duct liner. Figure 4.1-20 shows the acoustic impedance of LMMS HTP-11097 (3.65 pcf) and the acoustic reactance reaches its optimal value (-0.5 ρc) between 2,000 Hz and 5,000 Hz. However, due to difficulties associated with inserting the lower HTP system (~3 pcf) into the titanium sandwich panels, this lower system (~3 pcf) cannot be considered for the bypass duct application now. A new fabrication method should be investigated to complete the acoustic insertion loss studies.

It should be noted that the ceramic foam filled sandwich structure was designed and fabricated solely to study the basic acoustic properties of the ceramic foam materials and not for liner optimization. Modification of perforate face sheet and core should improve the acoustic performance of ceramic foam filled sandwich structures (see Section 6.3).

5.0 ENVIRONMENTAL AND STRUCTURAL TESTS

Environmental and structural testing performed, either as part of the previous Rohr - LMMS joint efforts or this program are described in the following sections.

5.1 Environmental Evaluation

Several environmental concerns exist regarding the use of ceramic foam as a bulk absorber in acoustic structures applications. These include contamination of the large fillet region of sandwich structures constructed using standard Liquid Interface Diffusion (LID) bonding methods and susceptability of the foam to exposure to fluids, such as Skydrol.

In order to assess the potential for joint contamination due to the use of the ceramic bulk absorber in acoustic structure applications, four (4) 3" x 6" x 0.75" thick ceramic foam filled honeycomb titanium panels were fabricated. Since it has not been determined yet whether protective coatings for the ceramic foam are necessary, half of the panels contained colloidal alumina coated ceramic foam and half contained uncoated ceramic foam to investigate bonding effects of the foam to the face sheet due to the presence of the protective coating. The face sheet material was Ti-6Al-4V with Ti-3Al-2.5V core (3/8 inch cell size). One face sheet was solid, the other was perforated with a 20 percent open area (POA). The ceramic foam was HTP-5.4. Standard LID bonding methods and parameters were used to bond all panels. After fabrication, all four panels were sectioned to 3" x 3" sizes and tested for flatwise tension strength. The results are shown in Table 5.1-1 with the uncoated samples being superior.

Metallurgical evaluation was performed on both coated and uncoated samples to assess potential joint contamination. Energy Dispersive Spectroscopy (EDS) analysis was performed on the LID braze fillet regions. Evidence of voiding (high levels of porosity) was apparent on the coated samples, whereas no voiding was observed on the uncoated samples. Micro hardness indentations around a typical fillet were also assessed with calculated values in the normal range for both coated and uncoated samples. Based on the above, it was concluded that future efforts involving titanium bonded

sandwich/ceramic foam specimens/structures should use uncoated ceramic foam.

Skydrol exposure testing was also performed. Samples were exposed to Skydrol 500-B4 per MIL-4-5606 (20 hours at 120^{0}F), which is considered to be a very conservative test, and to a misting (four times per day - 2 minutes each time) for ten days. Significant weight pickup (120% increase) was incurred from the 20 hour/hot Skydrol soaking and the specimens sustained some loss of stiffness. The misting test produced far less weight pickup (15% increase) and the foam retained its stiffness characteristics. However weight pickup due to exposure to fluids, including moisture, and sensitivity to Skydrol were identified as issues that must be resolved before this material can be used in aeroacoustic applications.

5.2 Structural Evaluation

Since the ceramic foam is encapsulated in the honeycomb sandwich structure and is not a load carrying member, durability of the foam in a hot dynamic environment is considered the key structural issue for the foam. To address this issue, High Cycle Fatigue (HCF) testing was performed at both ambient and elevated temperatures (1000^{0}F). This temperature was used since it represents the capability limit of the Rohr shaker system and since it is close to the maximum value experienced by AST component applications. All specimens were tested using an Inconel duckbill assembly to grip the specimen at one end. The duckbill was attached directly to the head of an electrodynamic shaker to provide vibratory loading of the cantilever test specimens. Specimens were instrumented with strain gages at the duckbill gripline to measure uniaxial bending stresses along the gripline edge. The specimens were also instrumented with a tip accelerometer to monitor resonant frequency and tip displacement response. An accelerometer was attached to the shaker head to measure input loading to the specimen. Figure 5.2-1 shows the test setup and Figure 5.2-2 shows the test specimen details.

Random vibration tests were conducted according to the procedure described in Rohr Engineering Test Standard (RETS) 128D-90013, Method 10-85, "High Cycle Random Fatigue Test", with some slight procedural modifications. An outline of the testing sequence is described below:

Sine Sweep: The initial phase of testing consisted of a low level (0.5 G peak) sine sweep test from 20 - 1,000 Hz. This determined the resonant frequency corresponding to the maximum response with the first cantilever mode of the specimen. This resonant frequency was the center frequency used for the random loading phase of testing.

Random Vibration: A 1/3 octave band random signal, centered at the specimen resonant frequency, was used to excite the specimen for the random vibration screening tests. The strain gauge output signals were monitored during the test using a spectrum analyzer to generate strain frequency response spectra. The input loading of each test specimen was adjusted to generate a specified test strain level. A strain level of 300 $\mu\varepsilon$ was used for all tests. This value was assigned based on titanium perforate face sheet fatigue capabilities. Testing was performed for 10^6 cycles or until failure occurred which was defined as a 20% drop in natural frequency (indicating a major loss of stiffness), or visible evidence of damage to the part (cracking, etc.). Test results are shown in Table 5.2-1. No significant frequency drop was evidenced in any of the tests. It should be noted that for sandwich specimens, dynamic shaker testing causes deflections that exceed those that would normally be expected in a sonic environment (thus, this represents a conservative test when compared with anticipated service excursions). This has been confirmed through previous dynamic shaker/progressive wave tube sonic tests conducted at Rohr on other ceramic foam specimens.

Figures 5.2-3 through 5.2-10 show test results of the measured acoustic impedance for each test location prior to and after HCF tests at three SPLs. These test results indicate that the acoustic impedance of the specimens did not change significantly after HCF testing at room temperature or at high temperature. Changes in acoustic resistance were minimal, whereas slight differences were observed in the acoustic reactance, probably due to a measurement error.

5.3 Structural Testing of Downselected Materials Systems

Three high cycle fatigue (HCF) test specimens were fabricated using the downselected 4.78 pcf LMMS 1437 material (titanium sandwich structure) and

the same configuration as the flow duct test panel. The same test procedure described in Section 5.2 was used to test these specimens. Test results are provided in Table 5.3-1 along with acoustic impedance test results (prior to and after HCF testing) in Figures 5.3-1 through 5.3-9. No significant frequency drop was evidenced in any of HCF tests nor did the acoustic impedance of the specimens change significantly due to HCF testing at room temperature or at high temperature.

6.0 ACOUSTIC IMPEDANCE MODEL

6.1 Model Development Background

A key element in the optimization of acoustic treatment for specific applications is establishment of an acoustic impedance math model for predicting acoustic performance. This math model is typically highly dependent upon material type. Acoustic bulk absorbers can be made from flexible fibrous blankets (i.e., Kevlar 29), rigid reticulated foam (i.e., carbon foam) or fibrous foams (i.e., HTP ceramic foam). The Rohr bulk impedance model developed to predict the impedance characteristics of these materials is primarily based on theory derived from D. J. Sides, and K. A. Attenborough (References 1 & 2). Math models derived from A. Hersh (Reference 3), L. L. Beranek (Reference 4), and U. S. Shirahatti (Reference 5) were also used for specific options such as data comparison, flow resistance calculation and structure factor estimation. Moreover, since the bulk material is in close contact with a perforated facing sheet, the U. Ingard math model (Reference 6) was used to estimate the acoustic contribution from the facing sheet.

If the sound wave propagation in the air is expressed as $P = e^{(j\omega t - kx)}$, the basic equation for a bulk liner with a porous face sheet and solid back skin can be expressed as follows:

$$Z(f)/\rho c = R + jX = Z_o/\rho c + Z_b/\rho c \qquad (1)$$

$$Z_b = -j Z_c \cot(k_b d) \qquad (2)$$

where,

P is the sound pressure

f is the frequency.

ω is the angular frequency ($=2\pi f$)

k is the wave number ($=2\pi f/c$)

$Z(f)/\rho c$ is a complex number representing the normalized bulk liner impedance.

R is the normalized acoustic resistance.

j is the unit of imaginary number = $\sqrt{-1}$.

X is the normalized acoustic reactance.

$Z_O / \rho c$ is the normalized porous face sheet impedance over the bulk material.

$Z_b / \rho c$ is the normalized bulk material impedance.

ρ is the air density and c is the sound speed.

ρc is defined as the characteristic impedance for air (unit: cgs Rayl).

Z_c is defined as the characteristic impedance for a given bulk material.

k_b is the bulk material propagation constant (complex number).

d is the bulk thickness in inches or cm.

Section 6.2 details the math model used to calculate HTP ceramic foam impedance. Section 6.3 describes acoustic impedance contributions from the perforated sheet that is in close contact with the bulk material. Section 6.4 addresses the method used to determine the bulk material characteristic impedance and complex propagation constant. Section 6.5 provides a comparison between predicted and measured impedance results.

6.2 Ceramic Foam Impedance Model

At Rohr two math models are used to predict the acoustic impedance of bulk absorbers. The choice of math model is primarily dependent on bulk absorber type.

For both reticulated and fibrous ceramic foams, the complex propagation constant, k_b, and the characteristic impedance, Z_c, are based on Attenborough's Model (Reference 2) and can be described as follows:

$$k_b = q\, k\, [F(\mu) / G(\mu)]^{0.5} \qquad (3)$$

$$Z_c = \omega \rho_b / k_b \qquad (4)$$

where,

$$\mu = (1/n)\, (8\, \rho\, q^2\, S\, \omega)^{0.5} / (\delta\, R_d) \qquad (5)$$

$$F(\mu) = 1 + [2(\gamma - 1)/(\xi\, \mu \sqrt{-j})]\, (T(\xi\, \mu \sqrt{-j}) \qquad (6)$$

$$G(\mu) = 1 - [2/(\mu \sqrt{-j})]\, T(\mu \sqrt{-j}) \qquad (7)$$

$$T(\mu\sqrt{-j}) = J_1(\mu\sqrt{-j}) / J_0(\mu\sqrt{-j}) \text{ ——————} \quad (8)$$

$$T(\xi\mu\sqrt{-j}) = J_1(\xi\mu\sqrt{-j}) / J_0(\xi\mu\sqrt{-j}) \text{ ——————} \quad (9)$$

$$\rho_b = \rho\,(q/\delta)\,G(\mu) \text{ ——————} \quad (10)$$

and,

q is the tortuosity factor ($q \geq 1$).

k is the air propagation constant (or wave number = $2\pi f/c$) in real number.

n is the dynamic shape factor ($0.5 \leq n \leq 1$).

S is the steady flow shape factor ($S = 2 - n$).

ω is the angular frequency (= $2\pi f$).

δ is the bulk porosity.

R_d is the steady flow resistance per unit (Rayl/cm).

γ is the specific heat ratio ($\approx$1.4 for air).

ξ is the square root of Prandtls number ($\approx$ 1).

J_0 and J_1 are circular Bessel functions of the zero and first order, respectively.

For a given air characteristic impedance, ρc, and rigid bulk material thickness, d, the ceramic foam normalized impedance, $Z_b/\rho c$, can be calculated by substituting Equations (3) and (4) into Equation (2).

For flexible fibrous bulk materials, the D. J. Sides model (Reference 1) is normally used. This model can also be used for rigid fibrous foams such as HTP, but involves more complicated equations and input parameters (i.e., Poisson's ratio and Young's modulus of the fibers) than the Attenborough model for calculating the complex propagation constant, k_b, and characteristic impedance, Z_c. In this report, the Attenborough model is the only math model used to compare predicted impedance data with measured results.

6.3 Impedance Contribution From The Perforated Facing Sheet Over the Bulk Material

Ingard (Reference 6) has reported that the effect of the perforate face sheet really depends on whether the facing is in close contact with the backing

bulk material or whether a small gap exists between the two. Figure 6.3-1 illustrates how the perforated facing distorts the flow in the contact area. This ordinarily does not extend further than about one perforation diameter from the facing.

If the distorted part of the flow is confined to the bulk material, the facing causes a reactance as well as a resistive contribution to the total impedance. Ingard explained that this effect is due to the near field (higher mode) losses in the bulk material around the perforations.

The equations used for the perforated facing contribution can be expressed as follows:

$$Z_o/\rho c = R_o/\rho c + j X_o/\rho c \quad \text{——————} \quad (11)$$

$$R_o/\rho c = S_P f(\delta_P) R_d/\rho c \quad \text{——————} \quad (12)$$

$$X_o/\rho c = k[(t/\delta_P) + f(\delta_P)(1+S_f) S_P] \quad \text{——————} \quad (13)$$

where,

$R_o/\rho c$ is the normalized porous face sheet acoustic resistance.
$X_o/\rho c$ is the normalized porous face sheet mass reactance.
S_p is the perforate plate hole spacing.
$f(\delta_P)$ is the correction function as defined in Figure 6.3-2.
t is the perforate facing sheet thickness.
δ_P is the perforate plate open area ratio.
S_f is the bulk material structure factor

For a single degree of freedom (SDOF) bulk liner, the bulk material is in close contact with the perforate face sheet plate liner. The total acoustic impedance, $Z(f)$, is the combination of bulk material impedance, Z_b and face sheet impedance over the bulk material, Z_o (See Equation (1)).

6.4 Characteristic Impedance and Propagation Constant Assessment

The complex propagation constant, k_b , and the characteristic impedance, Z_c, of the bulk material can be determined from normal incident impedance tube test data as described in Section 4.

For example, rewriting Equation (2) for two test specimens of different thickness, d_1 and d_2, from the same bulk material type yields:

$$Z_{b1} = -j\, Z_c \cot(k_b\, d_1) \qquad (14)$$

$$Z_{b2} = -j\, Z_c \cot(k_b\, d_2) \qquad (15)$$

Equations (14) and (15) can be reconstructed to yield:

$$Z_{b1} / Z_{b2} = \cot(k_b\, d_1) / \cot(k_b\, d_2) \qquad (16)$$

Since d_1 and d_2 are known and Z_{b1} *and* Z_{b2} are measured impedance data, a numeric process, such as the Newton-Raphson method, can be used to solve for k_b at each measured frequency. Two common problems exist in the use of such a numeric process. The first is the starting value (initial guess) selection. The second is that the solution may not converge during the process. Both problems were experienced in attempting to determine k_b for the HTP bulk material, especially for the samples with limited property data. To help resolve this problem, test specimens can be constructed such that the value of d_1 is equal to one half of the value of d_2, thus simplifying Equation (16) as follows:

Let $Z_{b12} = Z_{b1} / Z_{b2}$, and substitute $d_1 = (1/2)\, d_2$ into Equation (16), yielding

$$Z_{b12} = \cot(k_b(1/2)\, d_2) / \cot(k_b\, d_2)$$

$$= [\sin(k_b\, d_2) / \cos(k_b\, d_2)] / \tan(k_b(1/2)\, d_2) \qquad (17)$$

From Reference 7 (Handbook of Mathematical Functions), it is shown that

$$\tan(k_b\, (1/2)\, d_2) = \sin(k_b\, d_2) / [1 + \cos(k_b\, d_2)] \qquad (18)$$

Substituting Equation (18) into Equation (17) and eliminating $\sin(k_b\, d_2)$ yields

$$Z_{b12} = [1 + \cos(k_b d_2)] / \cos(k_b d_2) \text{ ——————} \quad (19)$$

Equation (19) can be further reduced:

$$\cos(k_b d_2) = 1/(Z_{b12} - 1) \text{ or}$$

$$(k_b d_2) = \text{Arccos}[1/(Z_{b12} - 1)] \text{ ——————} \quad (20)$$

Applying Inverse Circular Function ***ArccosZ*** from Reference 7 yields an exact solution for $(k_b d_2)$. The propagation constant, k_b, and characteristic impedance, Z_c, can then be calculated from Equation (15) at each frequency. Since a computer solution only provides the principal mode value for the ***ArccosZ*** function, it is import to carefully examine the results and adjust the solution to higher mode value if necessary. The best way to verify the solution is to substitute calculated k_b and Z_c values into Equation (14). If the calculated Z_{b1} value is equal to the measured Z_{b1} value within the round-off error range (accuracy up to second decimal number), then the solution is correct.

6.5 HTP Foam Impedance Model Verification

The impedance model verification is based on room temperature data and ignores the non-linear factor effect due to sound pressure change. High temperature turbulence and the non-linear factor can affect bulk material impedance characteristics, but the change may not be significant for HTP foam used for AST applications. Future studies which would involve more test data and modeling techniques to assess the impact of these two factors should be considered.

Additionally, no data was obtained for in-tube impedance measurements of the HTP foam with a perforate face sheet. This was due to the fact that the existing sample holder can not hold the HTP foam specimen with a perforate face sheet at the proper position. A special adapter ring is required for this evaluation. Therefore, the effect of facing sheet will not be evaluated in this report, but should be included in future study.

Figure 6.5-1 through 6.5-6 provide a comparison between predictions and data measurements of the Characteristic Impedance and Propagation Constant

for three different HTP foams (11093, 1438, and 1433A defined in Table 3-1). Attenborough's math model (Section 6.2) was used to generate the predictions. The math model described in Section 6.4 and the impedance measurement results found in Section 4 (see Figures 4.1-18, 4.1-24, and 4.1-25) were used to determine the measured characteristic impedance and propagation constant data. The quality of the measured data for the 3.3 pcf system is high for both the characteristic impedance and the propagation constant throughout the frequency range. This is attributed to the fact that reasonable differences exist (no overlap) between the various sets (thickness based) of impedance data. Execllent agreement exists between the predictions and measurement data when the values of the Tortuosity Factor, q, and the Dynamic Shape Factor, n, are 1.095 (q^2=1.2) and 0.91 respectively.

For the higher density HTP foams, measured impedance data at two different thicknesses overlap exists above certain frequencies (e.g., greater than 4,500 Hz for the 4.91 pcf foam (Figure 4.1-24) and greater than 3,000 Hz for the 5.36 pcf system (Figure 4.1-25)), resulting in calculation difficulties and anomalies in the generated propagation constant values (Figures 6.5-4 & 6.5-6). However, it does not affect the results of the characteristic impedance calculation because at the overlap region the values of characteristic impedance are equal to the measured impedance data. In future studies, ceramic foam thicknesses should be selected that provide sufficient differences in data sets, reducing calculation difficulties and the resultant anomalies. When compared with math model predictions, fair agreement is observed when the abnormal measured propagation constant data (derived from impedance measured data using two different foam thicknesses) in the high frequency range are excluded. For the 4.91 pcf foam sample, the values of Tortuosity Factor and the Dynamic Shape Factor, are the same as the 3.3 pcf foam sample. It shows predictions of the characteristic impedance to be slightly less than the measured data for the resistance curve at all frequencies and the reactance curve at frequencies below 3000 Hz. Several attempts were made to adjust the Tortuosity Factor and Dynamic Shape Factor but no improvement in the correlation was observed. This could be the result of poor sample quality. For the 5.36 pcf foam sample, the values of 1.342 (q^2=1.8) and 0.75 were used for the Tortuosity Factor, and the Dynamic Shape Factor respectively. These values provide the best fit between predicted and measured results for both characteristic impedance and

propagation constant. No relationship has been found between foam density, flow resistance, tortuosity, and dynamic shape. Further efforts are required to establish this relationship.

Figures 6.5-7, 6.5-8, and 6.5-9 show the comparison between impedance predictions and measurements using the bulk material samples discussed in previous Section 6.5-1. Good agreement is shown for the 3.3 and 5.36 pcf samples. For the 4.91 pcf sample, the impedance is slightly under predicted. However, excellent agreement exists between the predicted and measured impedance data in a similar sample (ID#1437, 4.78 pcf) which is shown in Figure 6.5-10.

The sound pressure effect is not significant at sound pressure levels below 148 dB. Figure 6.5-11 provides a comparison between predicted data and measured impedance data for the 3.94 pcf sample (ID # 11107T). The measured data include the sound pressure levels at 140 dB, 145 dB, and 148 dB. It is demonstrated that the impedance data to be insensitive to the sound pressure effects. Figures 6.5-11 also shows an unexpected upturns at the up-end of the high frequency range. No particular explanation has been explored but the instrumentation limits and measurement errors are probably the reasons for this unexpected upturns.

The data obtained from the previous Rohr/LMMS joint program on ceramic systems development were also reported in Section 4.1. The calculated characteristic impedance and propagation constants are shown in Tables 6.5-1 through 6.5-3 and Figures 6.5-12 through 6-17 for HTP-4 (4.3 pcf), HTP-6 (7.2 pcf), and HTP-10 (8.2 pcf) ceramic foam samples. Material properties are shown for these systems in Table 3-1. Since the DC flow resistance data are not available for these samples, no predictions have been made. Of note is that the impedance values of the HTP systems do not degrade at high frequencies indicating that this material offers good potential for both inlet and aft fan tone treatment.

7.0 CONCLUSIONS AND RECOMMENDATIONS

7.1 Conclusions

A study has been undertaken to evaluate the acoustic, environmental, and structural properties of HTP ceramic foam systems and to validate their sub-scale structure integration capability. The following conclusions can be drawn from this study.

- The lightweight HTP ceramic foam system (3 to 5 pcf) provides good broadband bulk absorber capability for use in linear liner applications based on acoustic impedance evaluation (i.e., resistance target of 1.0 to 2.5 ρc and reactance target of -1.5 to 0.0 ρc).

- An approach for incorporating the HTP ceramic foam system into acoustic sandwich structure was demonstrated for foams with densities in excess of 4 pcf. Adequate structural integrity was exhibited under room and hot temperature load environments (dynamic shaker tests).

- Based on acoustic impedance testing, 4 - 5 pcf HTP material provides the best balance of broadband performance, structural integrity and minimum weight impact for AST applications. However, a 3 pcf HTP material system is desired since it would be lightweight and provide better acoustic characteristics for optimum acoustic liner design. A major issue with such a lightweight system is structural durability. It is anticipated that a denser system (~10 pcf) would be required for hypersonic applications.

- A Rohr-developed math model for the HTP material system has been demonstrated to accurately predict acoustic impedance characteristics.

- Currently environmental effects, specifically moisture pickup and sensitivity to Skydrol, limit the use of the HTP system in AST aeroacoustic applications on a production basis due to weight pickup and the effect fluids have on acoustic performance.

7.2 Recommendations

Based on the results of this study the following recommendations are made.

- Additional effort is needed to further optimize the use of ceramic foam filled acoustic structures. This includes examination of the effect of face sheet parameters (plate thickness, hole diameter, spacing, POA, etc.) on acoustic performance. High temperature impedance testing is also required for optimization as well as sound pressure effects on NLF. Efforts to obtain this data should be pursued.

- Airflow duct acoustic insertion loss studies, including low density specimen fabrication and prediction of HTP ceramic liner attenuation in the duct, should be completed.

- A relationship between HTP foam density, flow resistance, tortuosity, and dynamic shape should be established to finalize the impedance math model.

- Recent discussions with NASA, Pratt & Whitney and General Electric personnel involved in the High Speed Research Enabling Propulsion Materials (EPM) program indicate that a density of 8- 10 pcf would be optimum for hypersonic nozzle applications. Further study is required to assess the acoustic characteristics of these high density systems.

- It is imperative that all environmental issues (Skydrol sensitivity, moisture pickup, etc.) be resolved before HTP materials can be used for AST aeroacoustic applications. LMMS is evaluating manufacturing processes and after-process additions to address these issues. Additionally, based on EPM community testing of HTP material of unknowm pedigree, one area of concern for hypersonic applications is the susceptibility to freeze-thaw cycling. LMMS has been informed of this situation and is attempting to understand the mechanisms that will reduce the effect of freeze-thaw cycling on the HTP materials to EPM-acceptable levels.

- While several technical issues exist that must be overcome, this class of material systems do offer great promise as broadband bulk absorbers and should be evaluated in engine rig test environments should those opportunities arise for further verification of their utility.

8.0 REFERENCES

1. "Application of a Generalized Acoustic Propagation Theory to Fibrous Absorbents", by D. J. Sides, K. Attenborough, and K. A. Mulholland, Journal of Sound and Vibration, Vol. 19 (1), pp. 49-64, 1971.

2. "Acoustic Characteristics of Rigid Fibrous Absorbents and Granular Materials", by K. Attenborough, J. Acoust. Soc. Am. Vol. 73 (3), pp. 785-799, 1983.

3. "Acoustic Behavior of a Fibrous Bulk Material", by A. S. Hersh and B. Walker, AIAA 5th Aeroacoustics Conference, 79-0599, 1979.

4. "Acoustic Impedance of Porous Materials", by L. L. Beranek, J. Acoust. Soc. Am. Vol. 13, pp. 248-260, 1942.

5. "Acoustic Characterization of Porous Ceramic Tiles", by U. S. Shrirahatti and M. L. Munjal, Noise Control Engineering Journal, Vol. 28 (1), pp. 26-32, 1987.

6. "Perforated Facing and Sound Absorption", by U. Ingard, J. Acoust. Soc. Am. Vol. 26 (2), pp. 151-154, 1954.

7. "Handbook of Mathematical Functions With Formulas, Graphs, and Mathematical Tables", Edited by M. Abramowitz and I. A. Stegun, National Bureau of Standards, Applied Mathematics Series – 55, 1964.

8. ASTM Measurement Standard No. E1050-90, "Standard Test Method for Impedance and Absorption of Acoustical Materials Using a Tube, Two Microphones, and a Digital Frequency Analysis System", 1990.

9. Rohr Report, RHR 89-191, "Calibration System Used in the Engineering Test Laboratories", March, 1989.

FIGURE 1.3-1 LIGHTWEIGHT CERAMICS FOR AEROACOUSTICS APPLICATIONS PROGRAM SCHEDULE

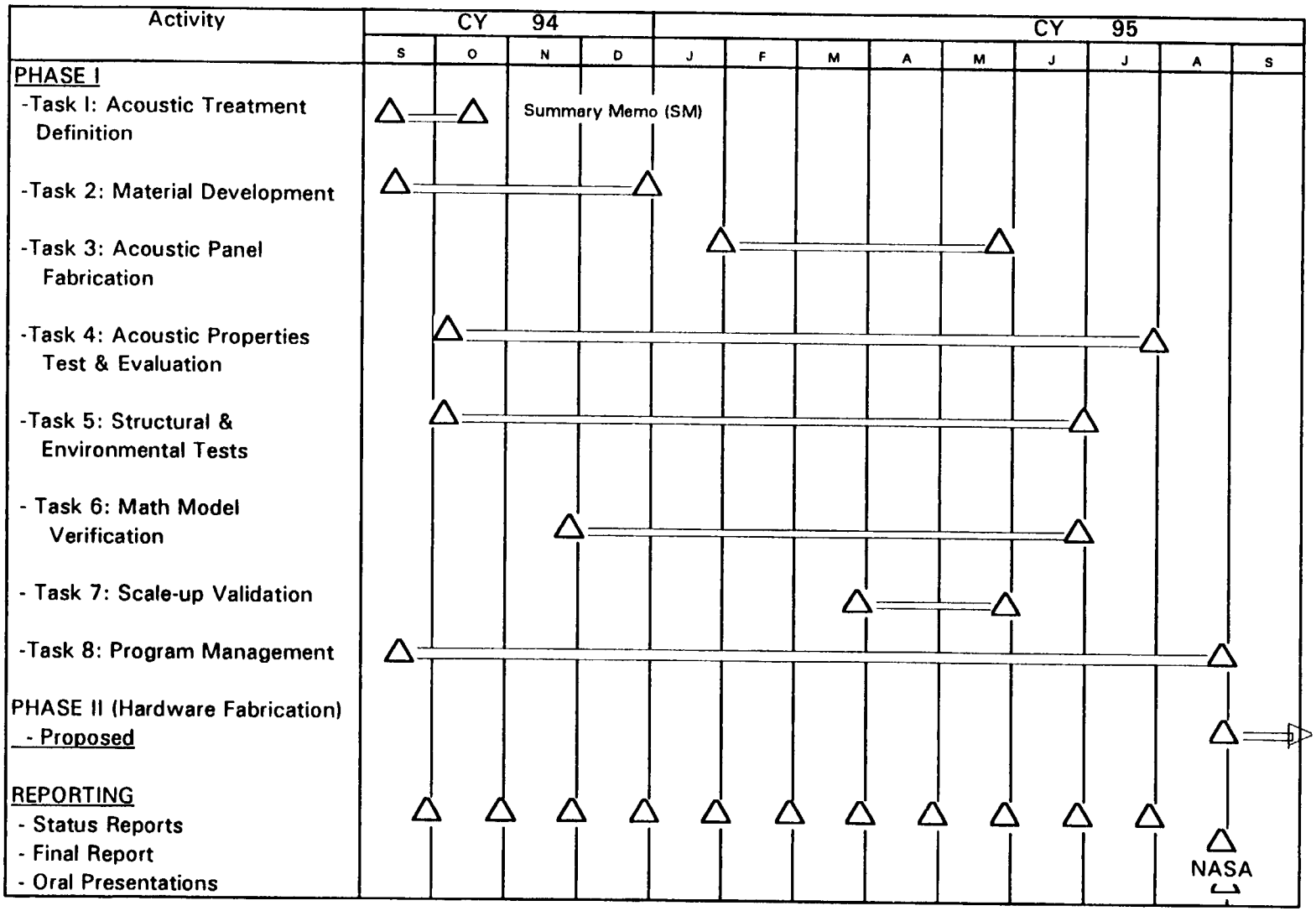

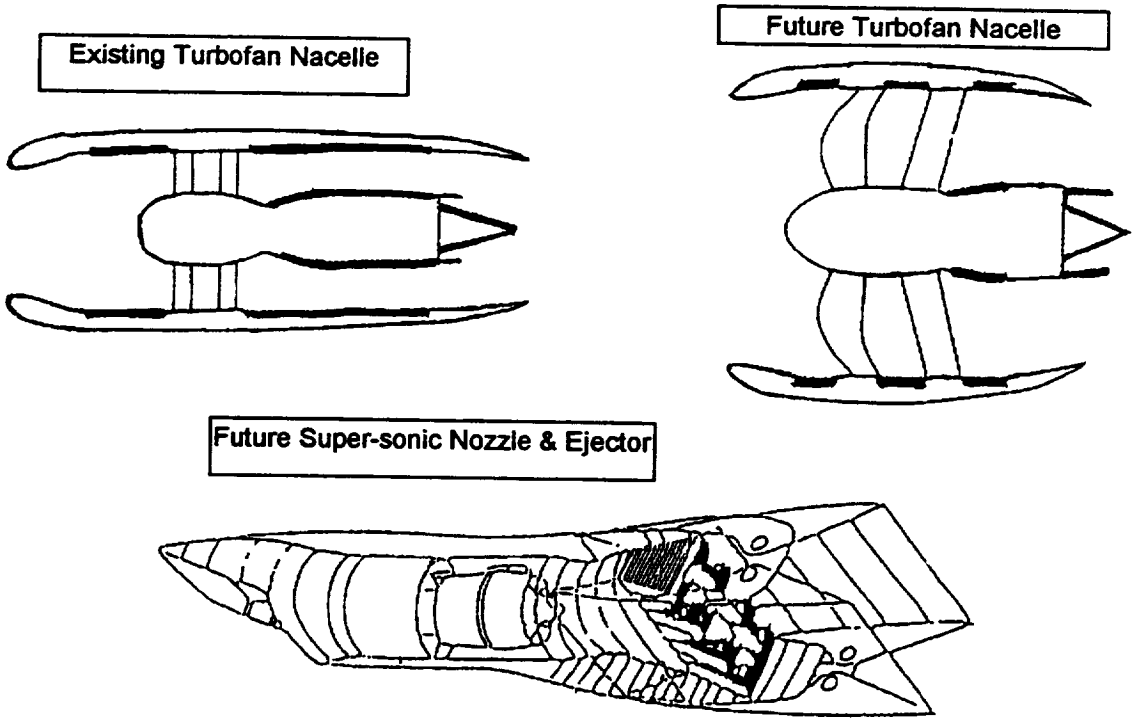

Figure 2-1 Potential Sound Suppression Systems that could Incorporate Ceramic Bulk Absorber Material/Structures

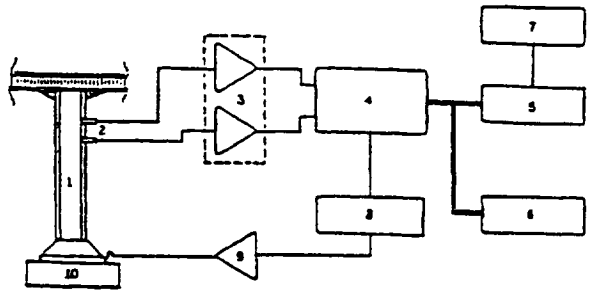

1. 3 cm impedance tube.
2. Kulite pressure transducer.
3. Microphone pre-amplifiers.
4. Dual channel signal analyzer.
5. Computer.
6. Graphics plotter.
7. Printer
8. Bandpass filter.
9. Power amplifier.
10. High power compression driver.

Figure 4.1-1 Schematic of the Rohr acoustic impedance system

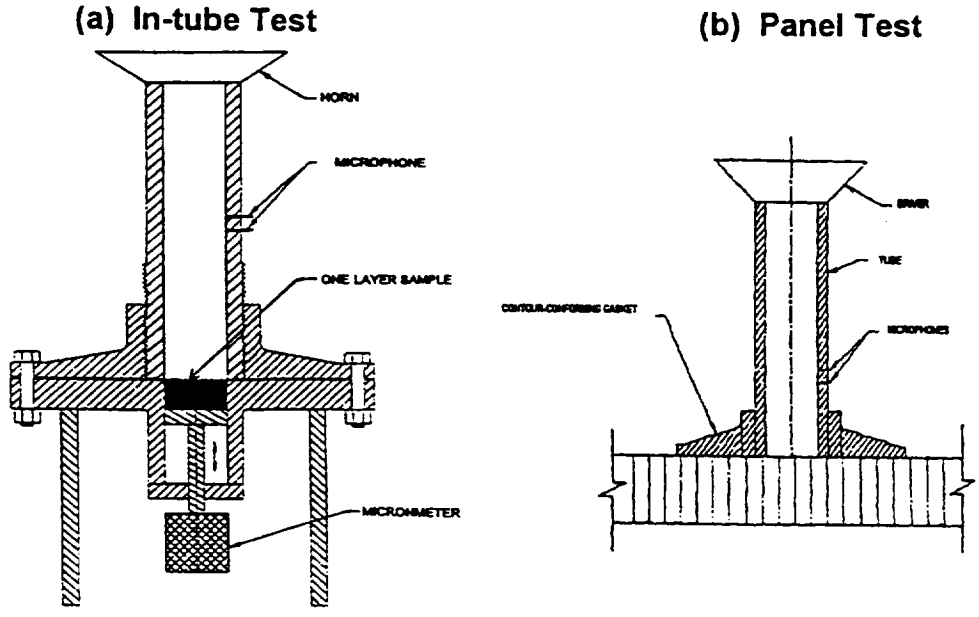

Figure 4.1-2 Rohr Impedance Test Apparatus

FIGURE 4.1-3 ACOUSTIC IMPEDANCE MEASUREMENT OF LMSC HTP-4 CERAMIC FOAM FOR VARIOUS THICKNESS

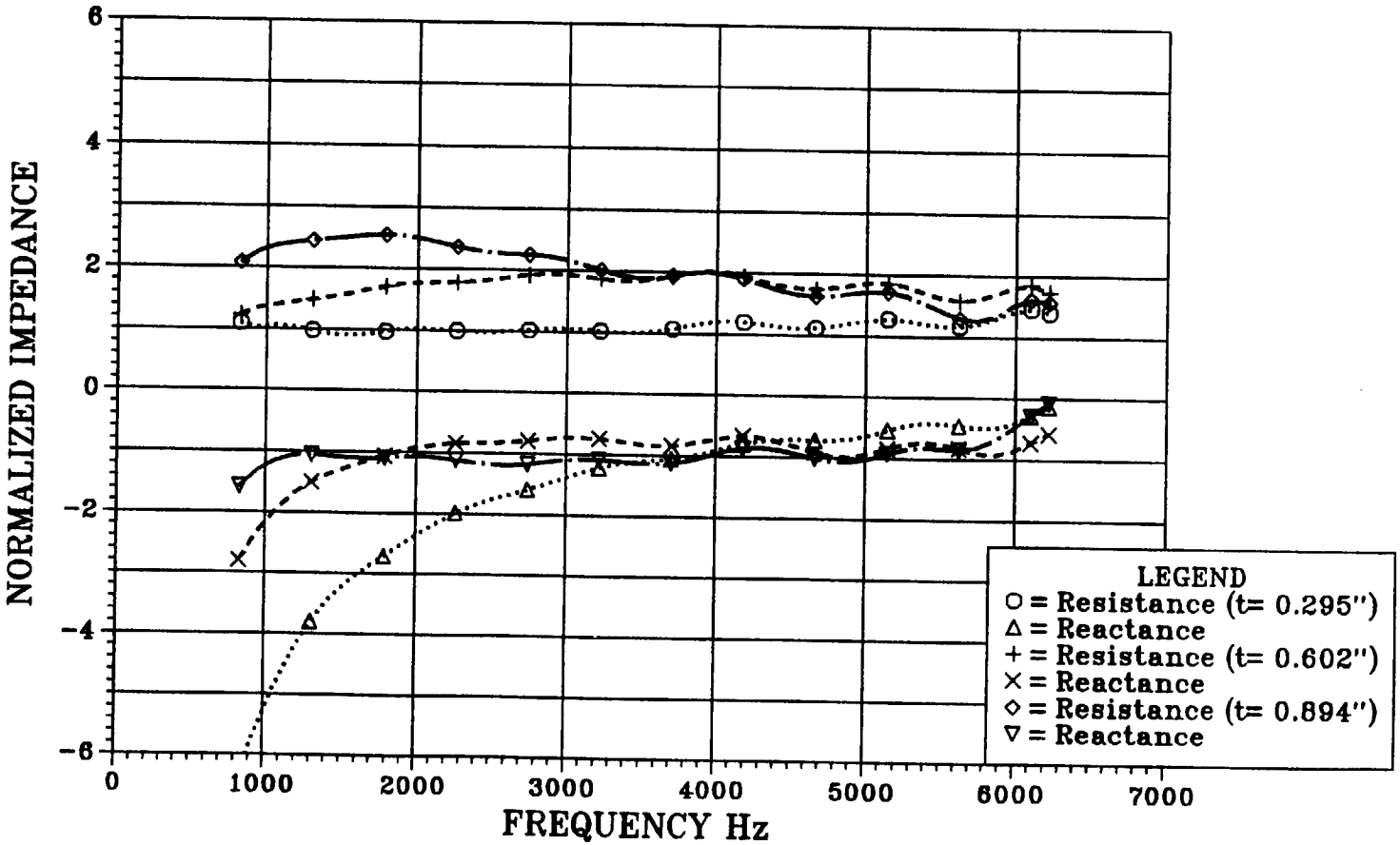

FIGURE 4.1–4 ACOUSTIC IMPEDANCE MEASUREMENT OF LMSC HTP–4
CERAMIC FOAM FOR VARIOUS THICKNESS

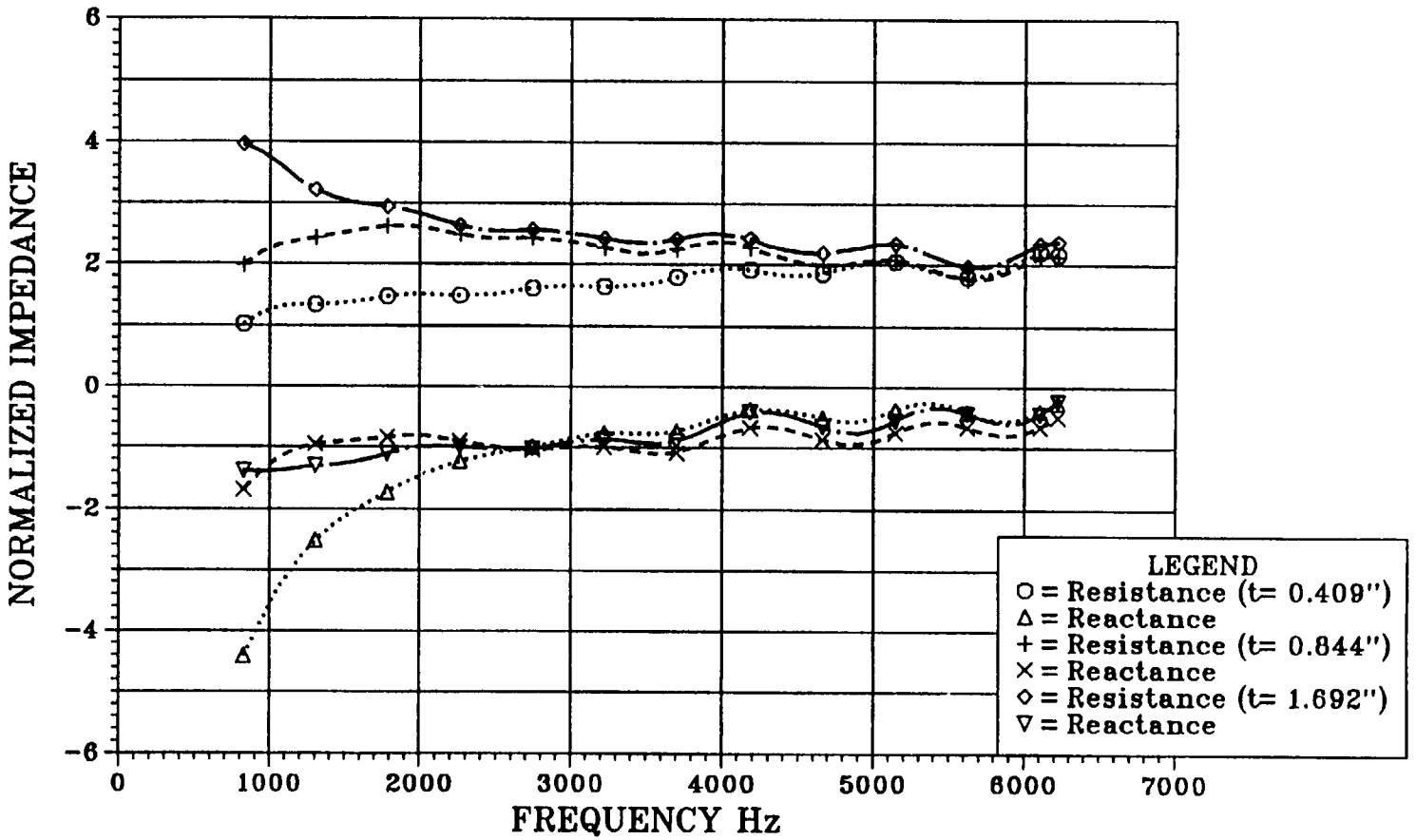

FIGURE 4.1-5 ACOUSTIC IMPEDANCE MEASUREMENT OF LMSC HTP-6
CERAMIC FOAM FOR VARIOUS THICKNESS

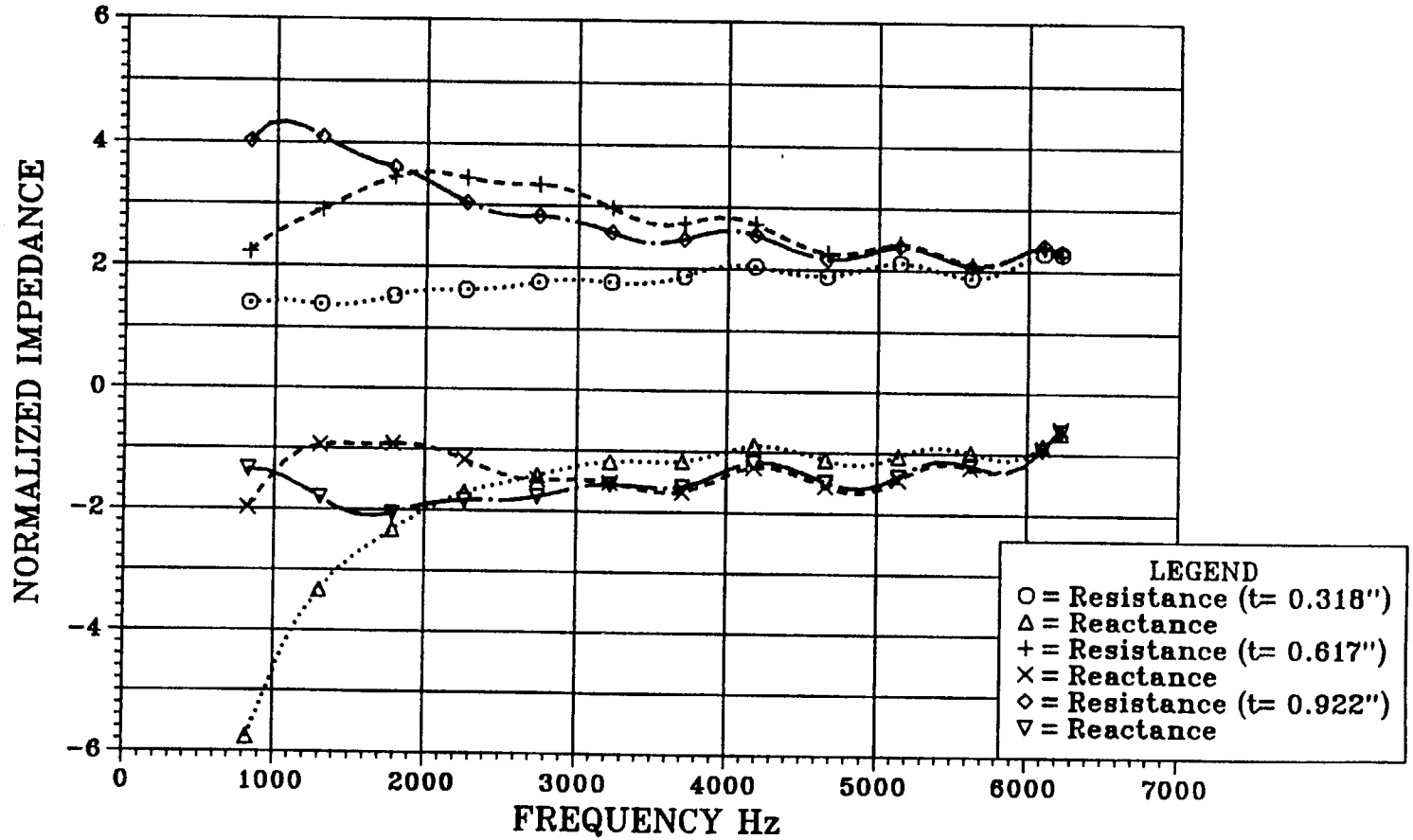

FIGURE 4.1-6 ACOUSTIC IMPEDANCE MEASUREMENT OF LMSC HTP-6 CERAMIC FOAM FOR VARIOUS THICKNESS

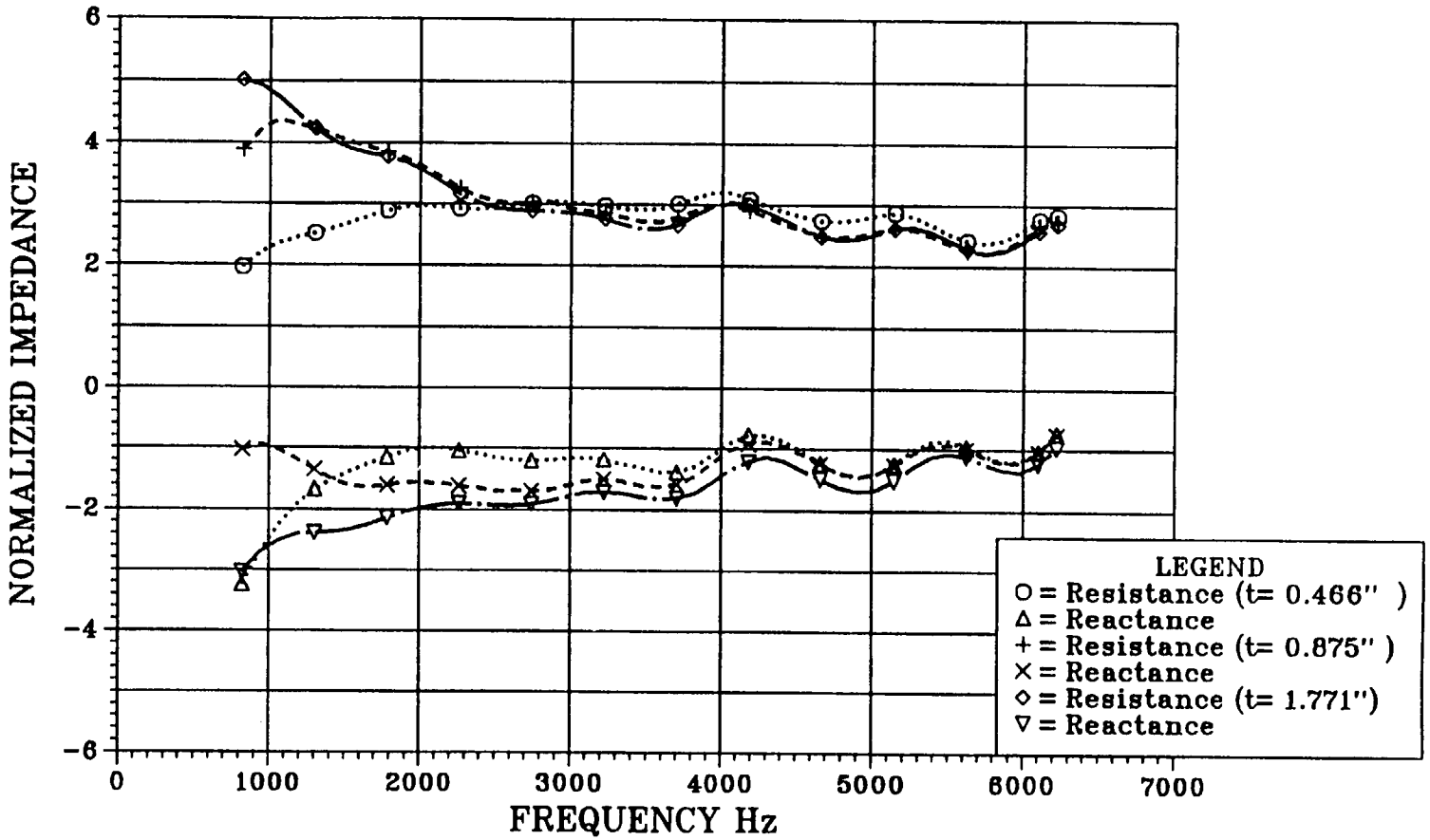

FIGURE 4.1-7 ACOUSTIC IMPEDANCE MEASUREMENT OF LMSC HTP-10 CERAMIC FOAM FOR VARIOUS THICKNESS

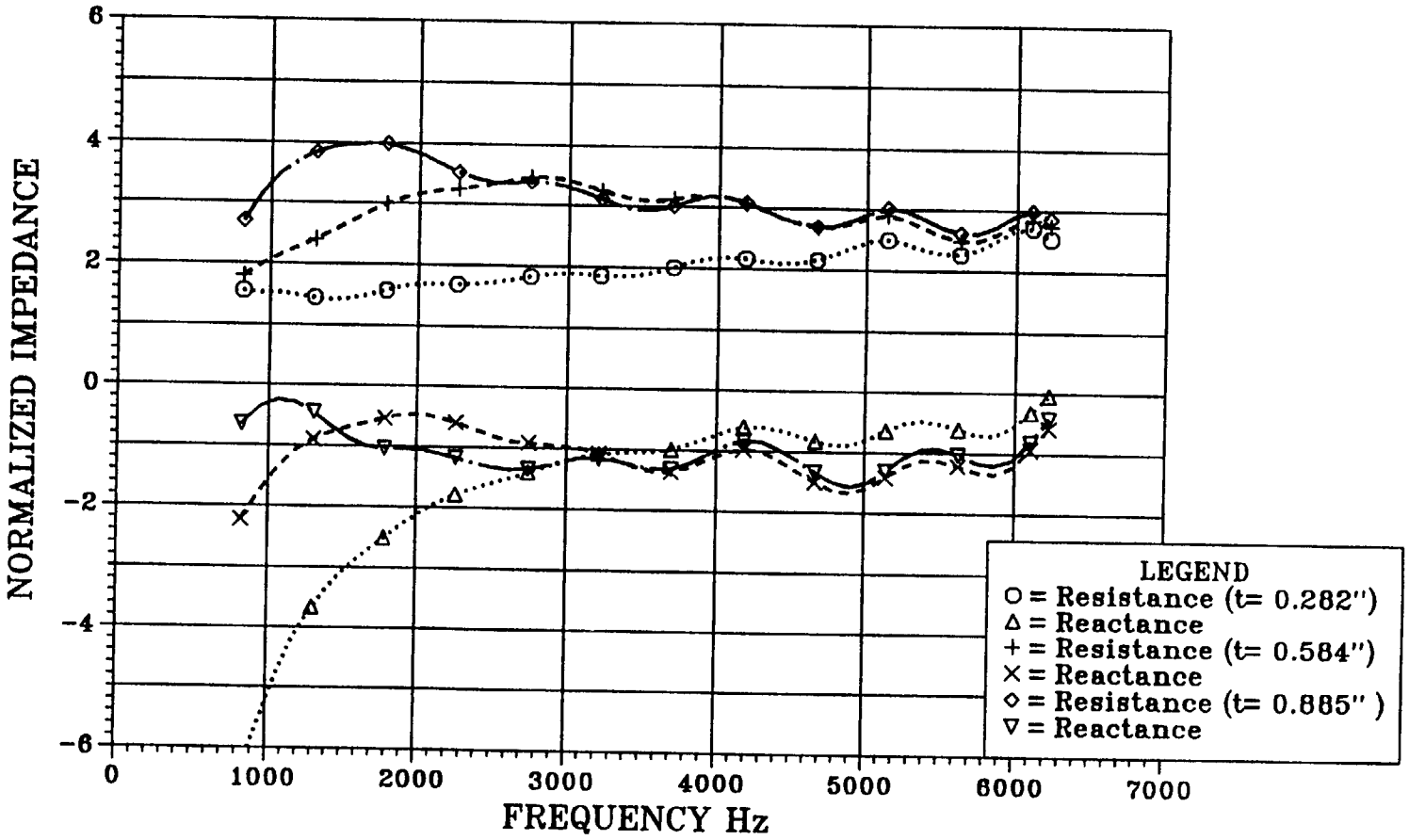

FIGURE 4.1–8 ACOUSTIC IMPEDANCE MEASUREMENT OF LMSC HTP–10 CERAMIC FOAM FOR VARIOUS THICKNESS

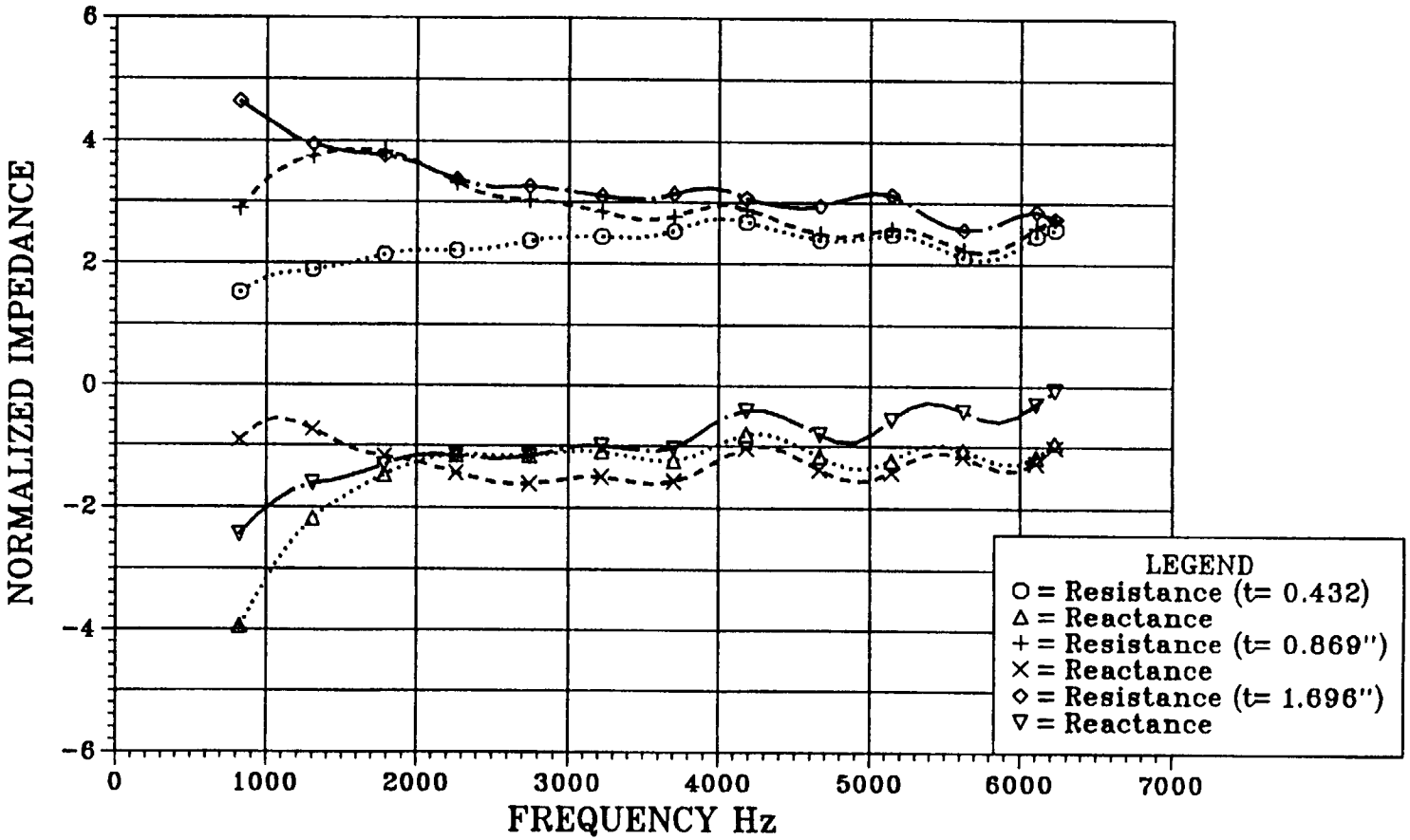

FIGURE 4.1–9 ACOUSTIC IMPEDANCE MEASUREMENT OF LMSC HTP–12
CERAMIC FOAM FOR VARIOUS THICKNESS

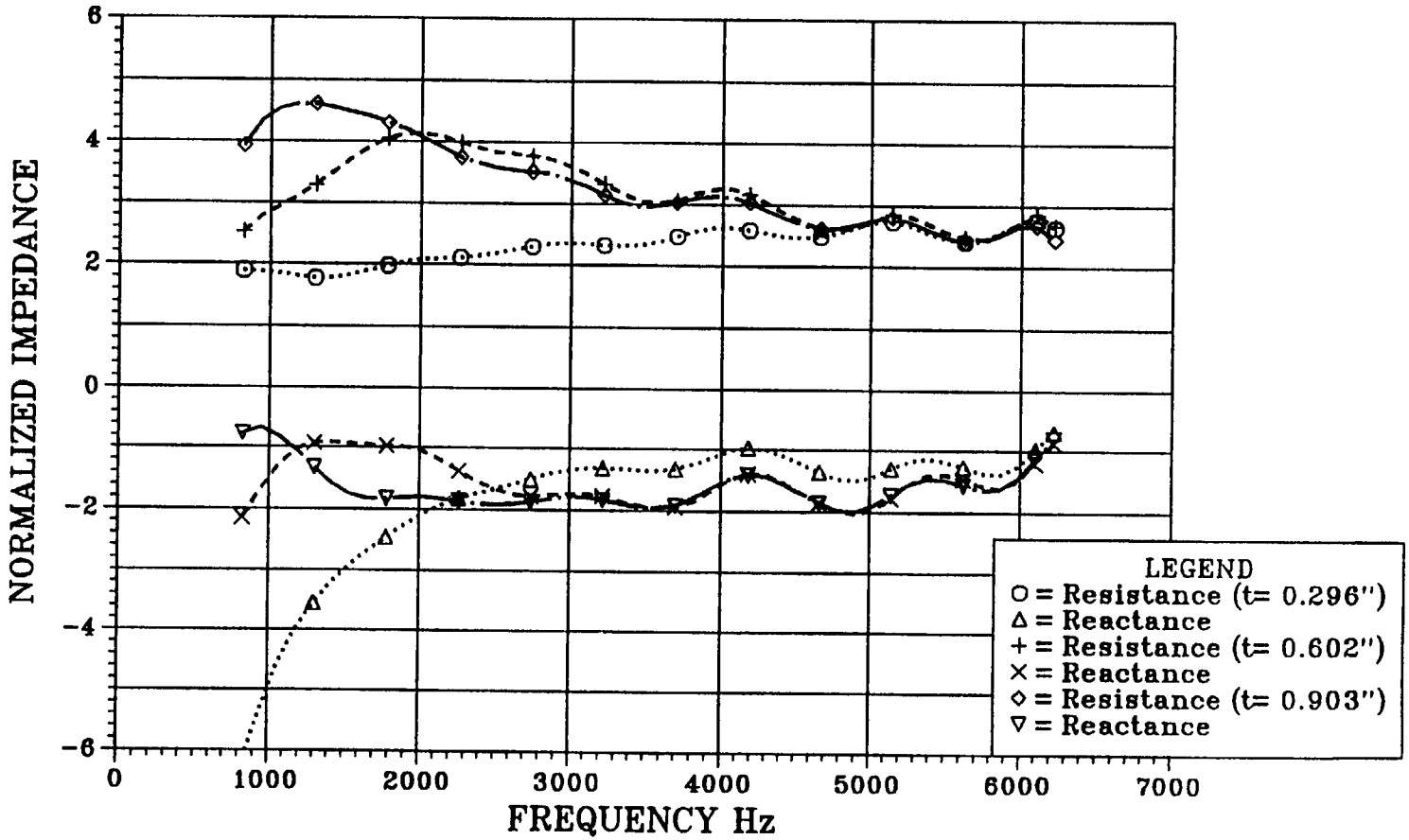

FIGURE 4.1-10 ACOUSTIC IMPEDANCE MEASUREMENT OF LMSC HTP-12
CERAMIC FOAM FOR VARIOUS THICKNESS

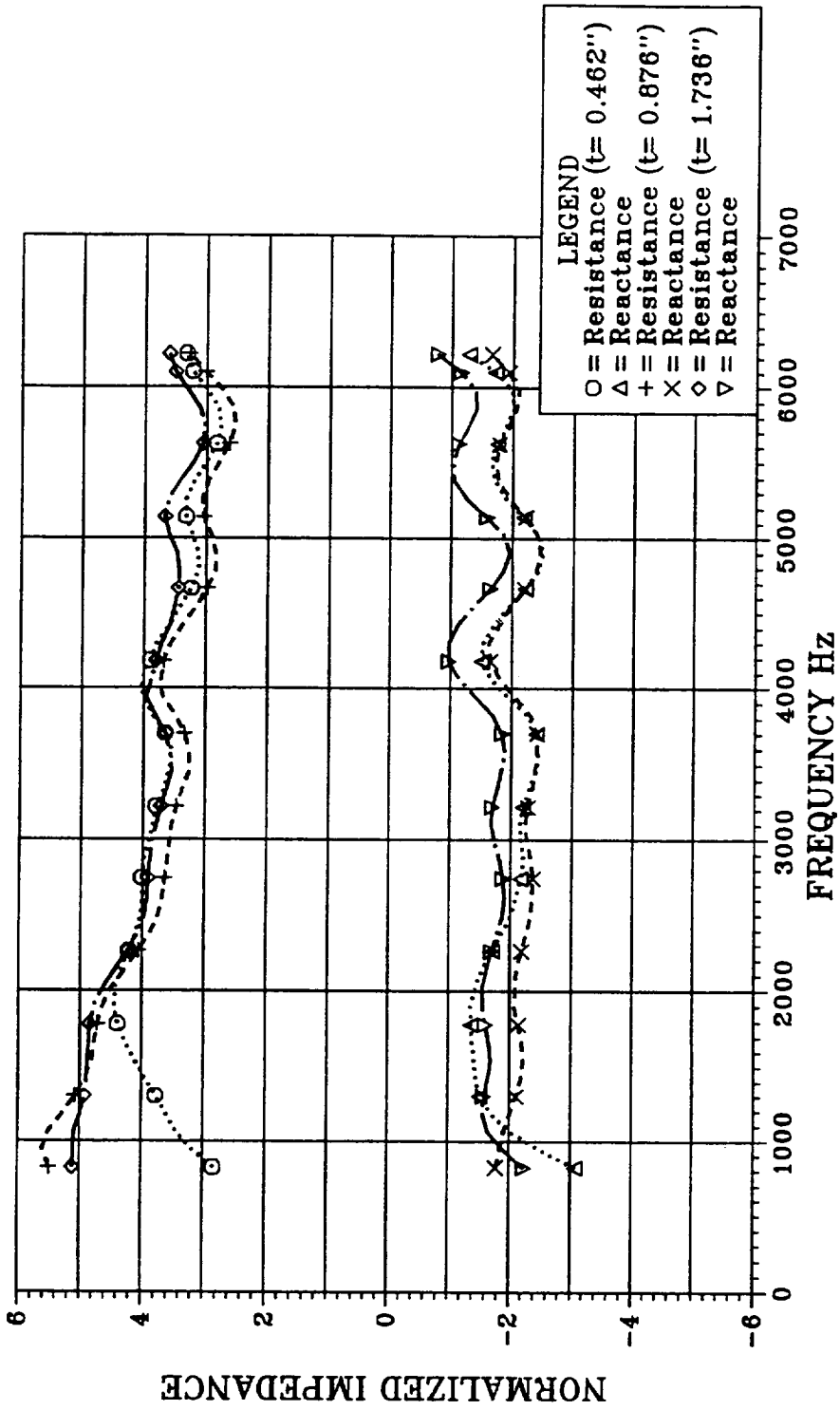

FIGURE 4.1–11 ACOUSTIC IMPEDANCE MEASUREMENT OF LMSC HTP–16
CERAMIC FOAM FOR VARIOUS THICKNESS

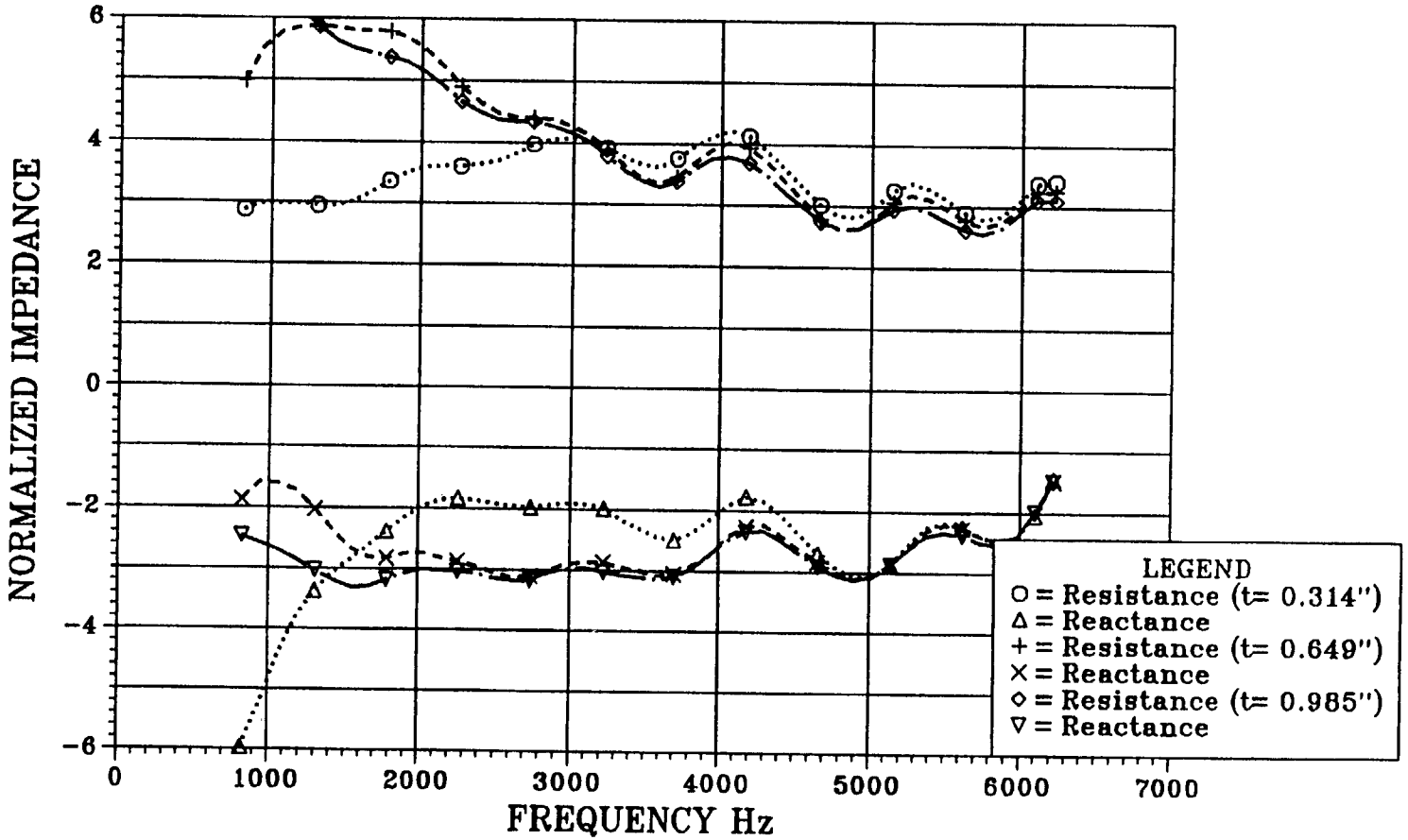

FIGURE 4.1–12 ACOUSTIC IMPEDANCE MEASUREMENT OF LMSC HTP–16 CERAMIC FOAM FOR VARIOUS THICKNESS

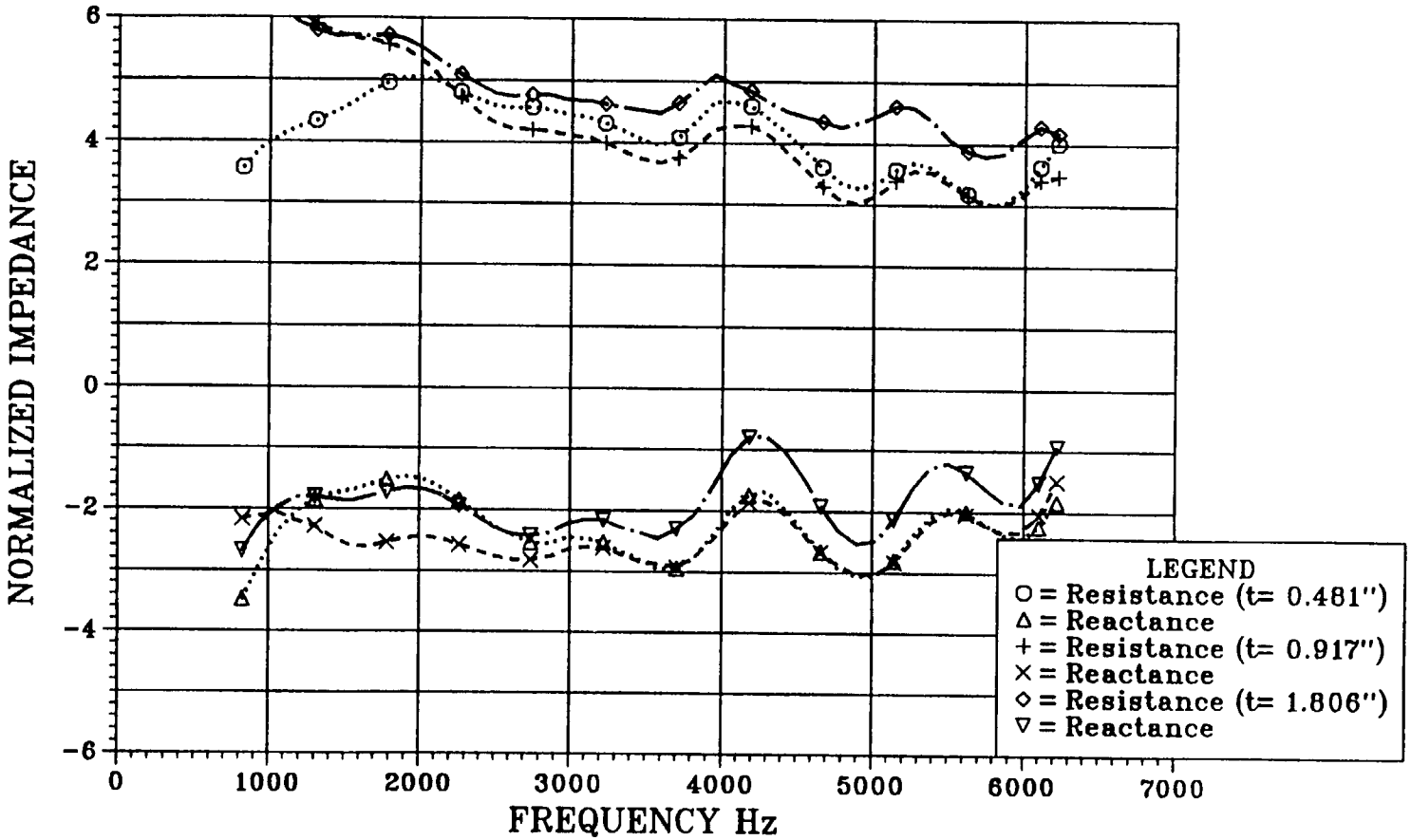

Figure 4.1-13 Average Acoustic Impedance of LMSC Material 14360B, 0.75" and 1.50" Thicknesses

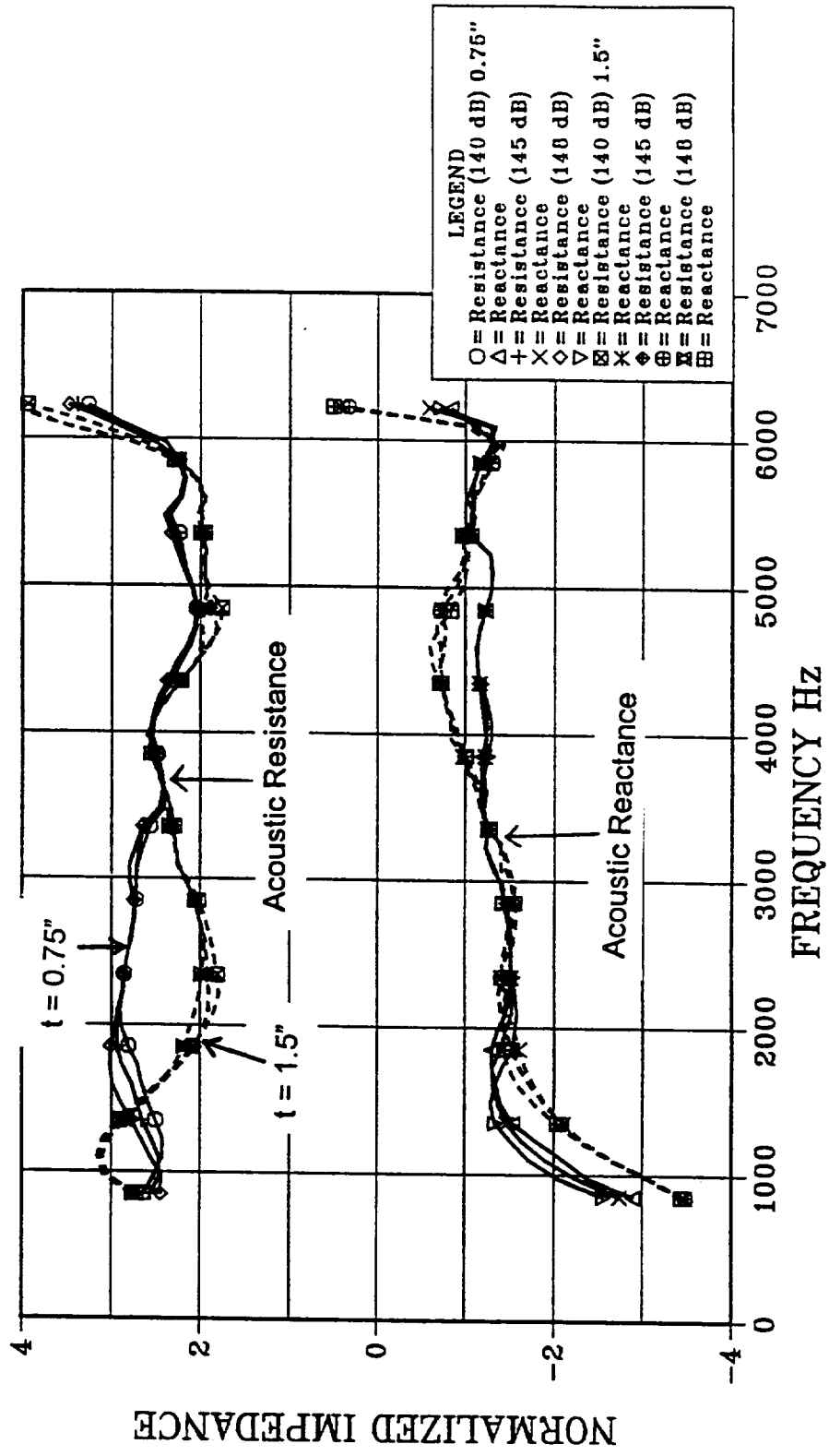

Figure 4.1-14 Average Acoustic Impedance of LMSC Material 14360D, 0.75" and 1.50" Thicknesses

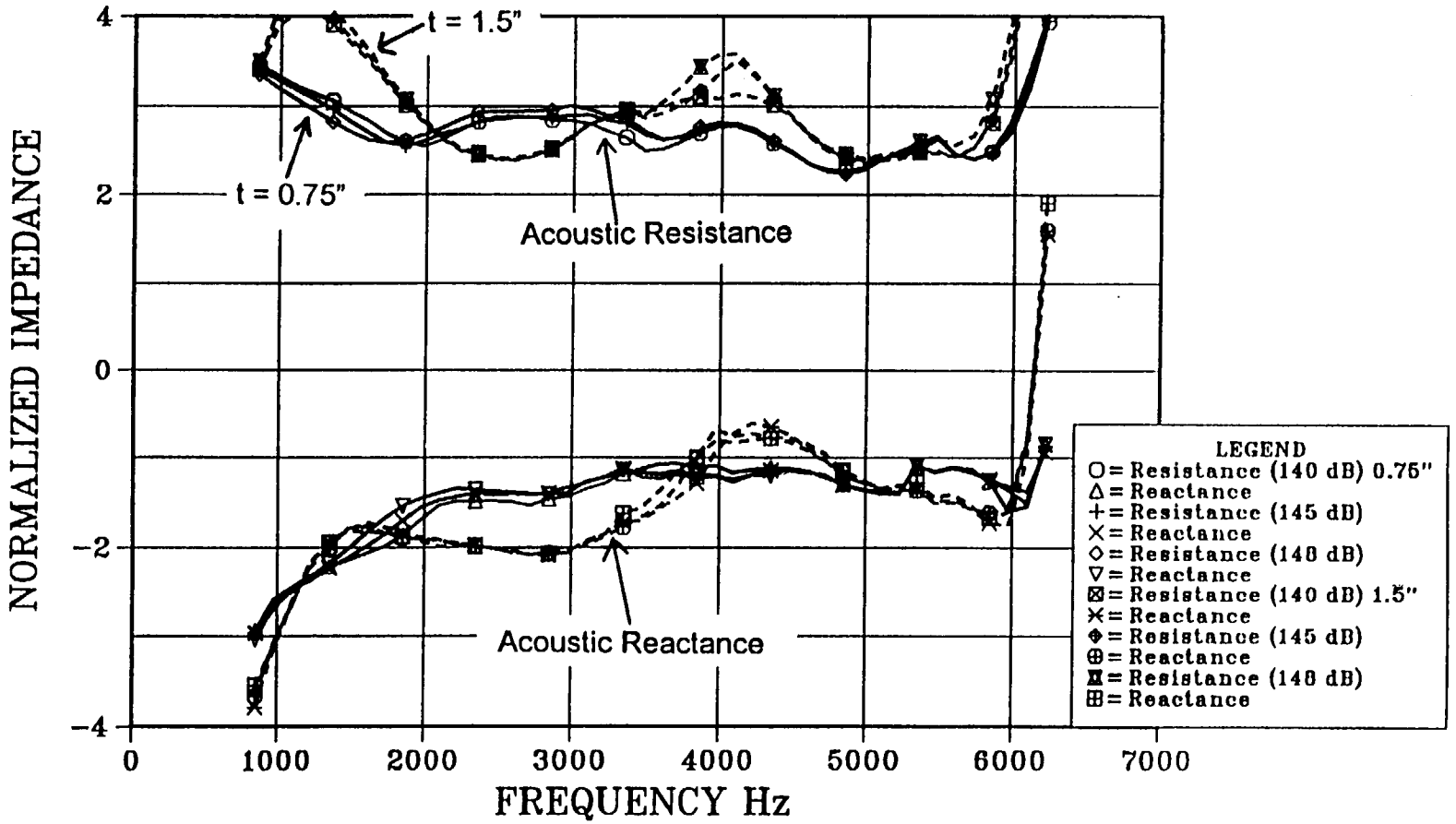

Figure 4.1-15 Average Acoustic Impedance of LMSC Material 14360F, 0.75" and 1.50" Thicknesses

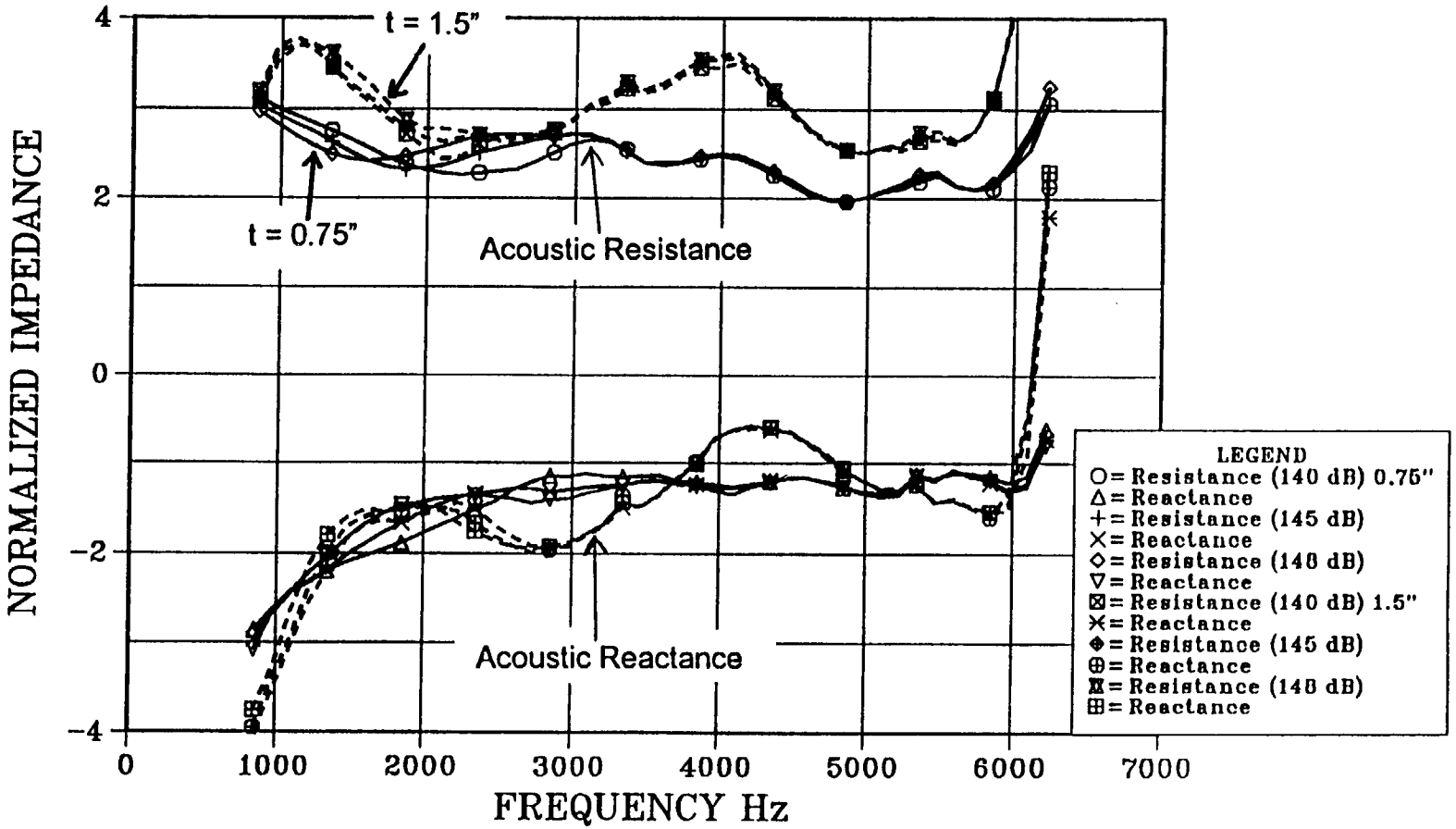

Figure 4.1-16 Average Acoustic Impedance of LMSC Material 14360G, 0.75" and 1.50" Thicknesses

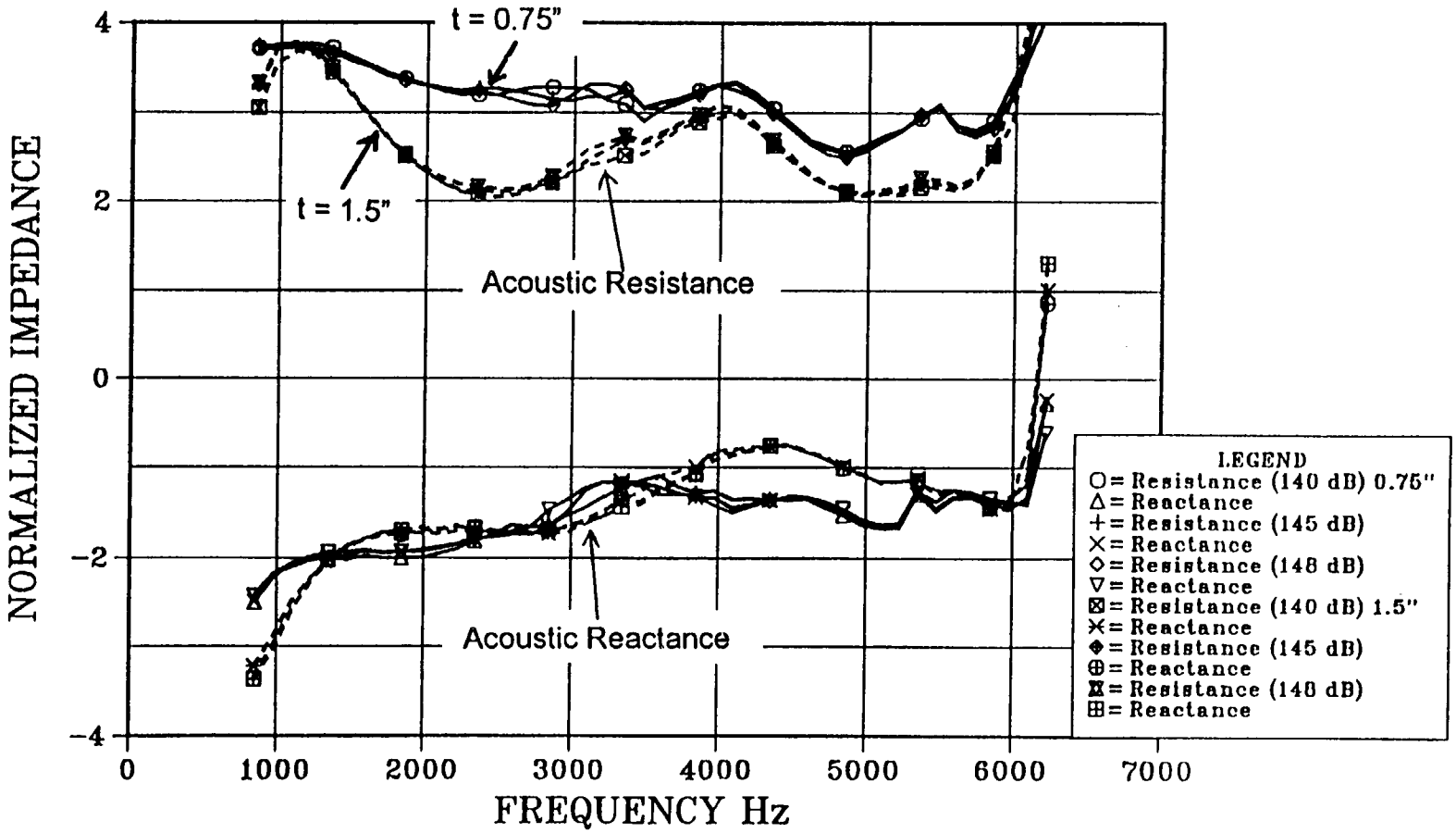

Figure 4.1-17 Average Acoustic Impedance of LMSC Material 14360J, 0.75" and 1.50" Thicknesses

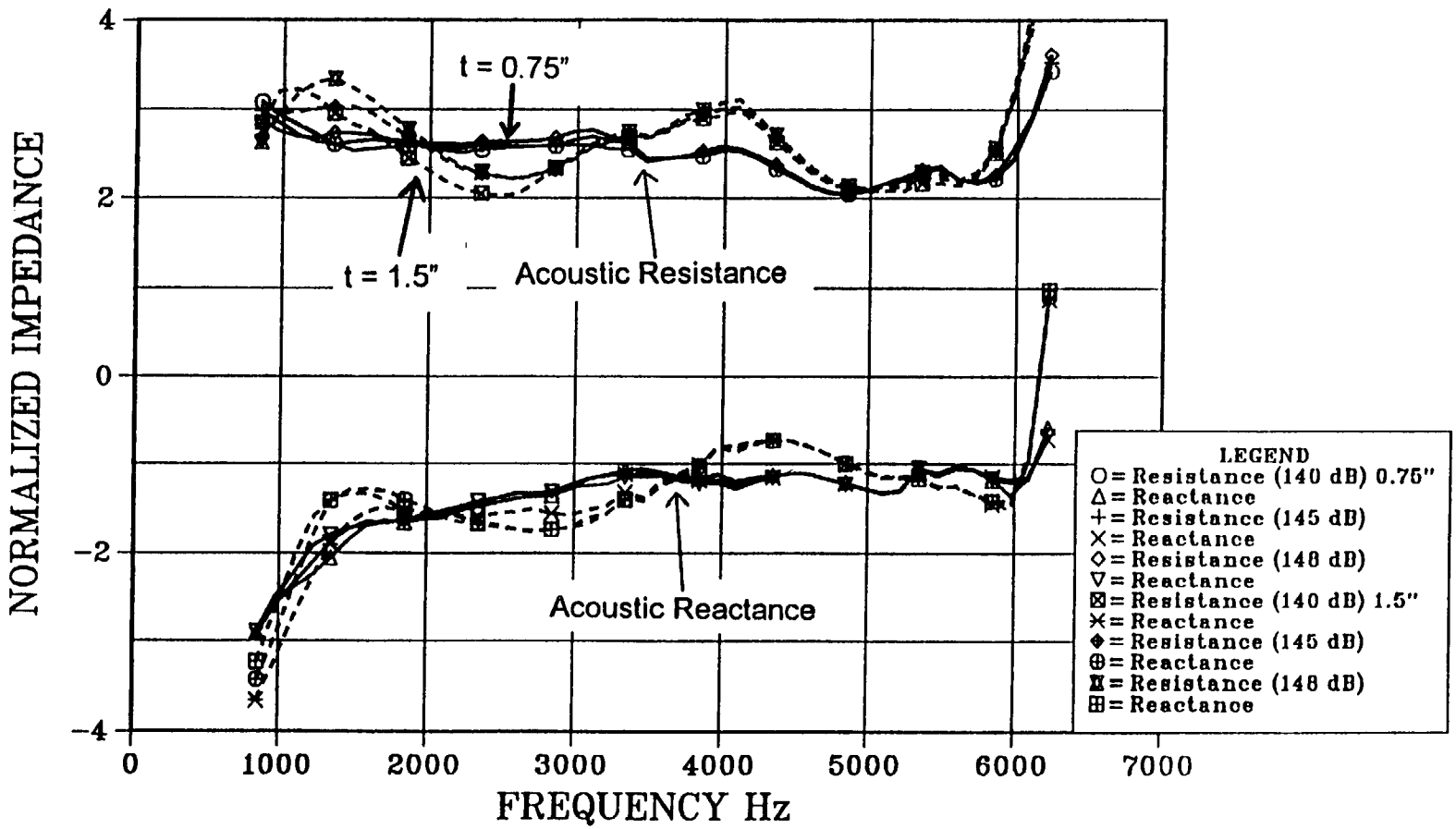

Figure 4.1-18 Average Acoustic Impedance of LMSC Material 11093T, 0.5", 1.0", 1.50" and 2.0" Thicknesses

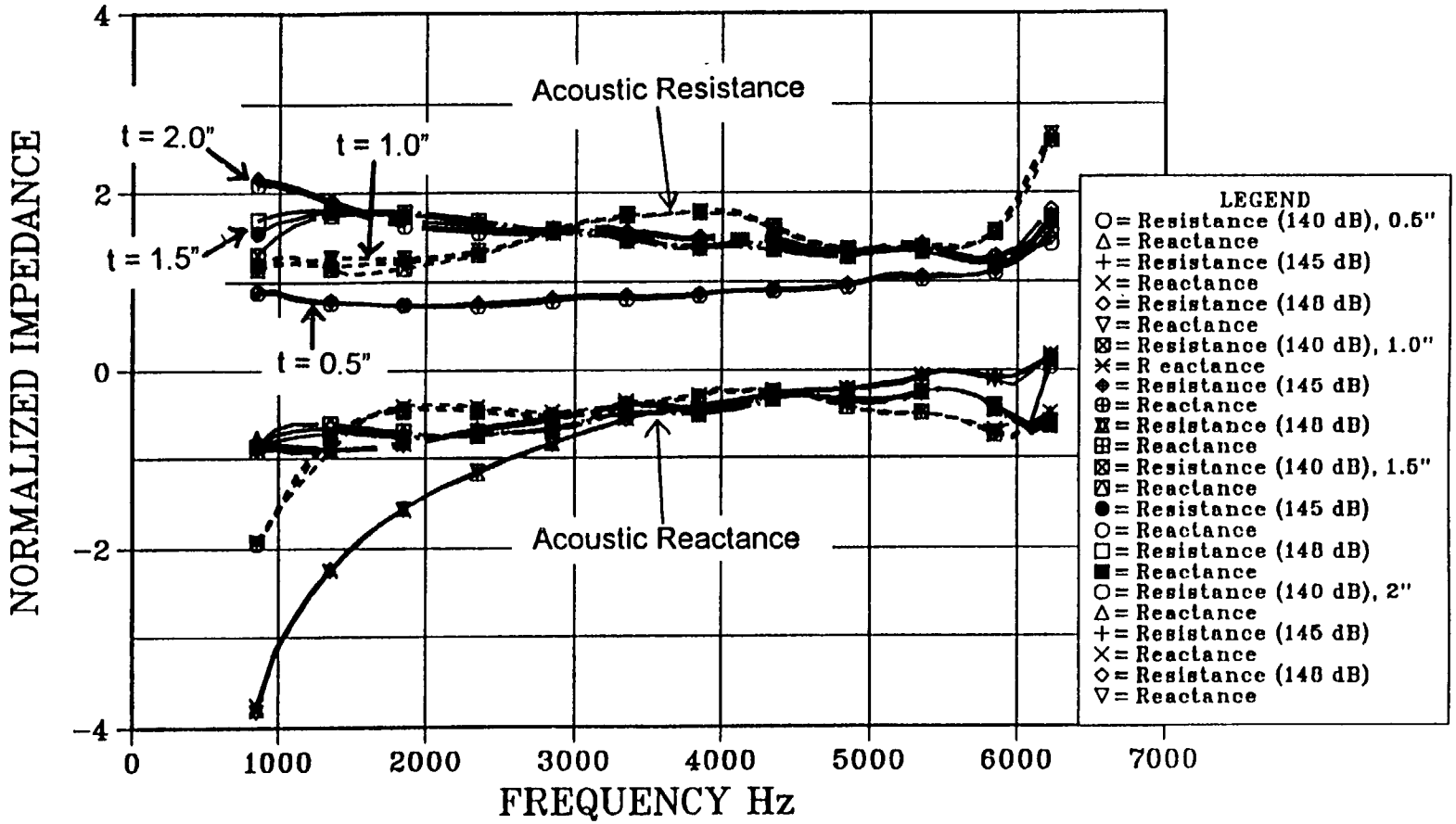

Figure 4.1-19 Average Acoustic Impedance of LMSC Material 11095T, 0.5", 1.0", 1.50" and 2.0" Thicknesses

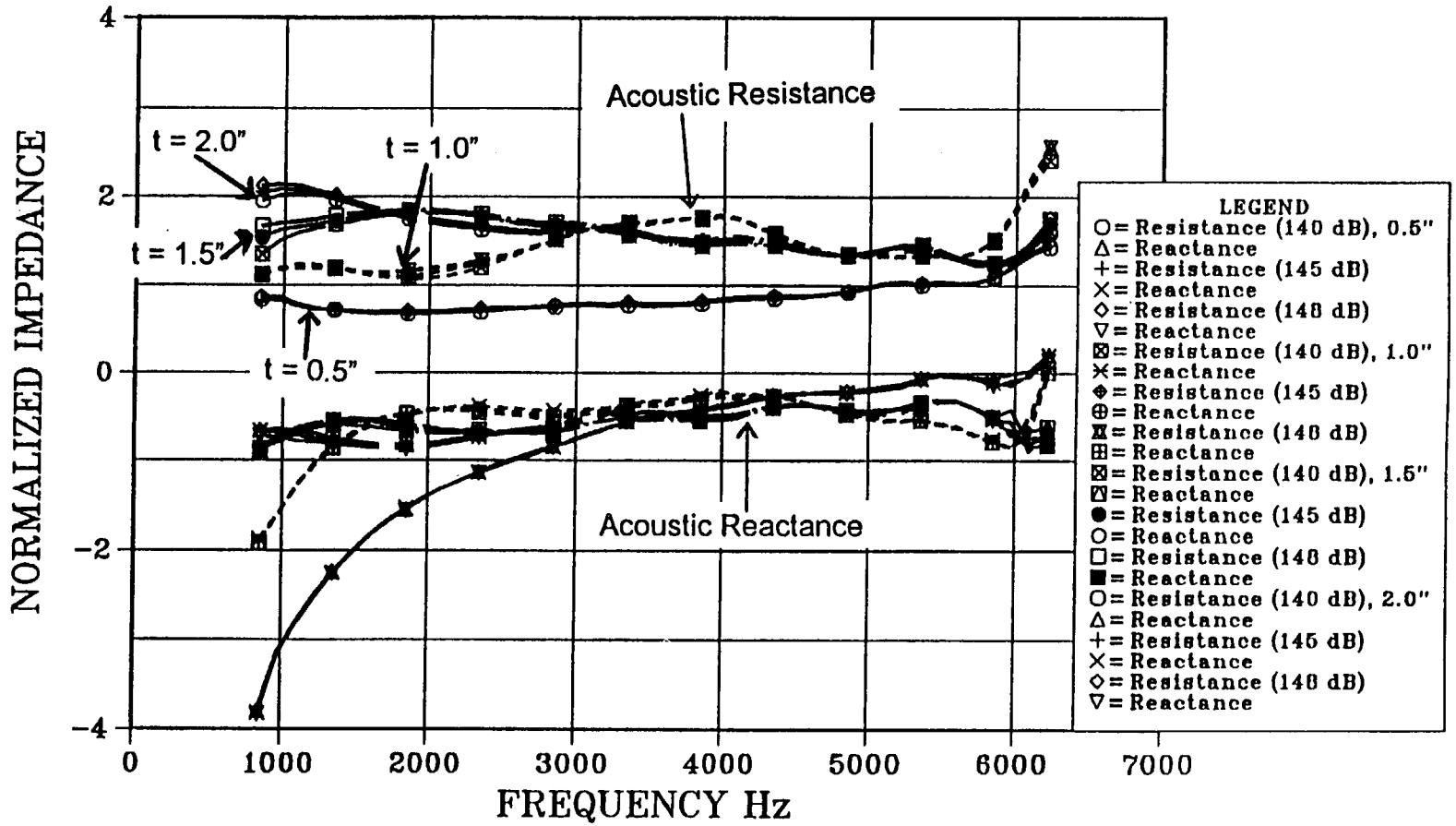

Figure 4.1-20 Average Acoustic Impedance of LMSC Material 11097T, 0.5", 1.0", 1.50" and 2.0" Thicknesses

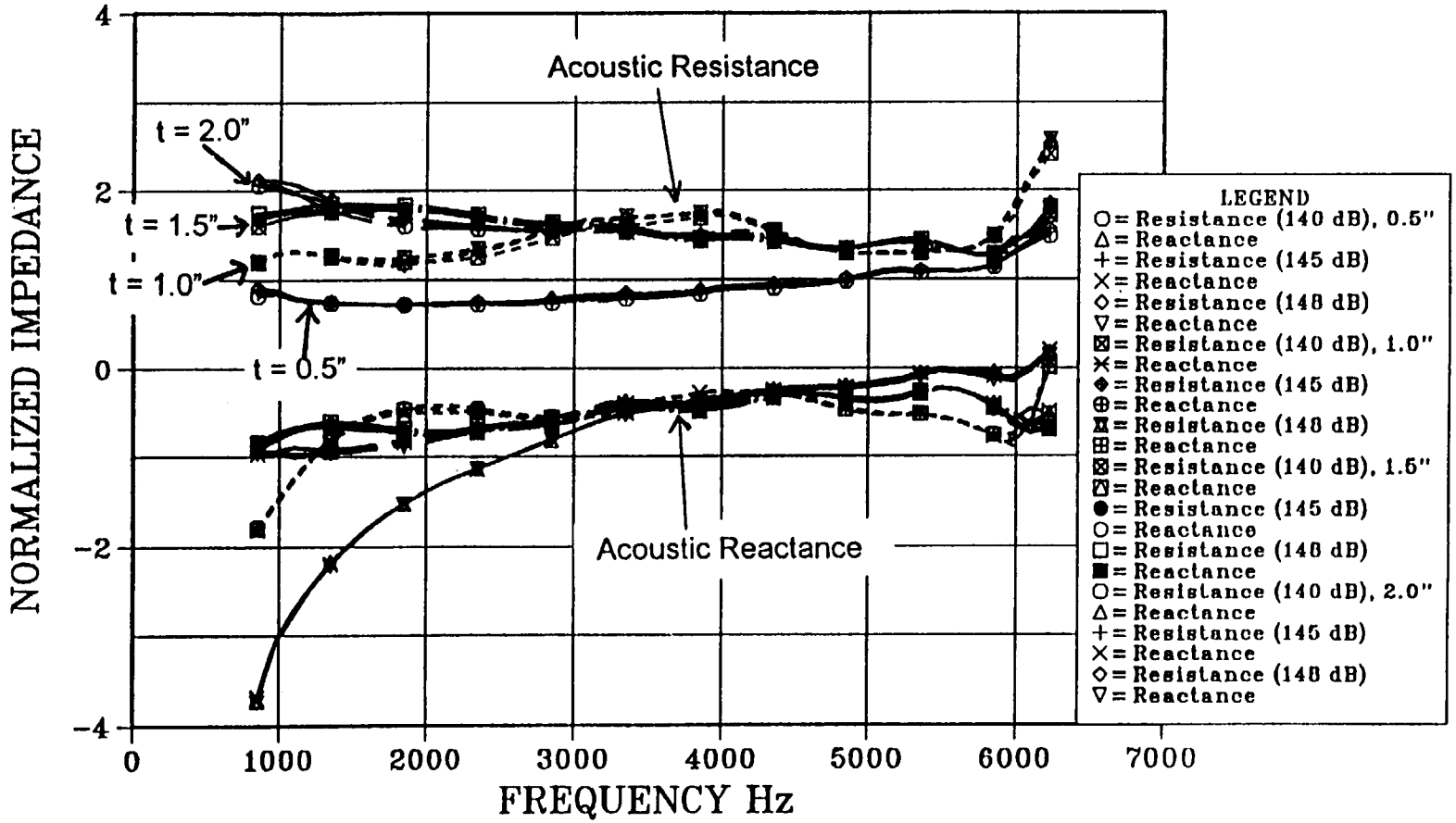

Figure 4.1-21 Average Acoustic Impedance of LMSC Material 11105T, 0.5", 1.0", 1.50" and 2.0" Thicknesses

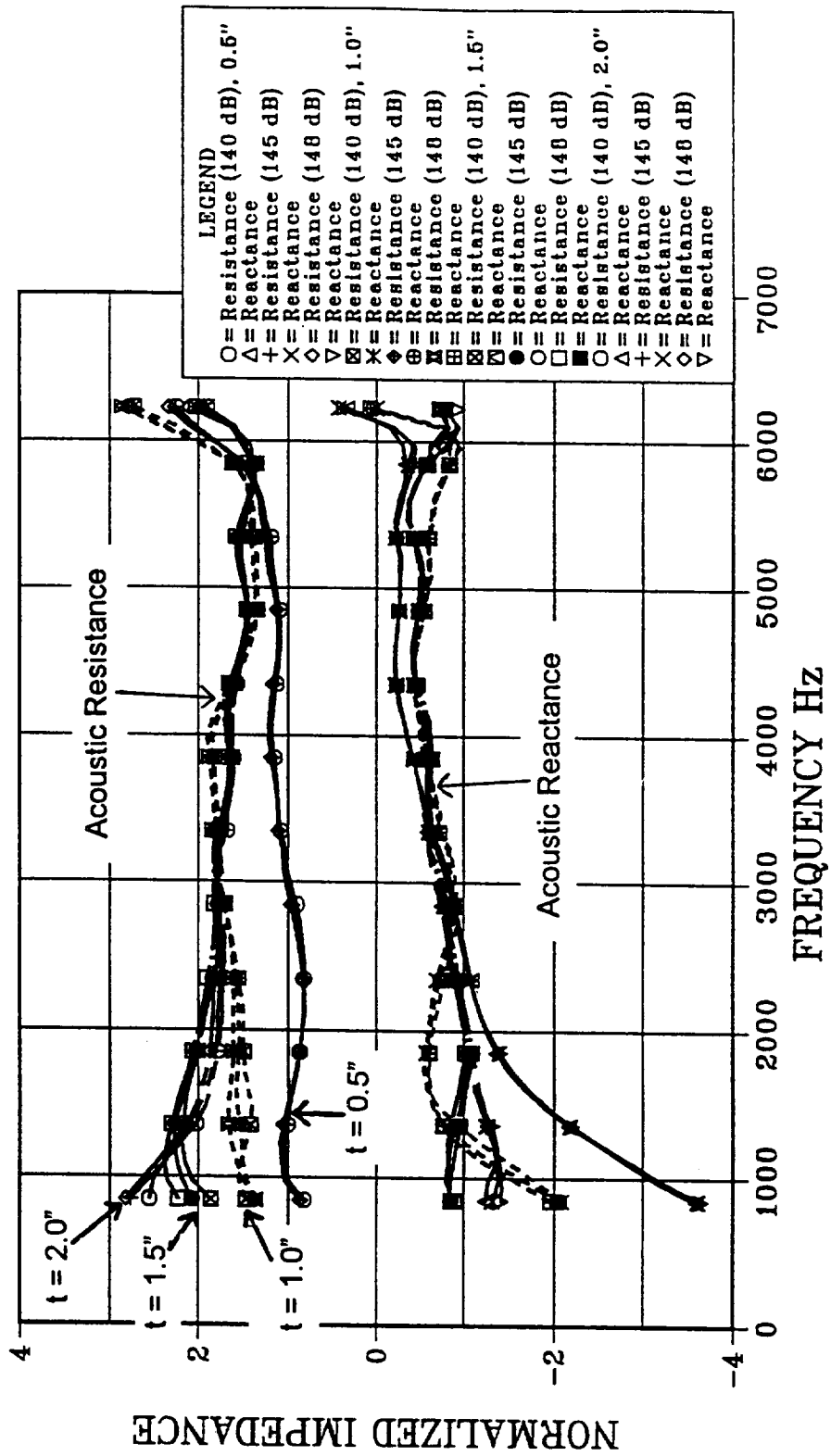

Figure 4.1-22 Average Acoustic Impedance of LMSC Material 11107T, 0.5", 1.0", 1.50" and 2.0" Thicknesses

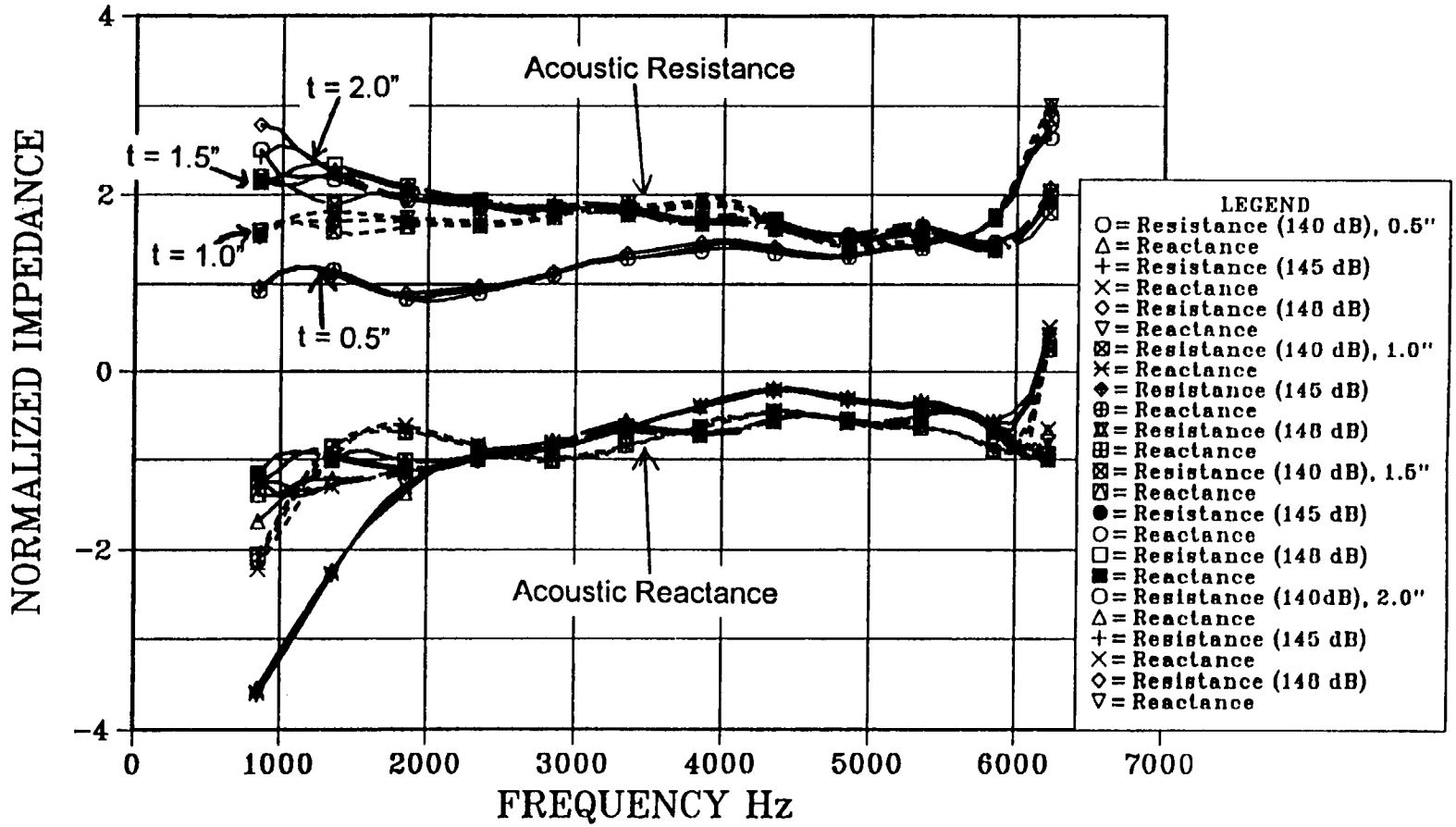

Figure 4.1-23 Average Acoustic Impedance of LMSC Material 13031T, 0.5", 1.0", 1.50" and 2.0" Thicknesses

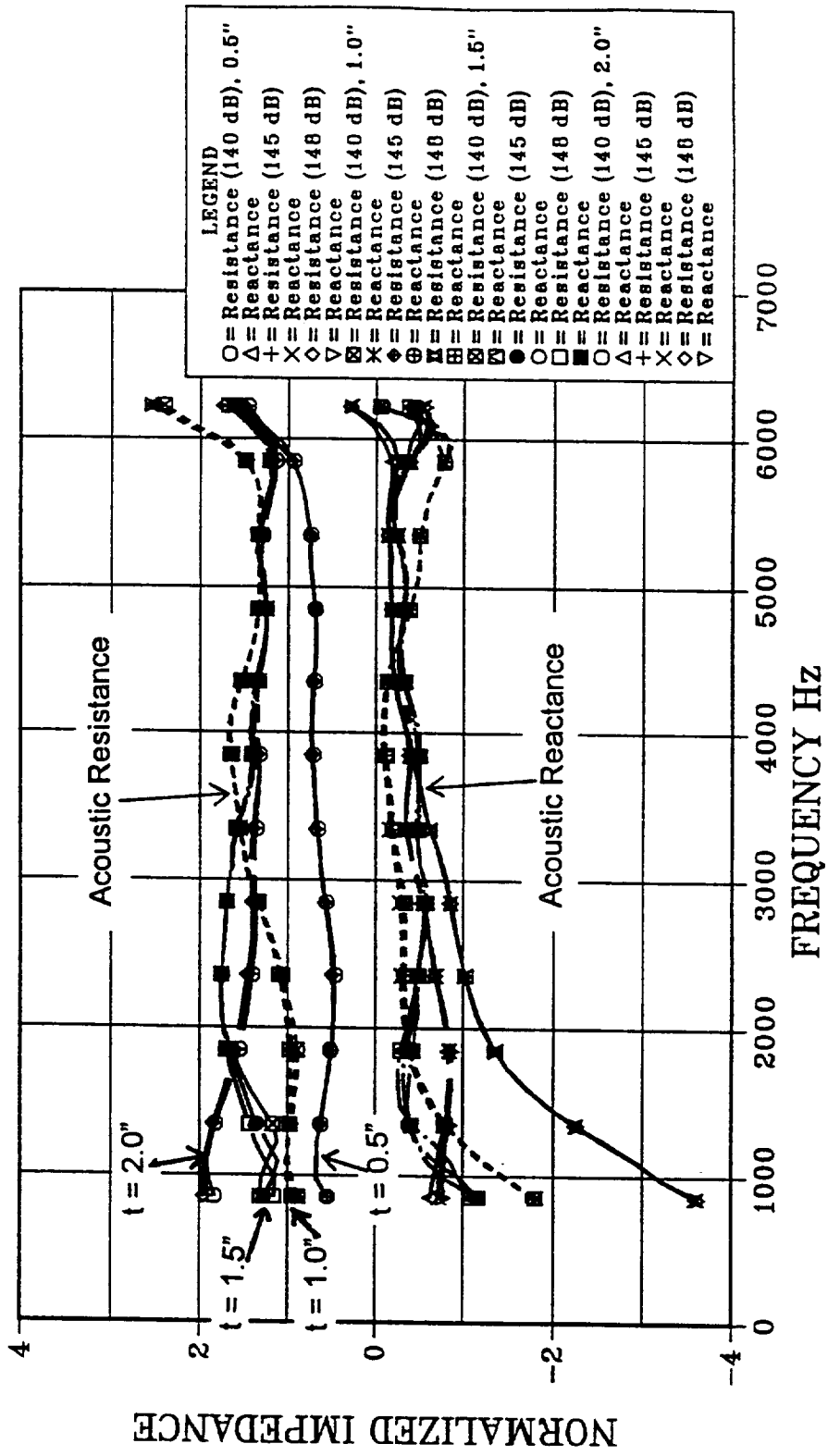

Figure 4.1-24 Average Acoustic Impedance of LMSC Material 1438, 0.55" and 1.10" Thicknesses at 145 dB

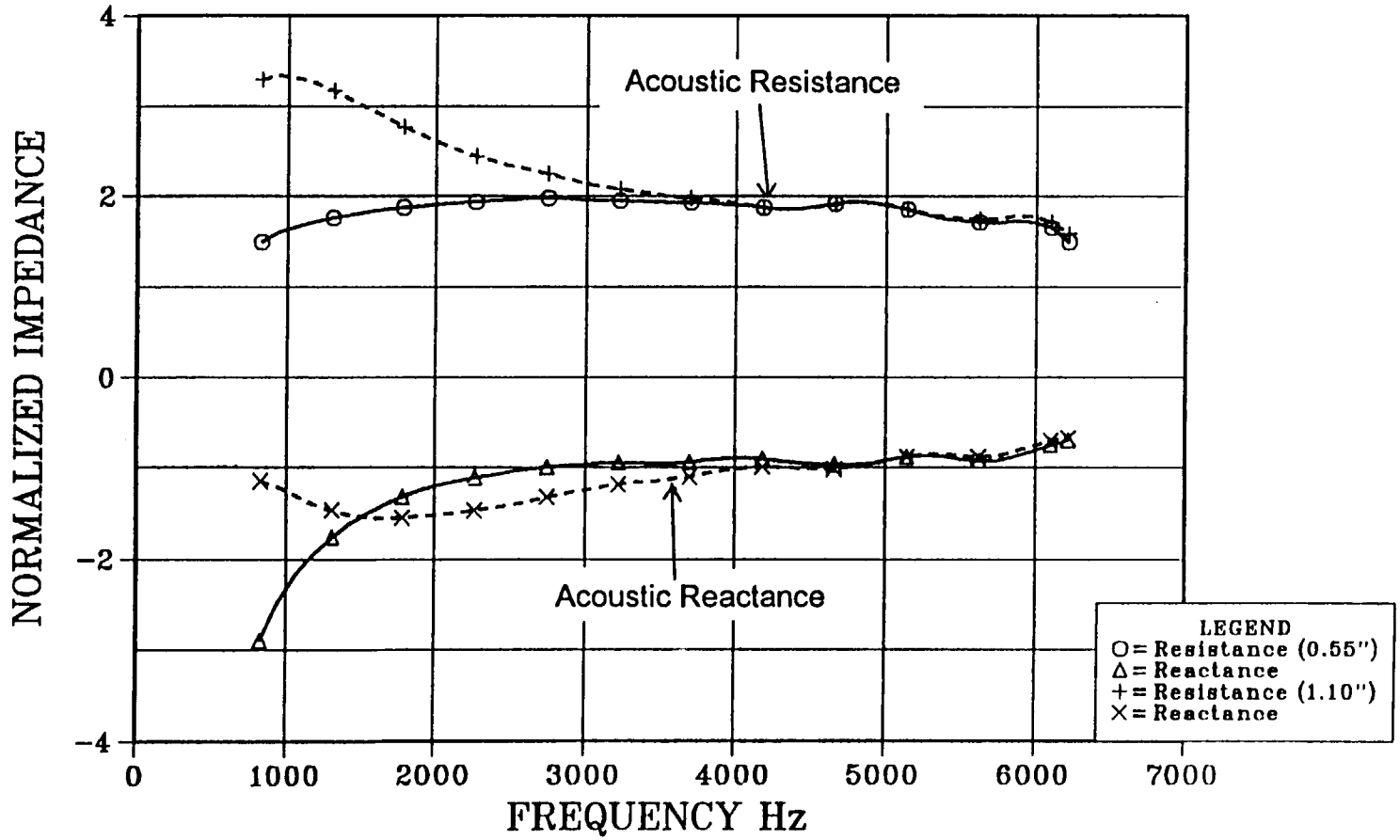

Figure 4.1-25 Average Acoustic Impedance of LMSC Material 1433A, 0.75" and 1.50" Thicknesses at 145 dB

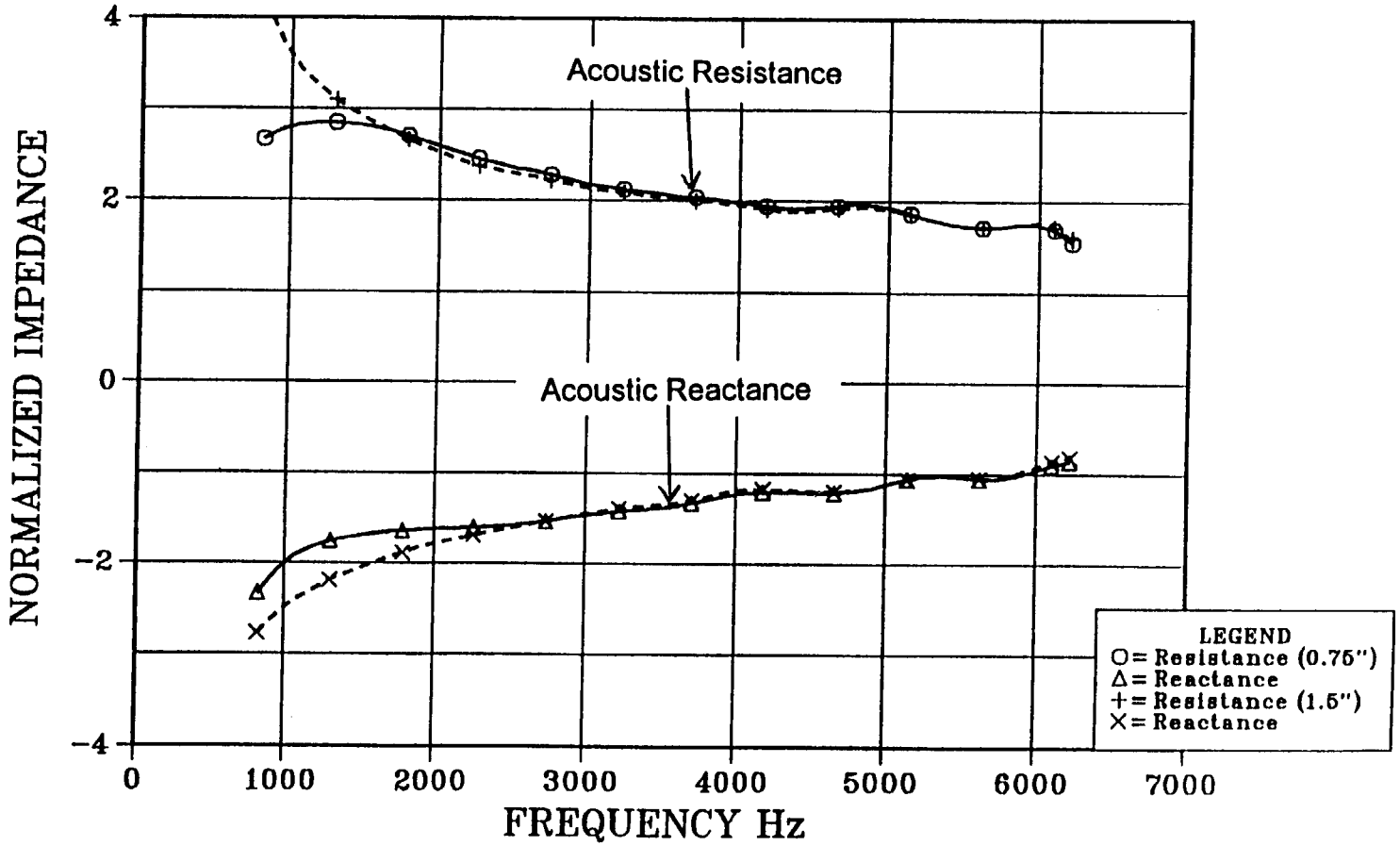

FIGURE 4.2-1 MEASURED ACOUSTIC IMPEDANCE OF LMSC HTP-1437
PANEL TEST AT 140 dB

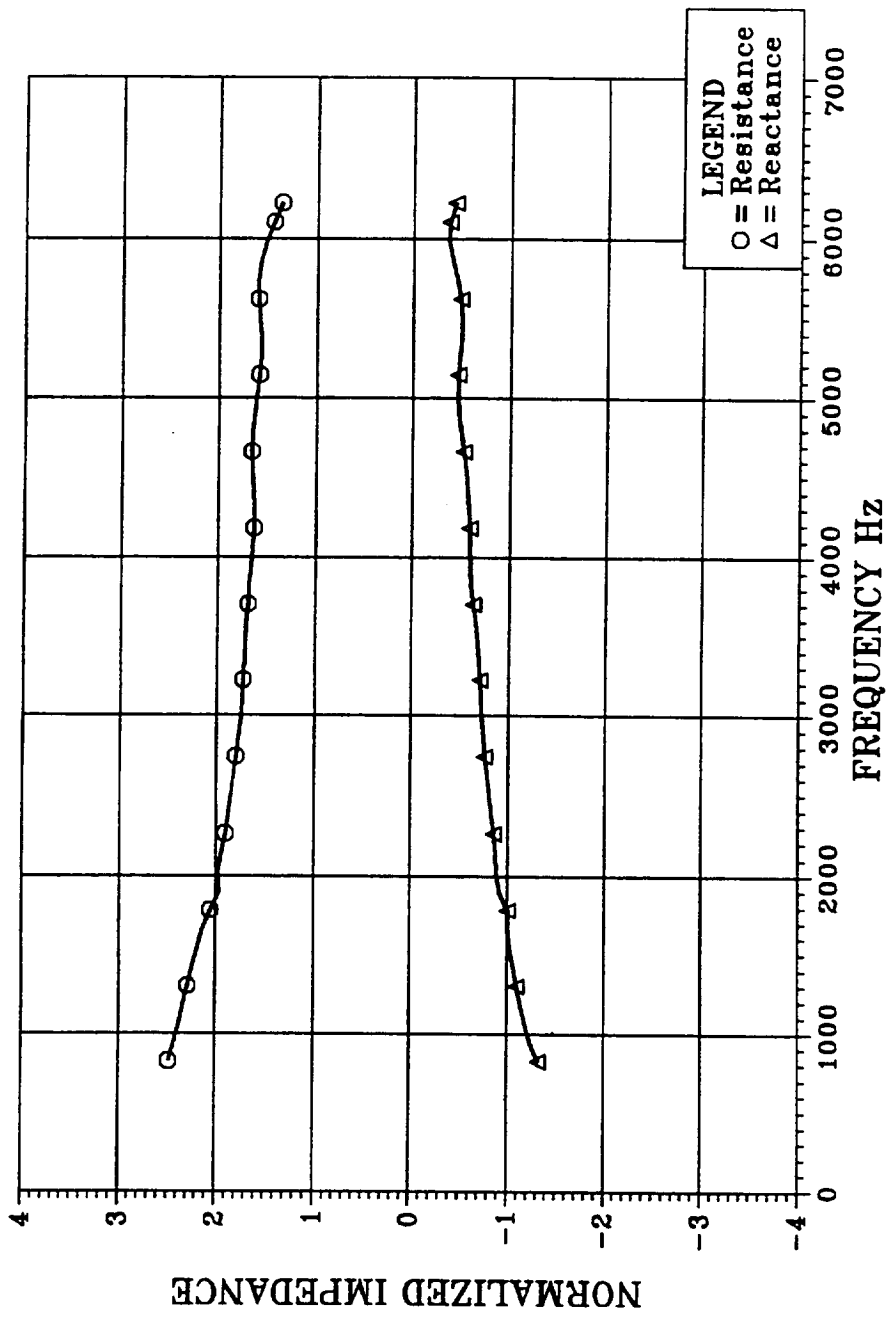

FIGURE 4.2–2 MEASURED ACOUSTIC IMPEDANCE OF LMSC HTP–1437
PANEL TEST AT 145 dB

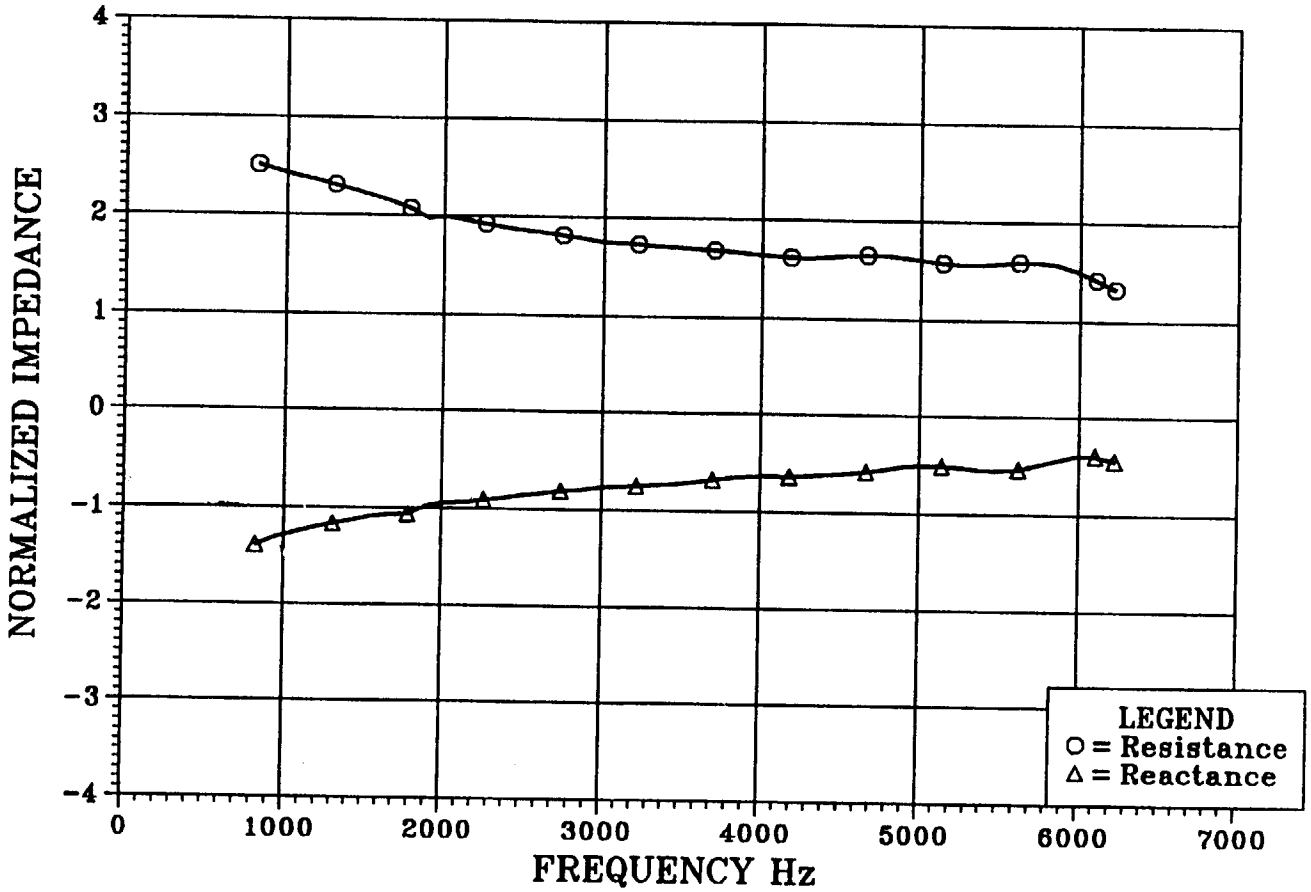

FIGURE 4.2-3 MEASURED ACOUSTIC IMPEDANCE OF LMSC HTP-1437
PANEL TEST AT 148 dB

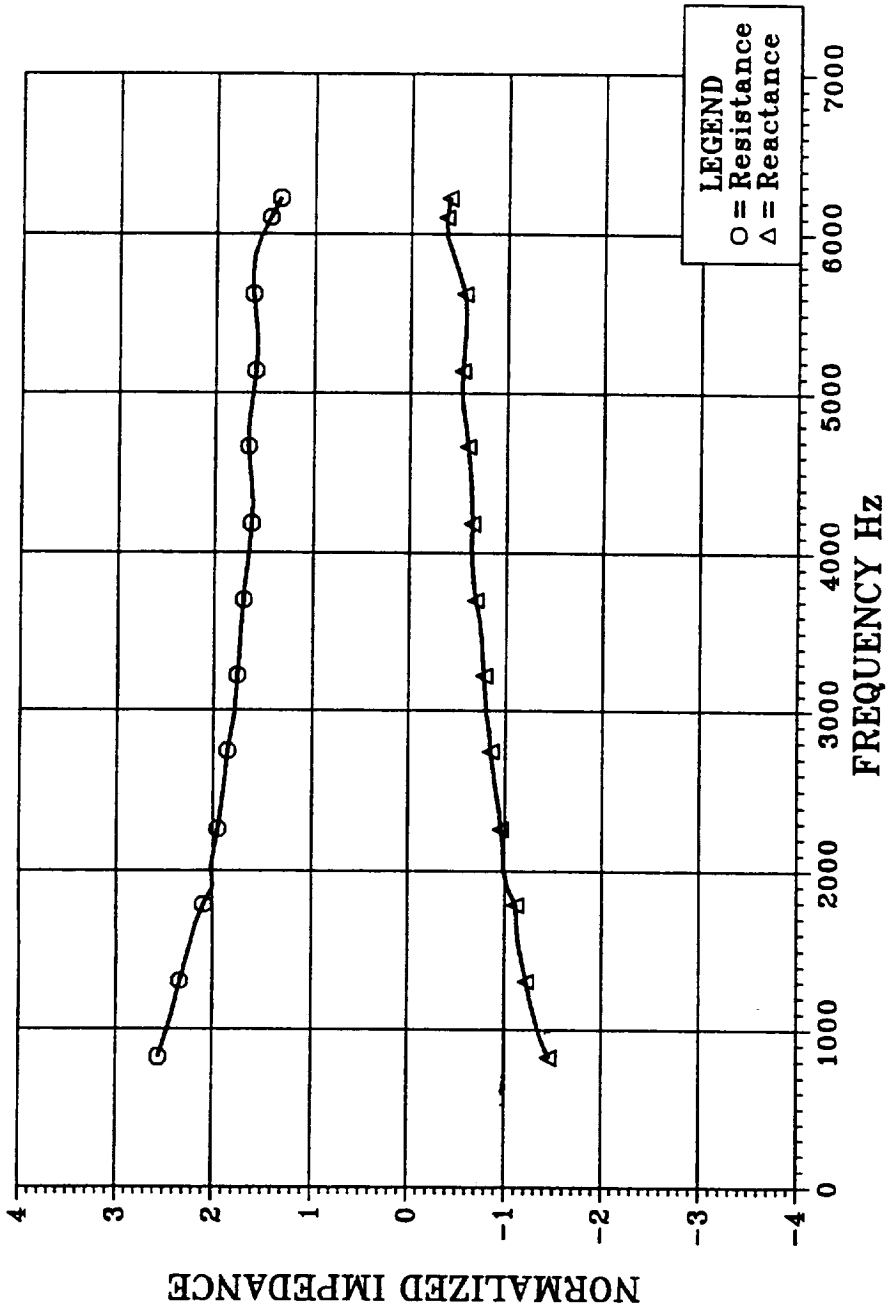

FIGURE 4.2-4 MEASURED ACOUSTIC IMPEDANCE OF LMSC HTP-1437
IN-TUBE TEST AT 140 dB (1" FOAM ONLY)

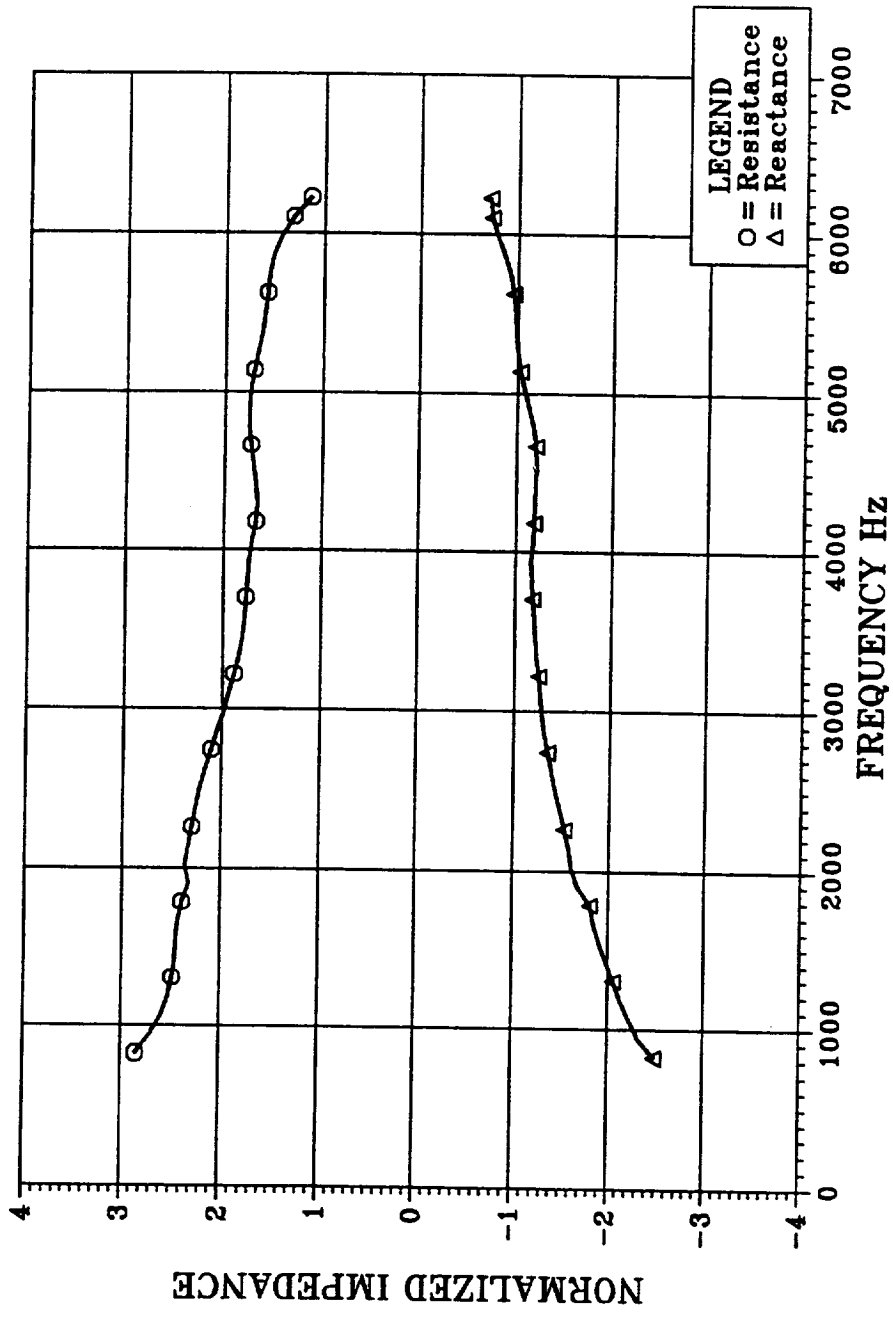

FIGURE 4.2–5 MEASURED ACOUSTIC IMPEDANCE OF LMSC HTP–1437
IN–TUBE TEST AT 145 dB (1" FOAM ONLY)

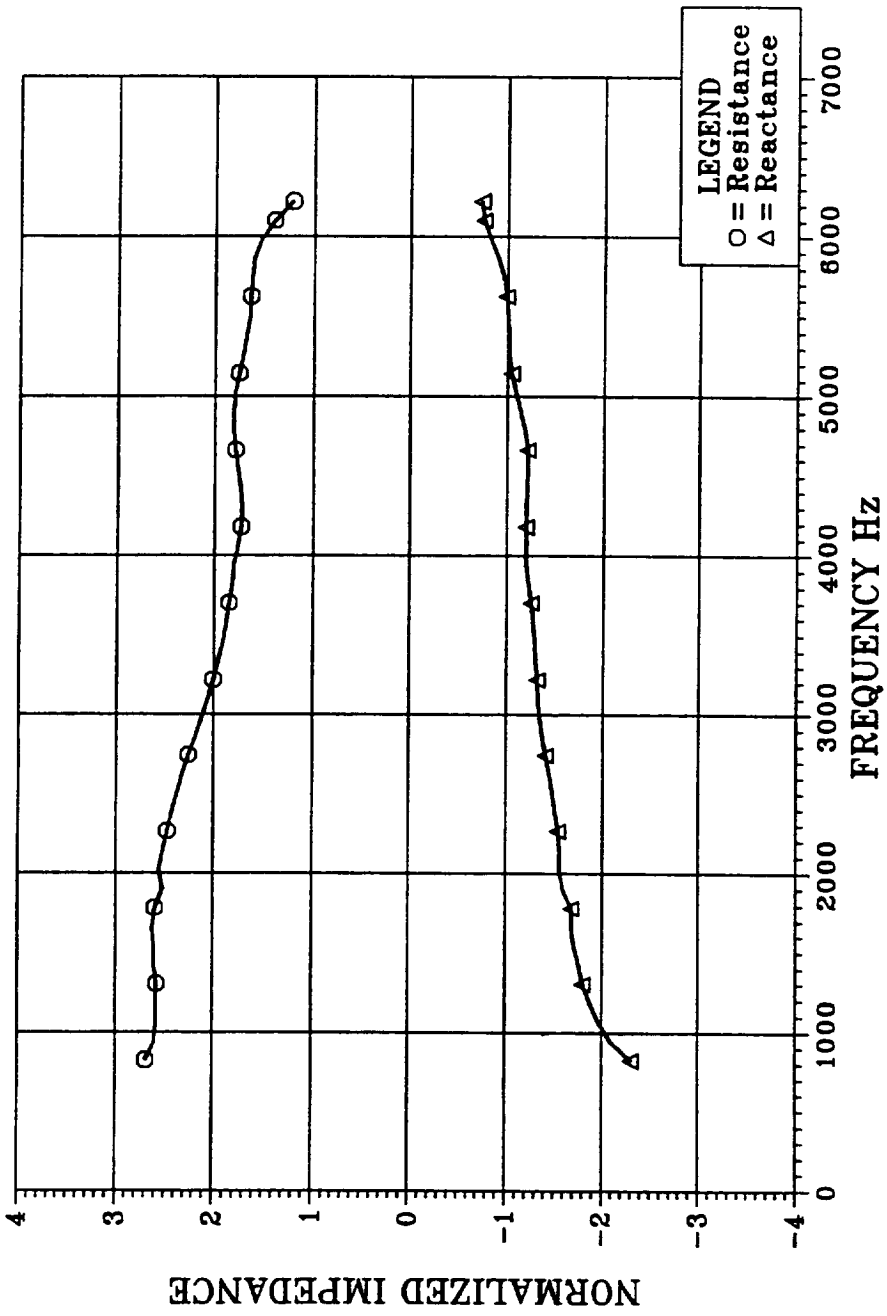

FIGURE 4.2-6 MEASURED ACOUSTIC IMPEDANCE OF LMSC HTP-1437
IN-TUBE TEST AT 148 dB (1" FOAM ONLY)

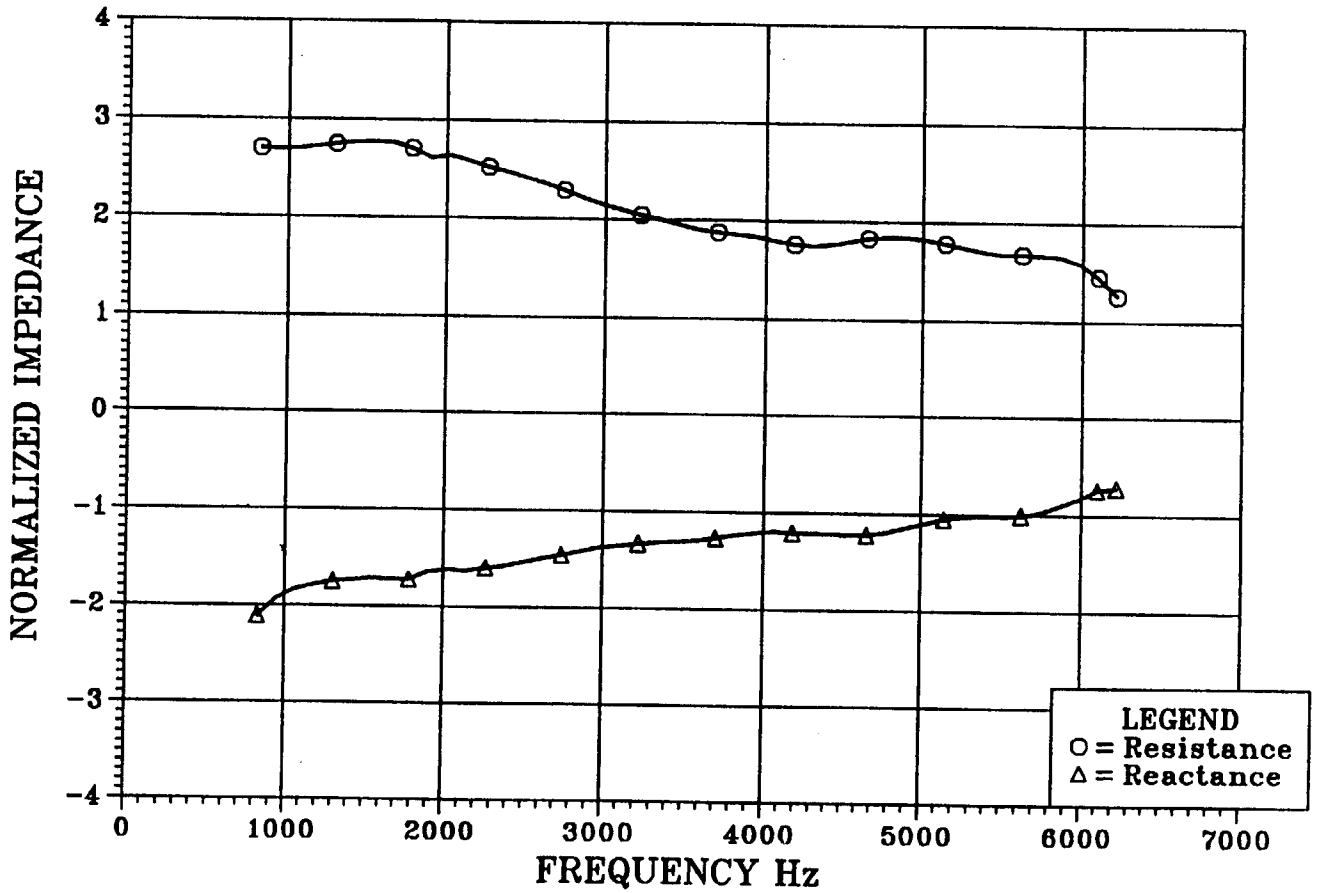

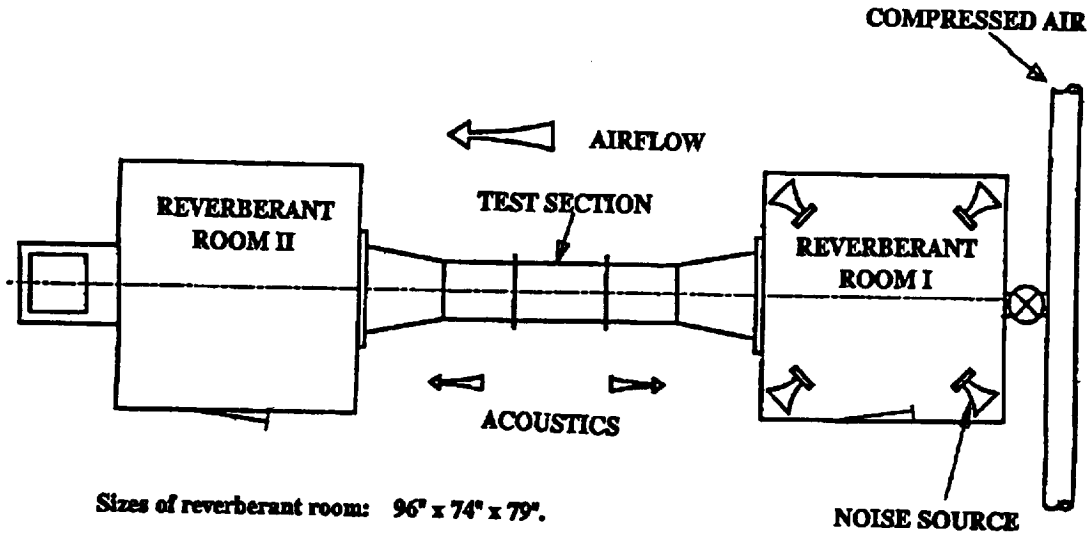

Figure 4.2-7 Schematic of Acoustic Air/Noise Flow Duct Facility

FIGURE 4.2-8 ACOUSTIC INSERTION LOSS OF LMSC HTP-1437 FOAM FILLED SANDWICH STRUCTURE AT MACH 0.0

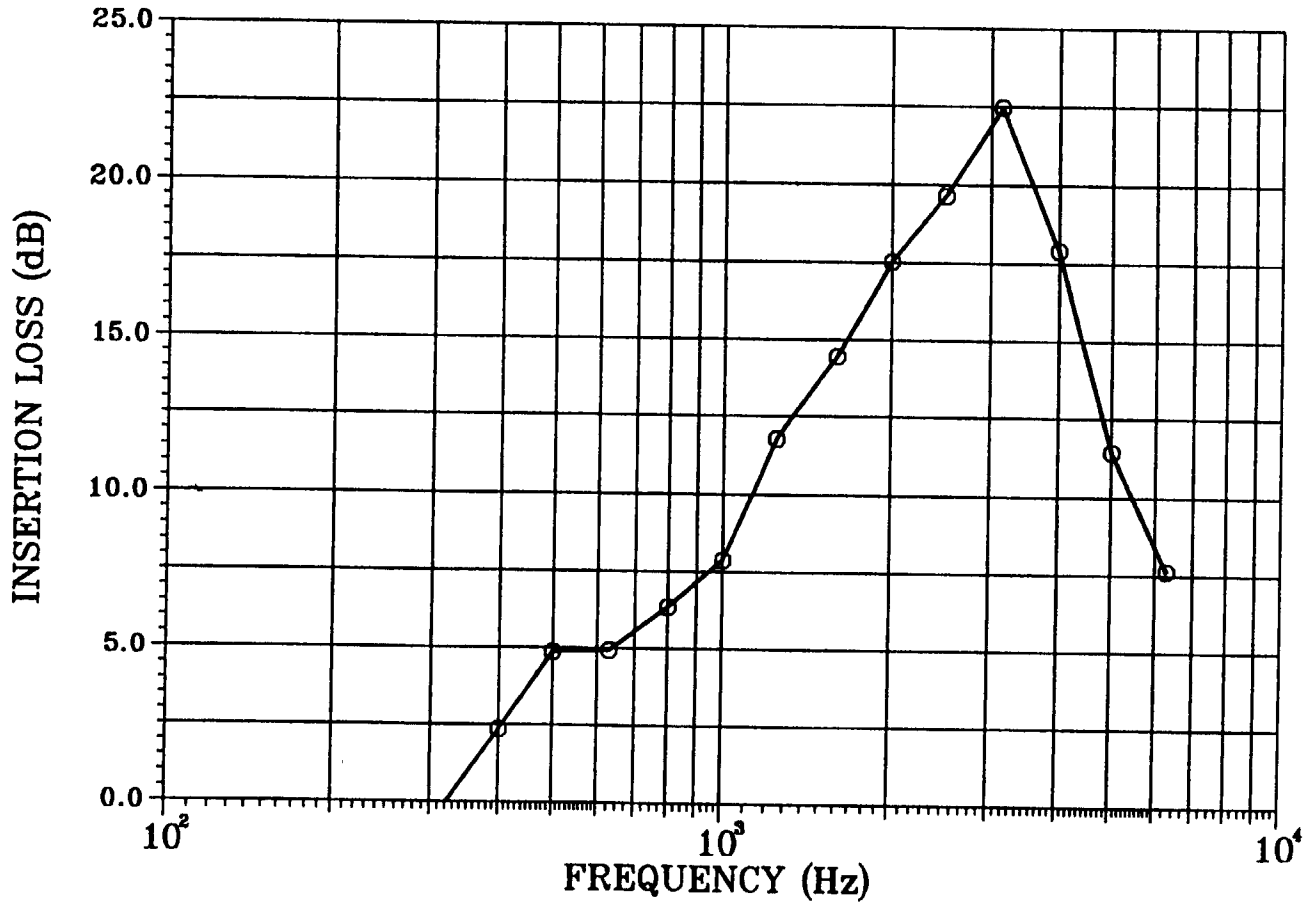

FIGURE 4.2-9 ACOUSTIC INSERTION LOSS OF LMSC HTP-1437 FOAM FILLED SANDWICH STRUCTURE AT MACH 0.2

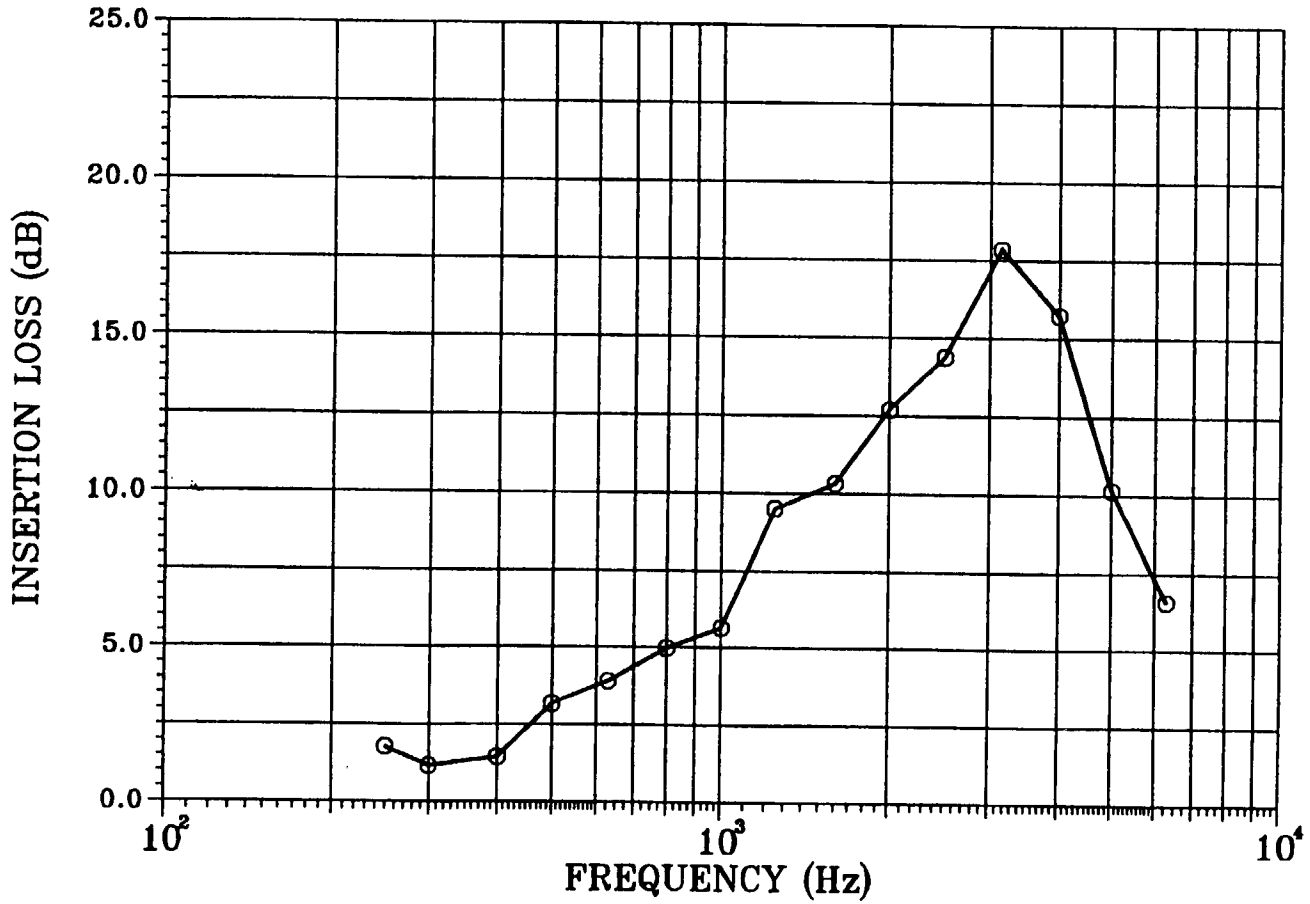

FIGURE 4.2–10 ACOUSTIC INSERTION LOSS OF LMSC HTP–1437 FAOM FILLED SANDWICH STRUCTURE AT MACH 0.3

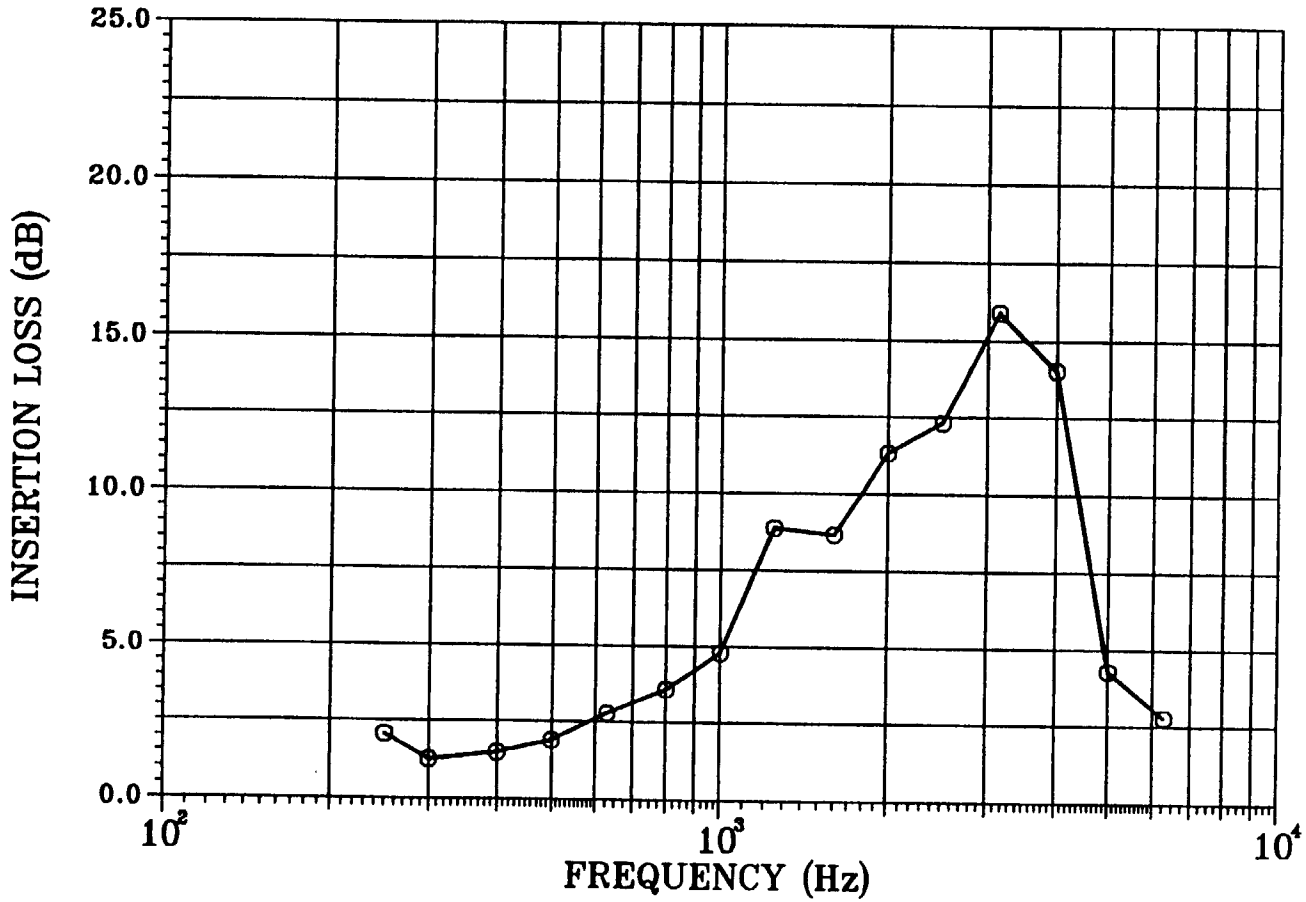

FIGURE 4.2–11 ACOUSTIC INSERTION LOSS OF LMSC HTP–1437 FOAM FILLED SANDWICH STRUCTURE AT MACH 0.4

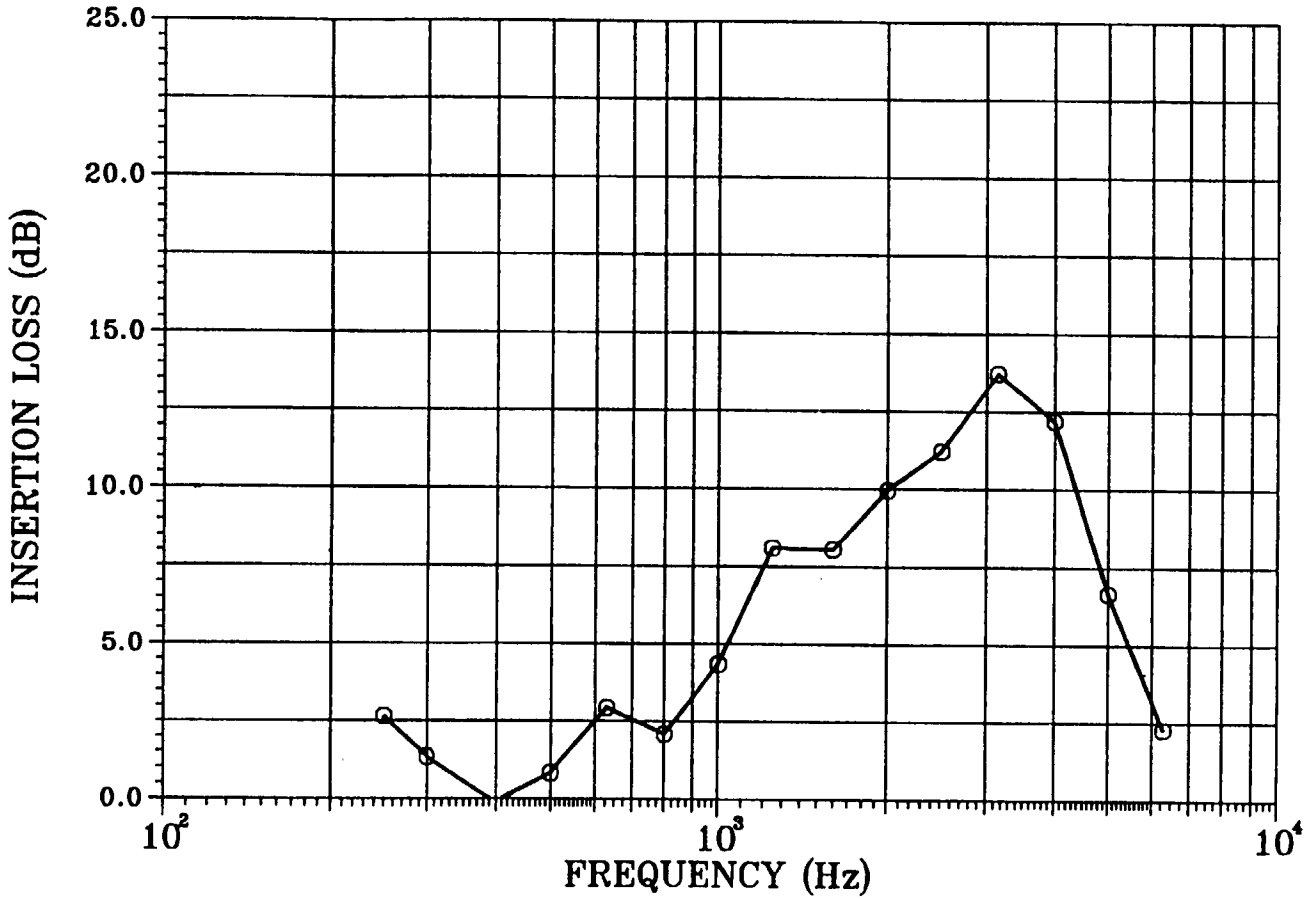

FIGURE 4.2–12 ACOUSTIC INSERTION LOSS OF LMSC HTP–1437 FOAM FILLED SANDWICH STRUCTURE AT MACH 0.5

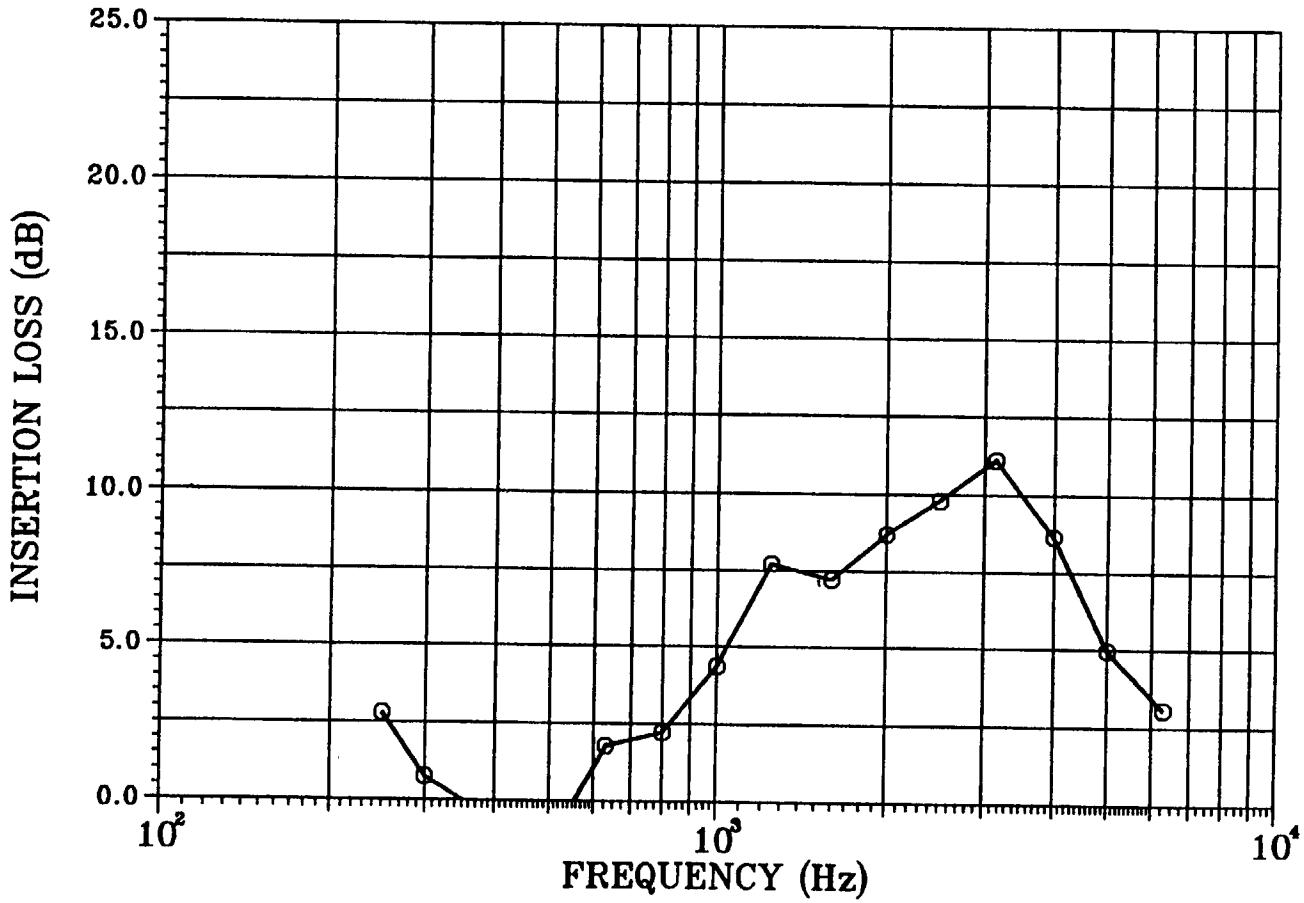

FIGURE 4.2-13 ACOUSTIC INSERTION LOSS OF LMSC HTP-1437 FOAM FILLED SANDWICH STRUCTURE AT MACH 0.6

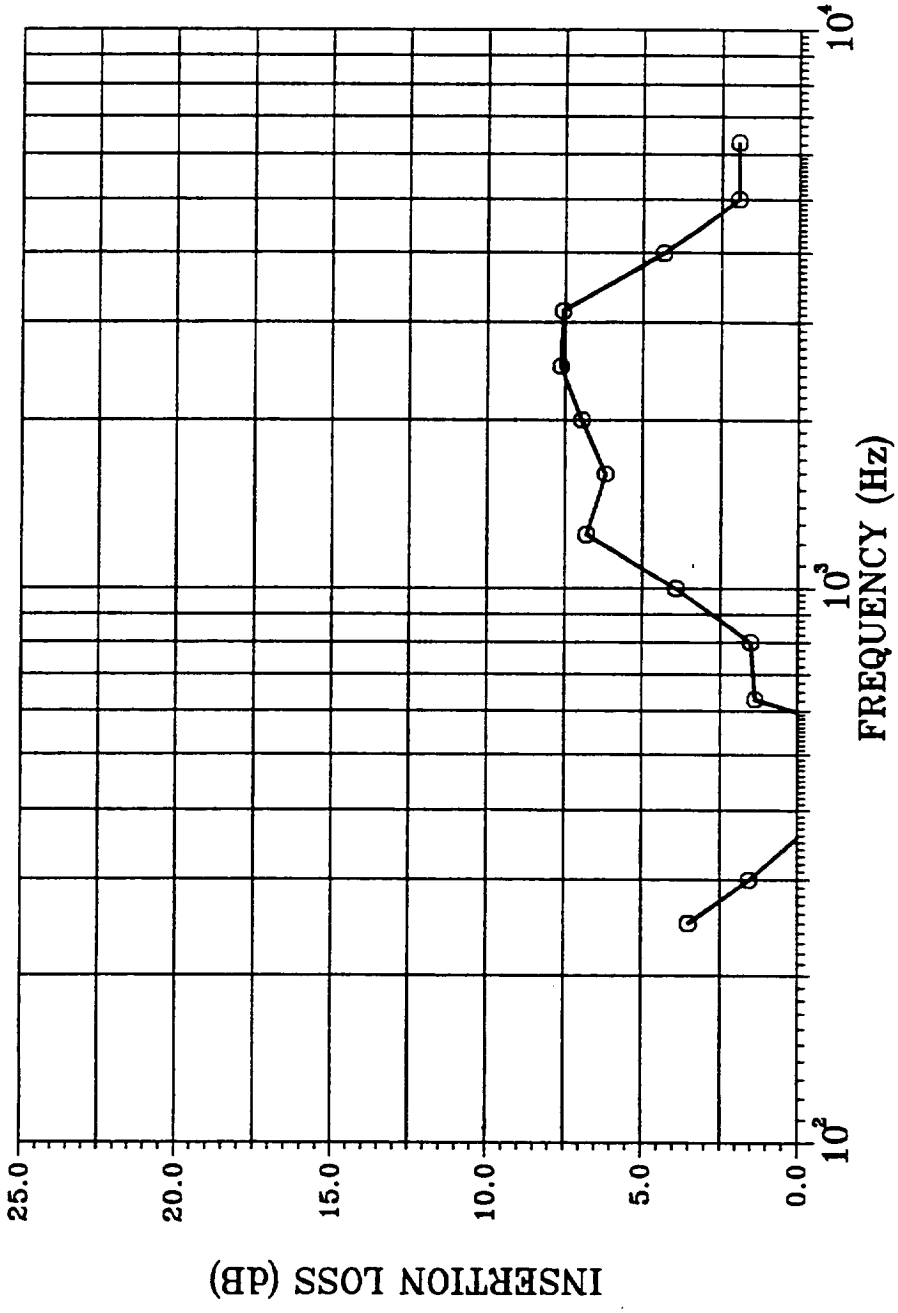

Figure 4.2-14 Comparison of Acoustic Insertion Loss for LMSC Material 1437 Filled Sandwich Structures (1" Thick) and 80-rayl SDOF DynaRohr (0.95" Thick) at Mach Number 0.4

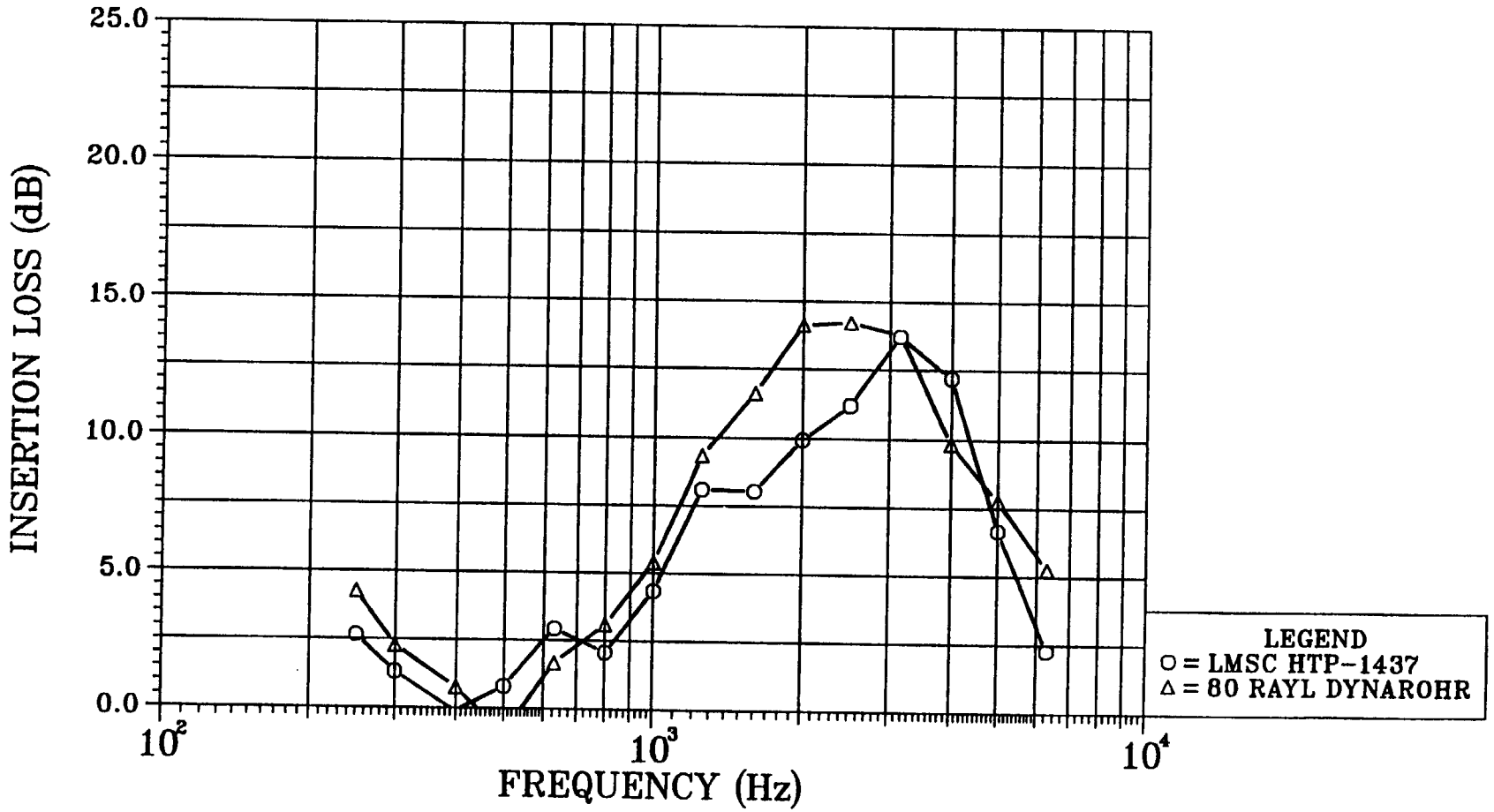

Figure 4.2-15 Comparison of Acoustic Insertion Loss for LMSC Material 1437 Filled Sandwich Structures (1" Thick) and 80-rayl SDOF DynaRohr (0.95" Thick) at Mach Number 0.5

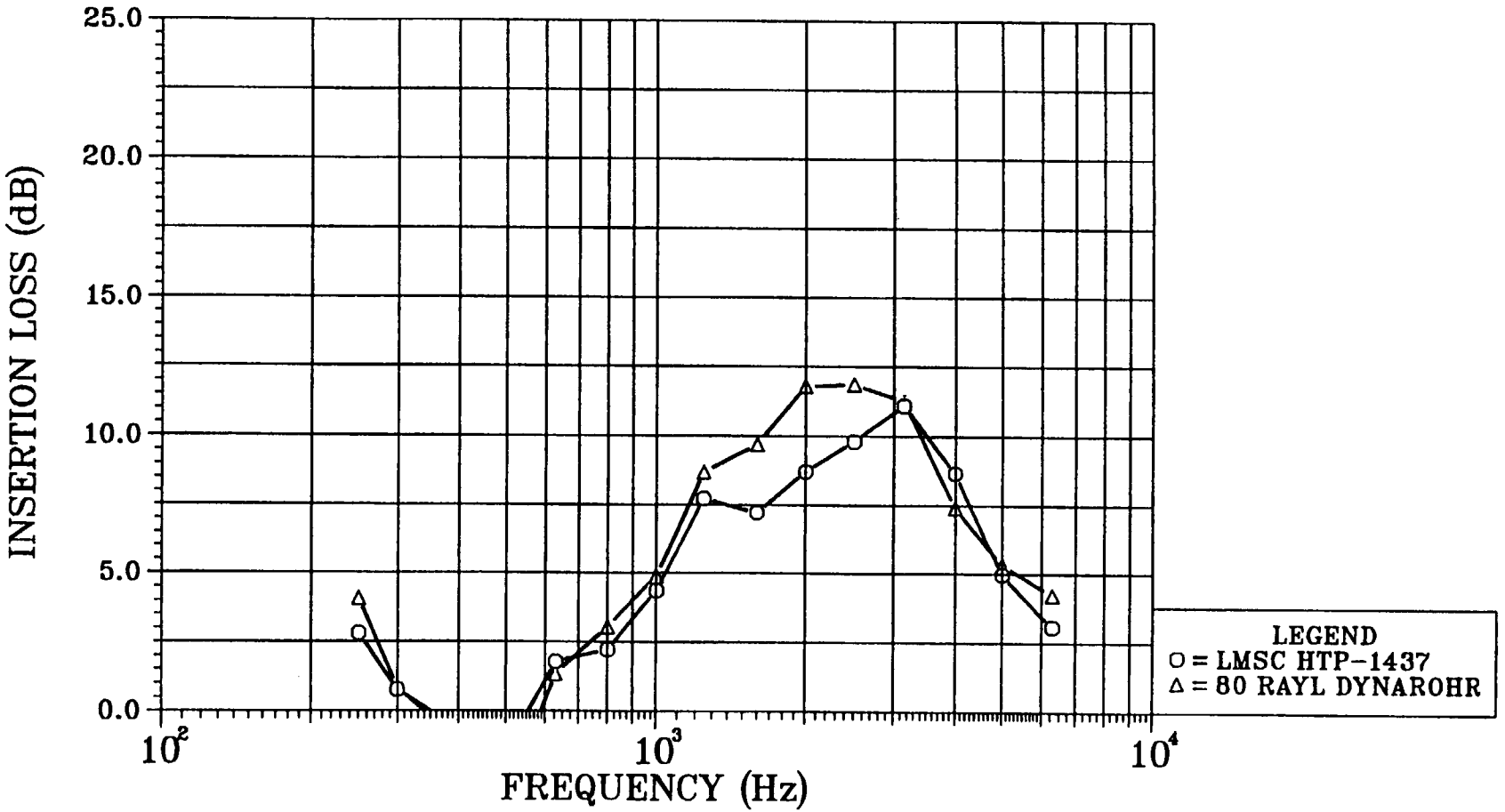

Figure 4.2-16 Comparison of Acoustic Insertion Loss for LMSC Material 1437 Filled Sandwich Structures (1" Thick) and 80-rayl SDOF DynaRohr (0.95" Thick) at Mach Number 0.6

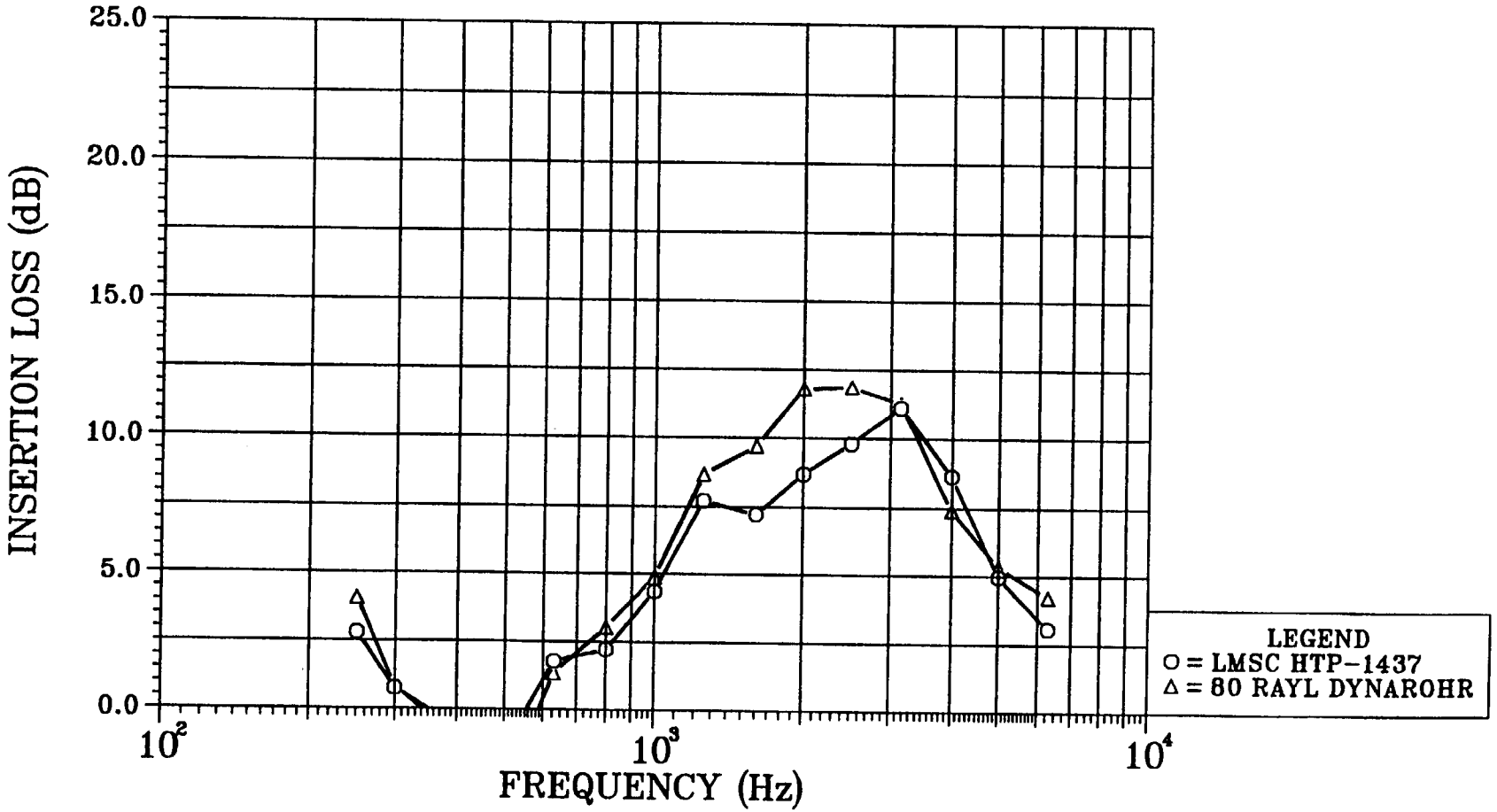

FIGURE 4.2-17 MEASURED ACOUSTIC IMPEDANCE OF 80-RAYL SDOF
DYNAROHR PANEL TEST AT 140 dB

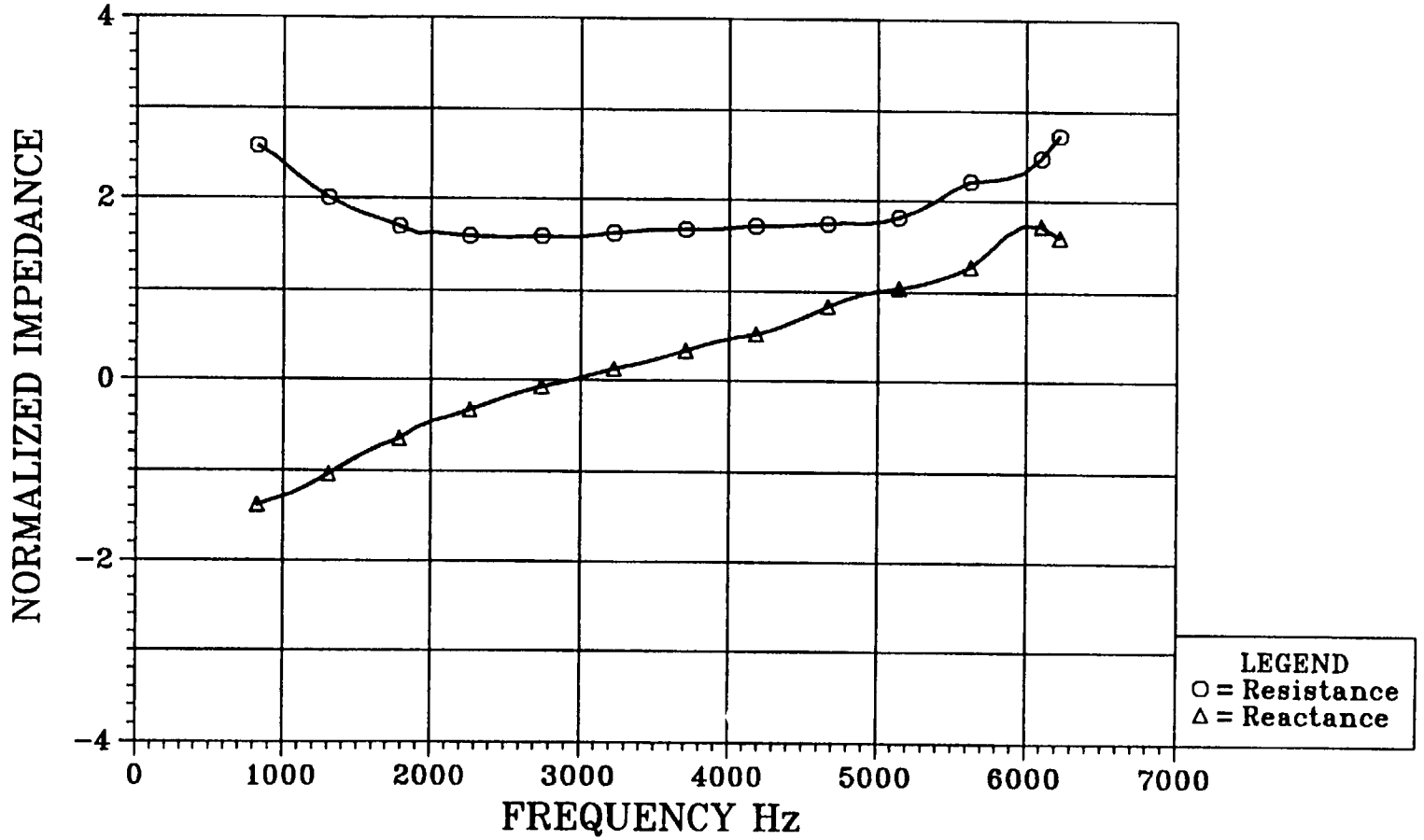

FIGURE 4.2–18 MEASURED ACOUSTIC IMPEDANCE OF 80–RAYL SDOF
DYNAROHR PANEL TEST AT 145 dB

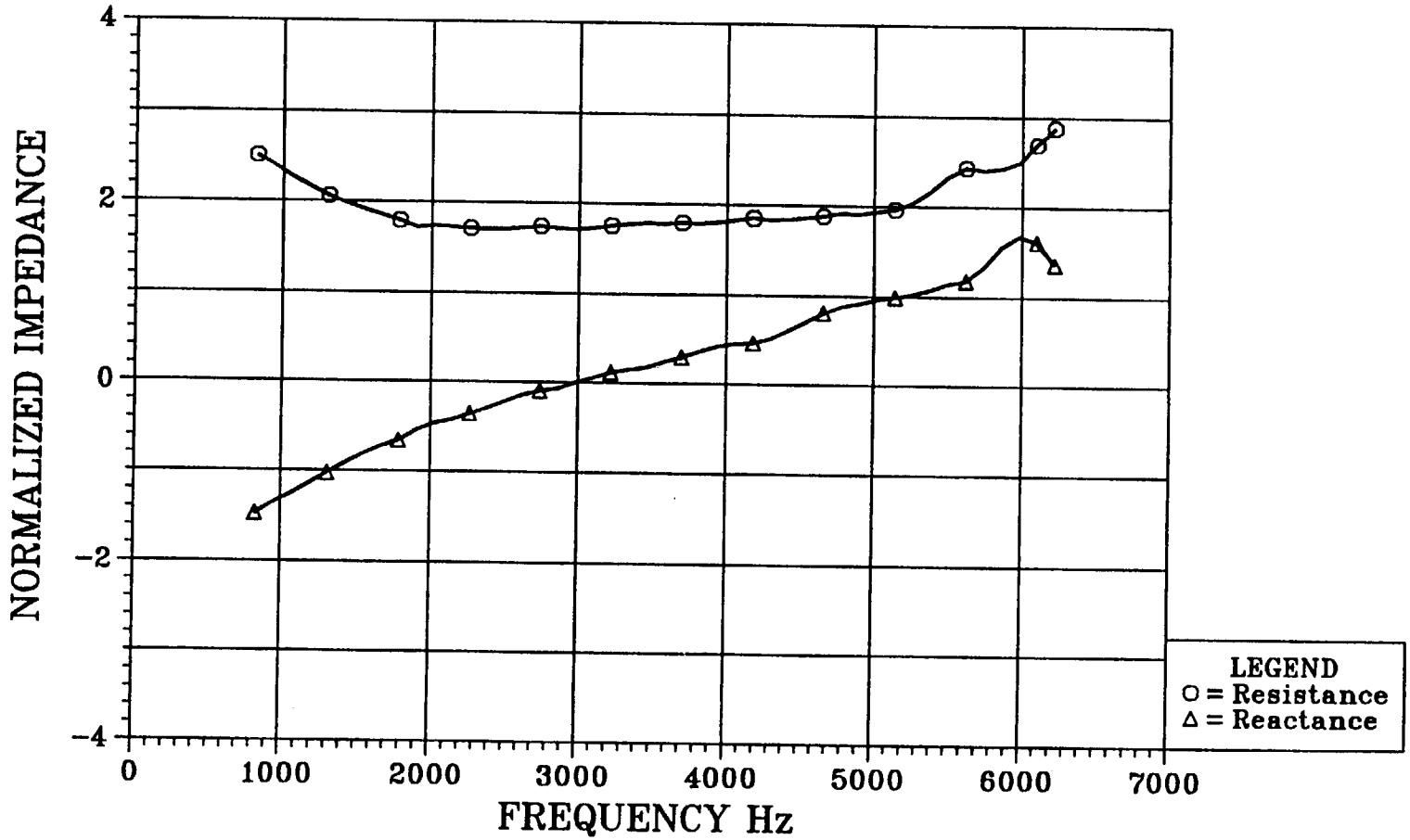

FIGURE 4.2–19 MEASURED ACOUSTIC IMPEDANCE OF 80–RAYL SDOF
DYNAROHR PANEL TEST AT 148 dB

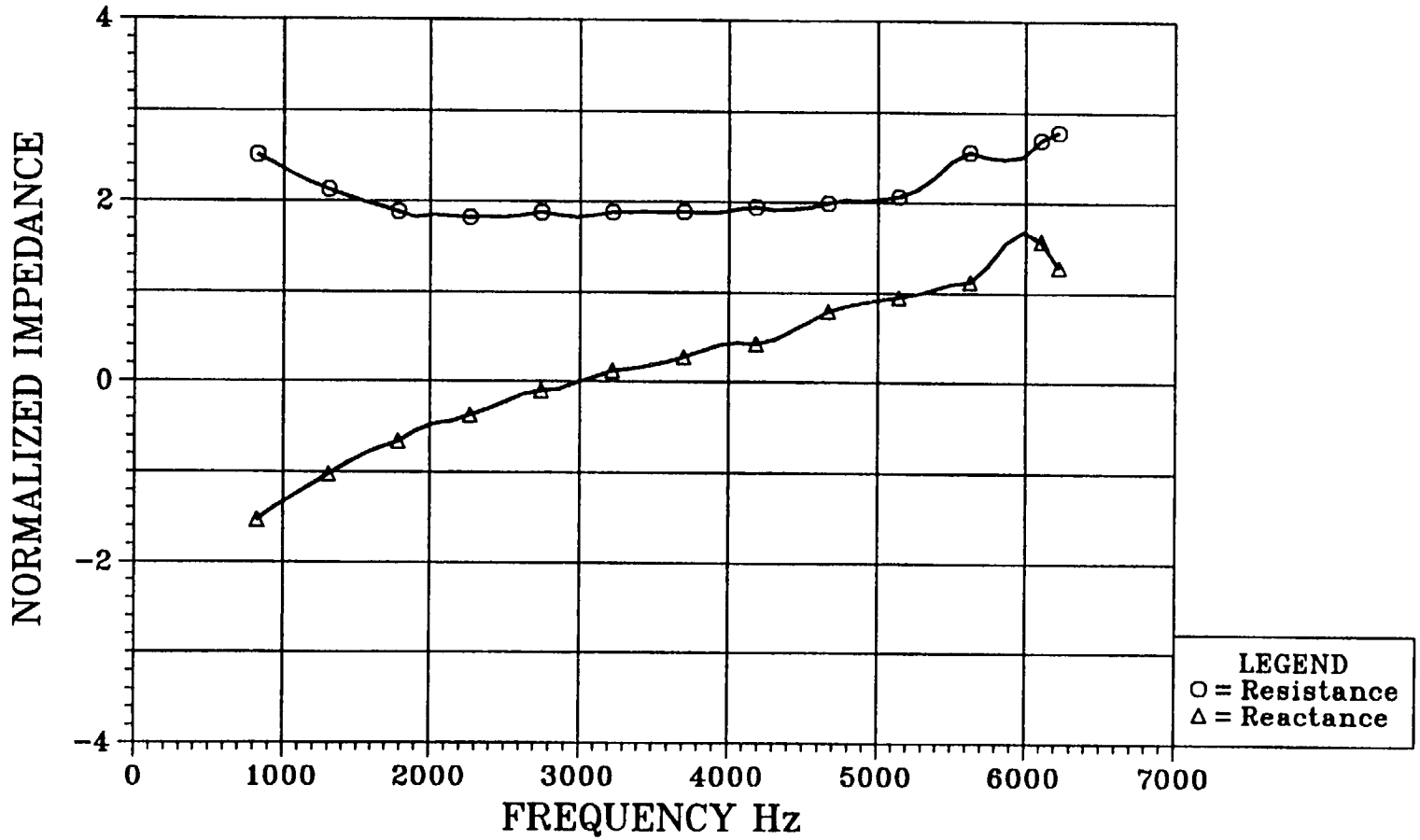

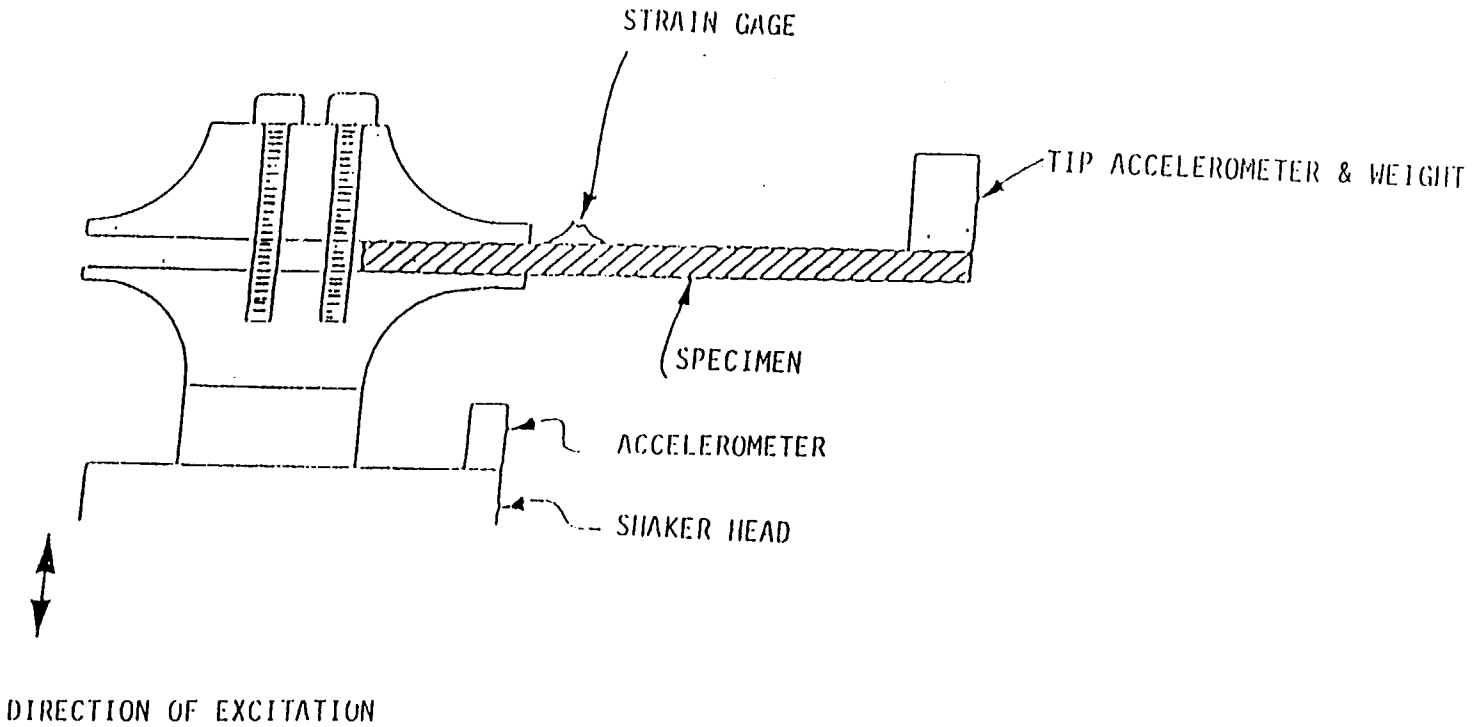

Figure 5.2-1 Dynamic Shaker General Test Setup

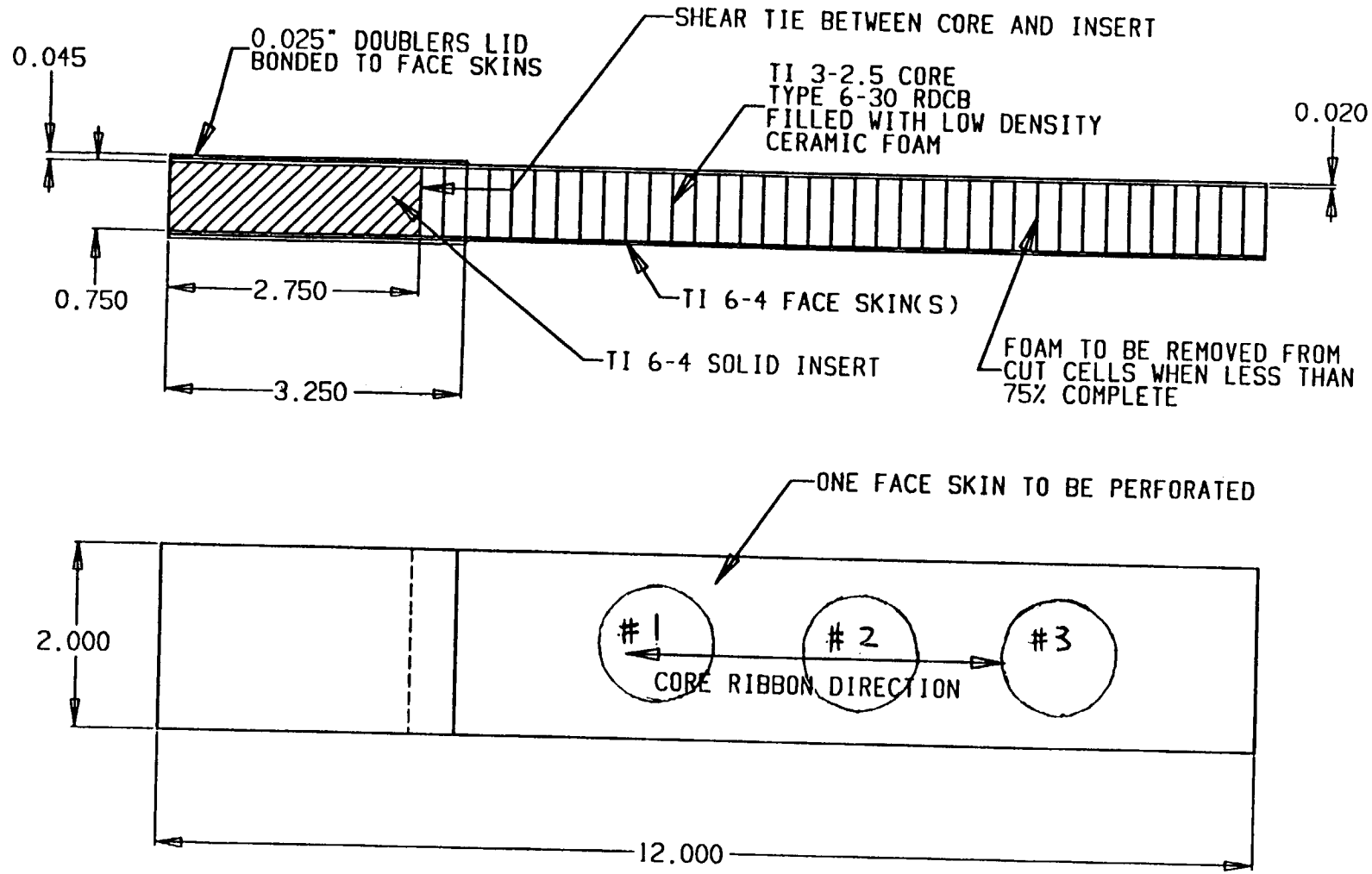

Figure 5.2-2 High Temperature Acoustic Structure Shaker (HCF) Test Specimen

Figure 5.2-3 Acoustic Impedance of Ceramic Foam Sandwich Structures Sample #1, Location 1, Prior/Post HCF Test

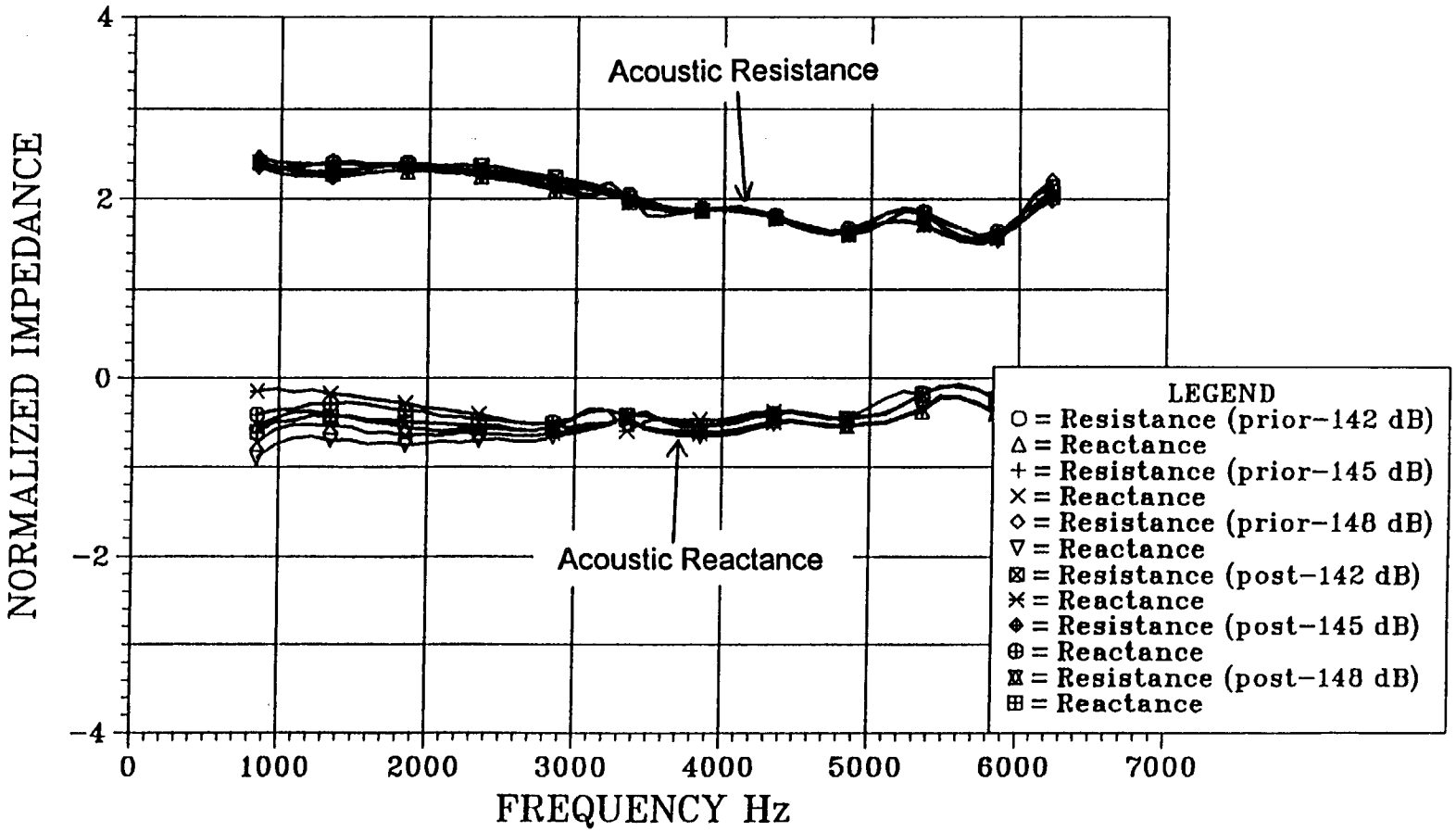

Figure 5.2-4 Acoustic Impedance of Ceramic Foam Sandwich Structures Sample #1, Location 2, Prior/Post HCF Test

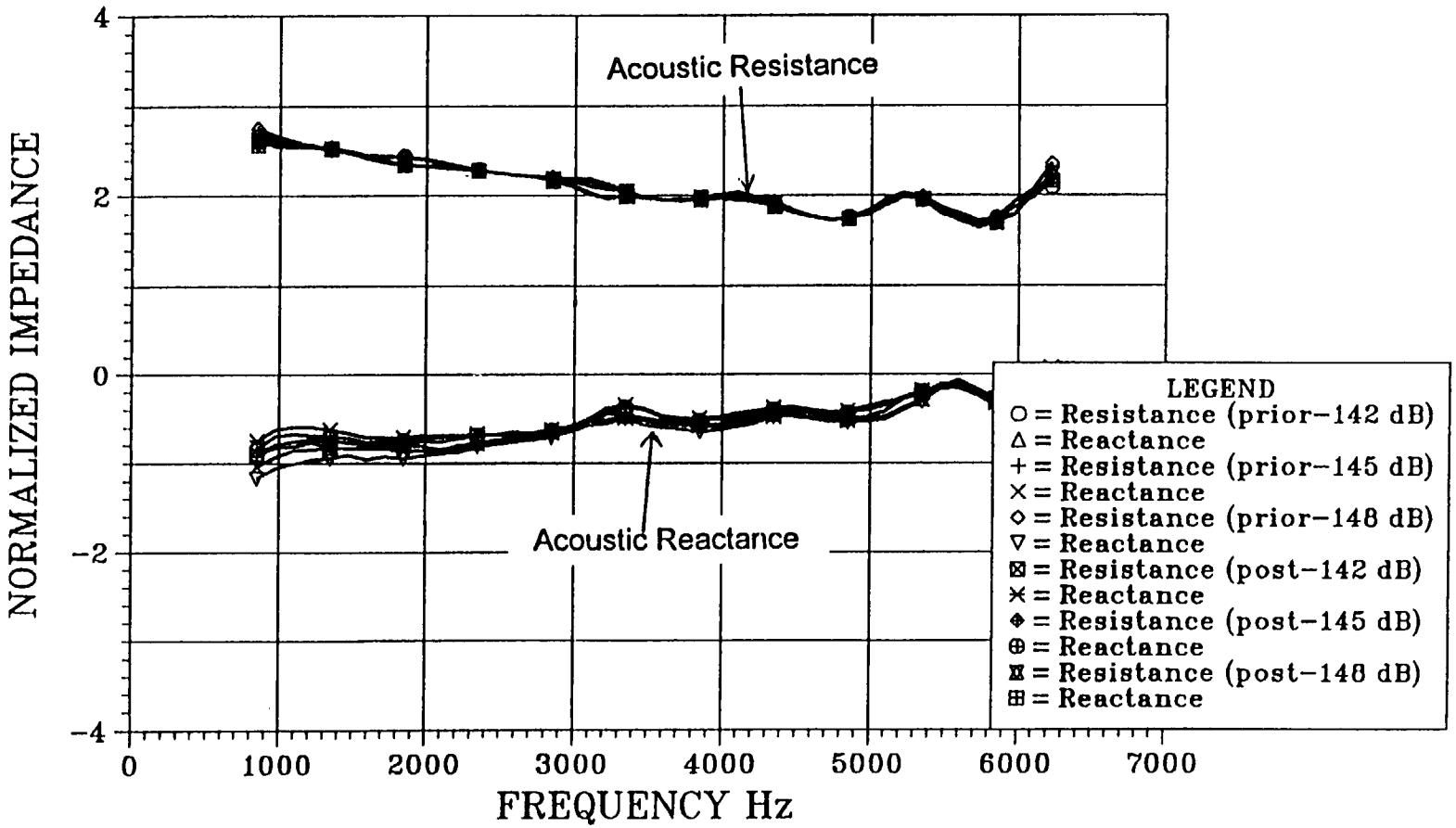

Figure 5.2-5 Acoustic Impedance of Ceramic Foam Sandwich Structures Sample #2, Location 1, Prior/Post HCF Test

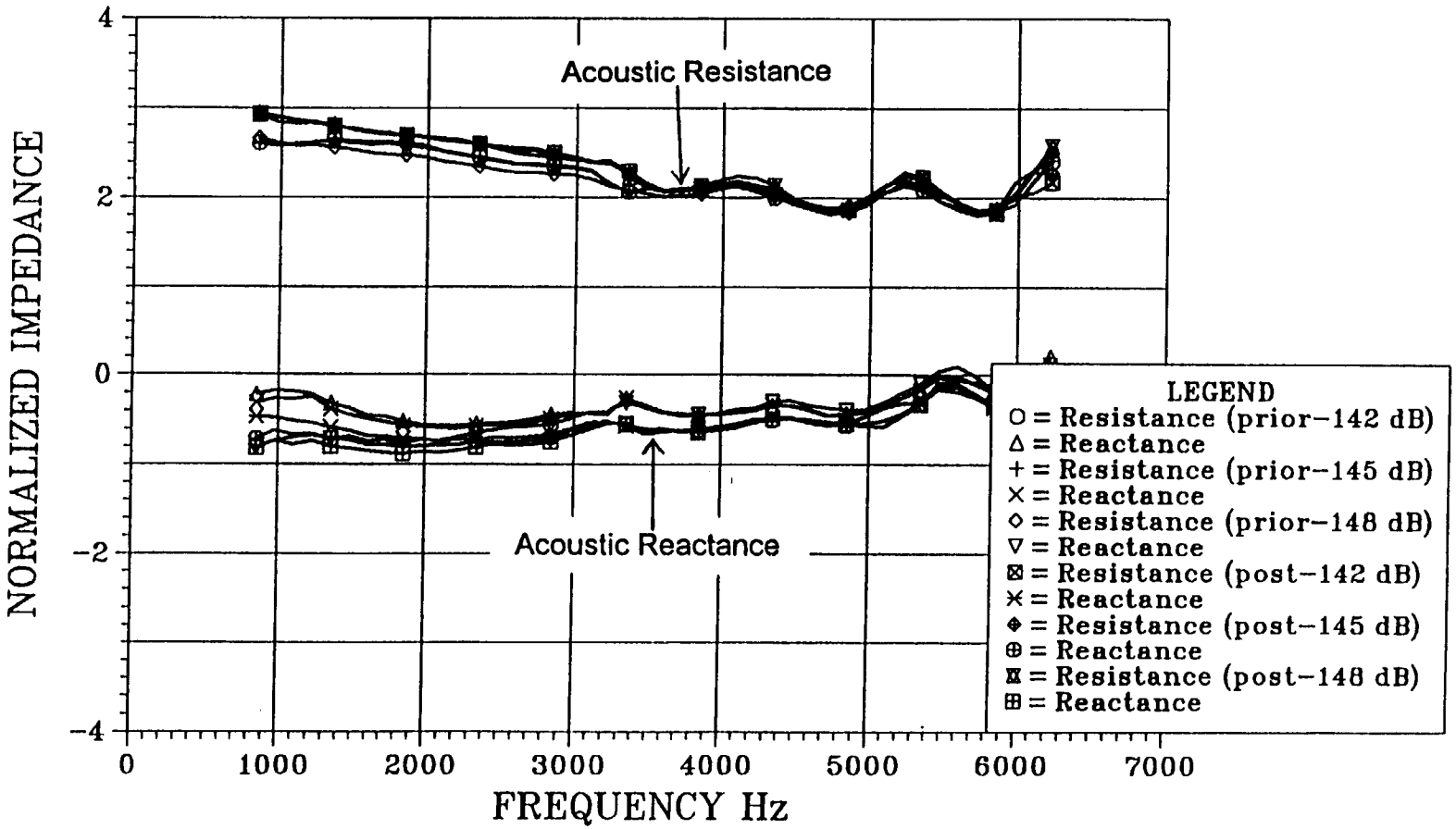

Figure 5.2-6 Acoustic Impedance of Ceramic Foam Sandwich Structures Sample #2, Location 2, Prior/Post HCF Test

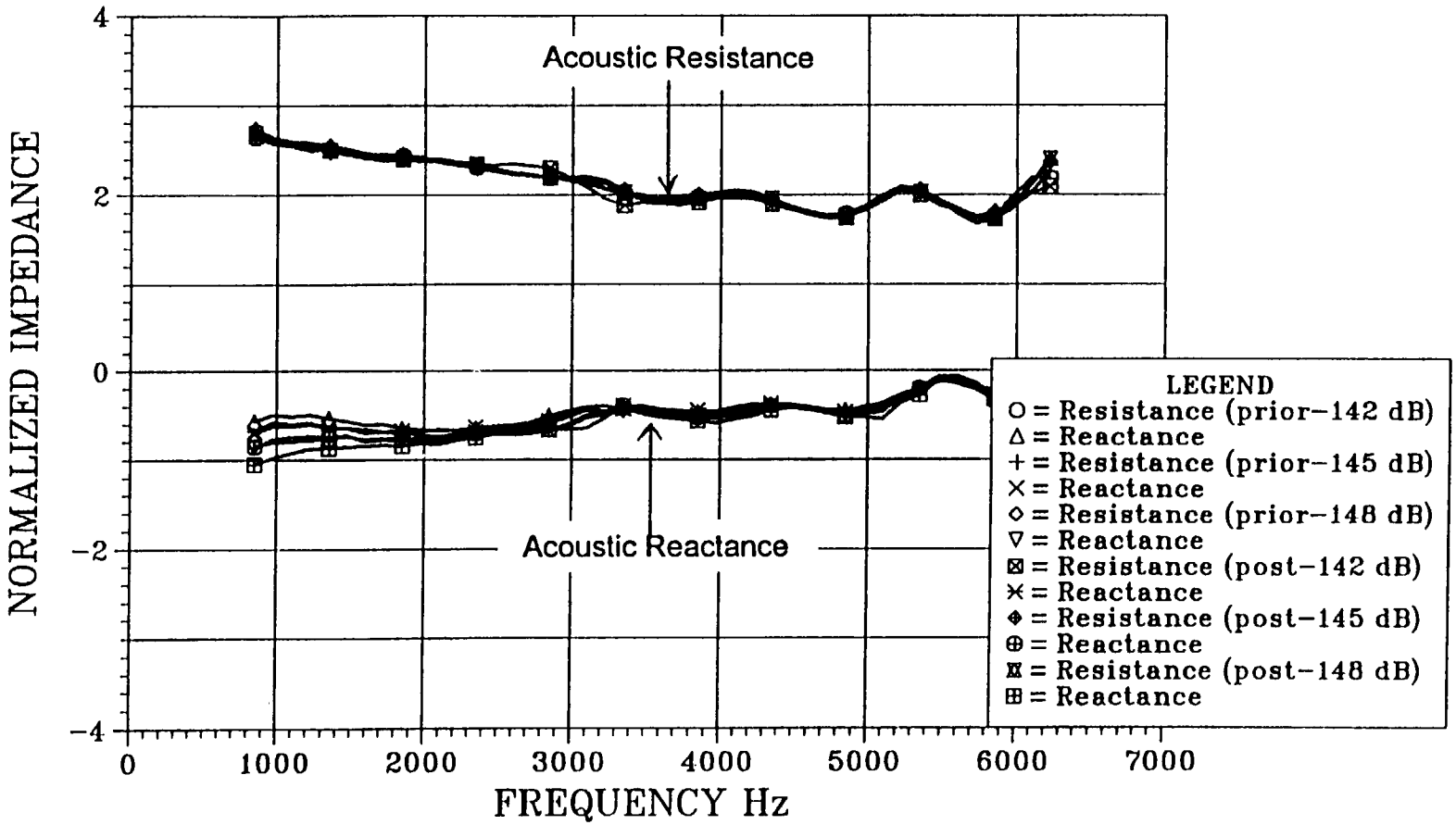

Figure 5.2-7 Acoustic Impedance of Ceramic Foam Sandwich Structures Sample #3, Location 1, Prior/Post HCF Test

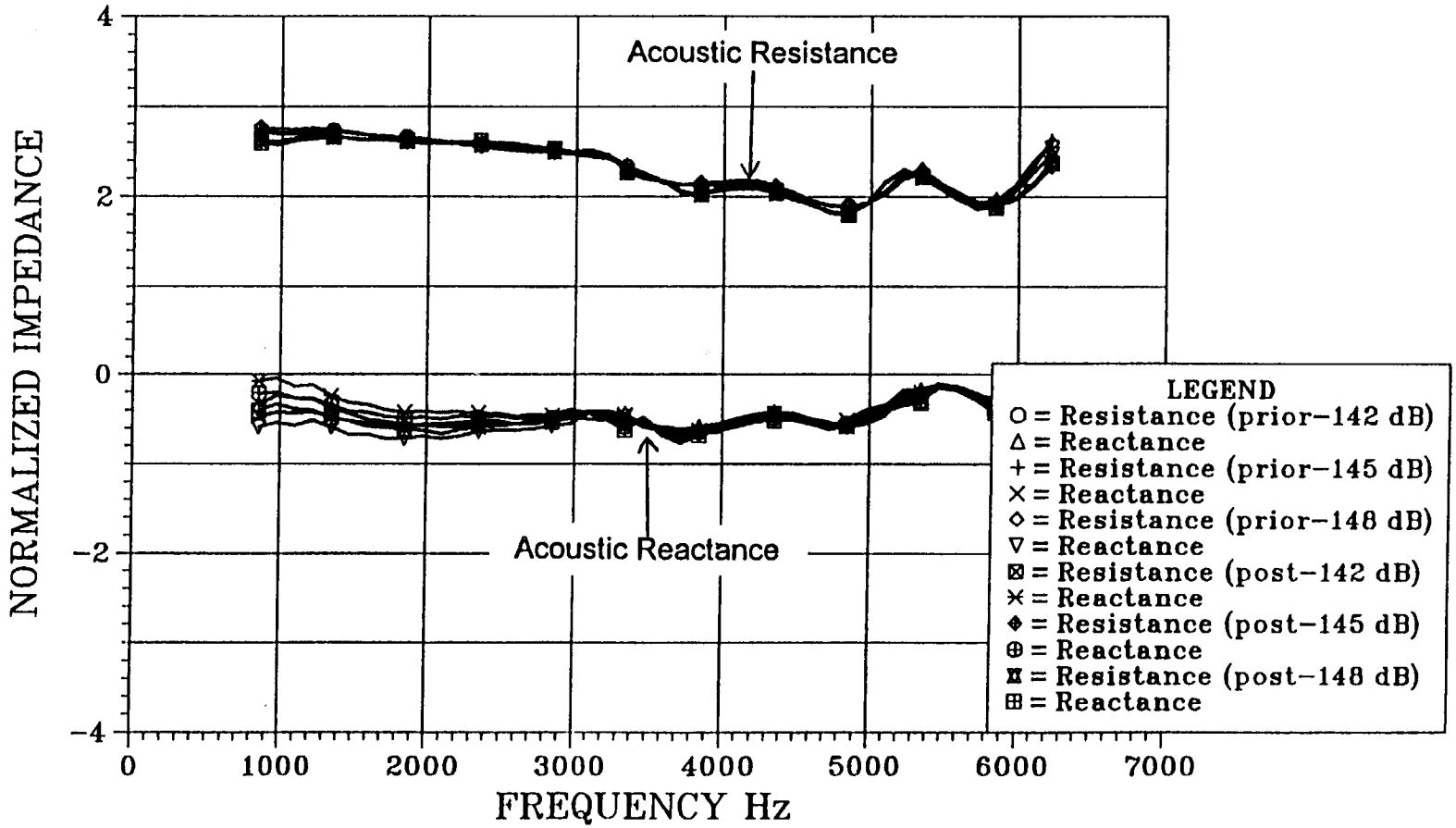

Figure 5.2-8 Acoustic Impedance of Ceramic Foam Sandwich Structures Sample #3, Location 2, Prior/Post HCF Test

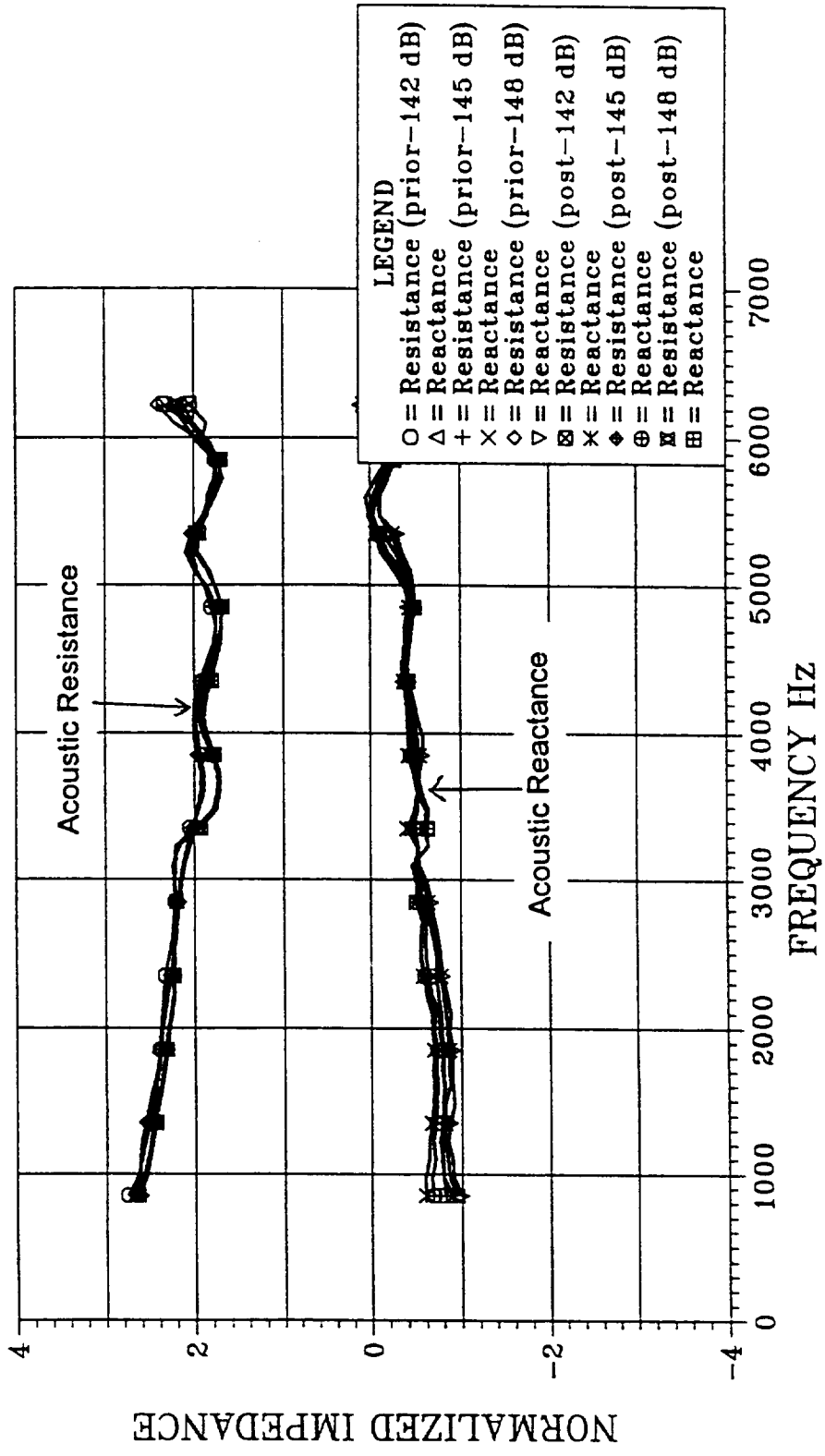

Figure 5.2-9 Acoustic Impedance of Ceramic Foam Sandwich Structures Sample #4, Location 1, Prior/Post HCF Test

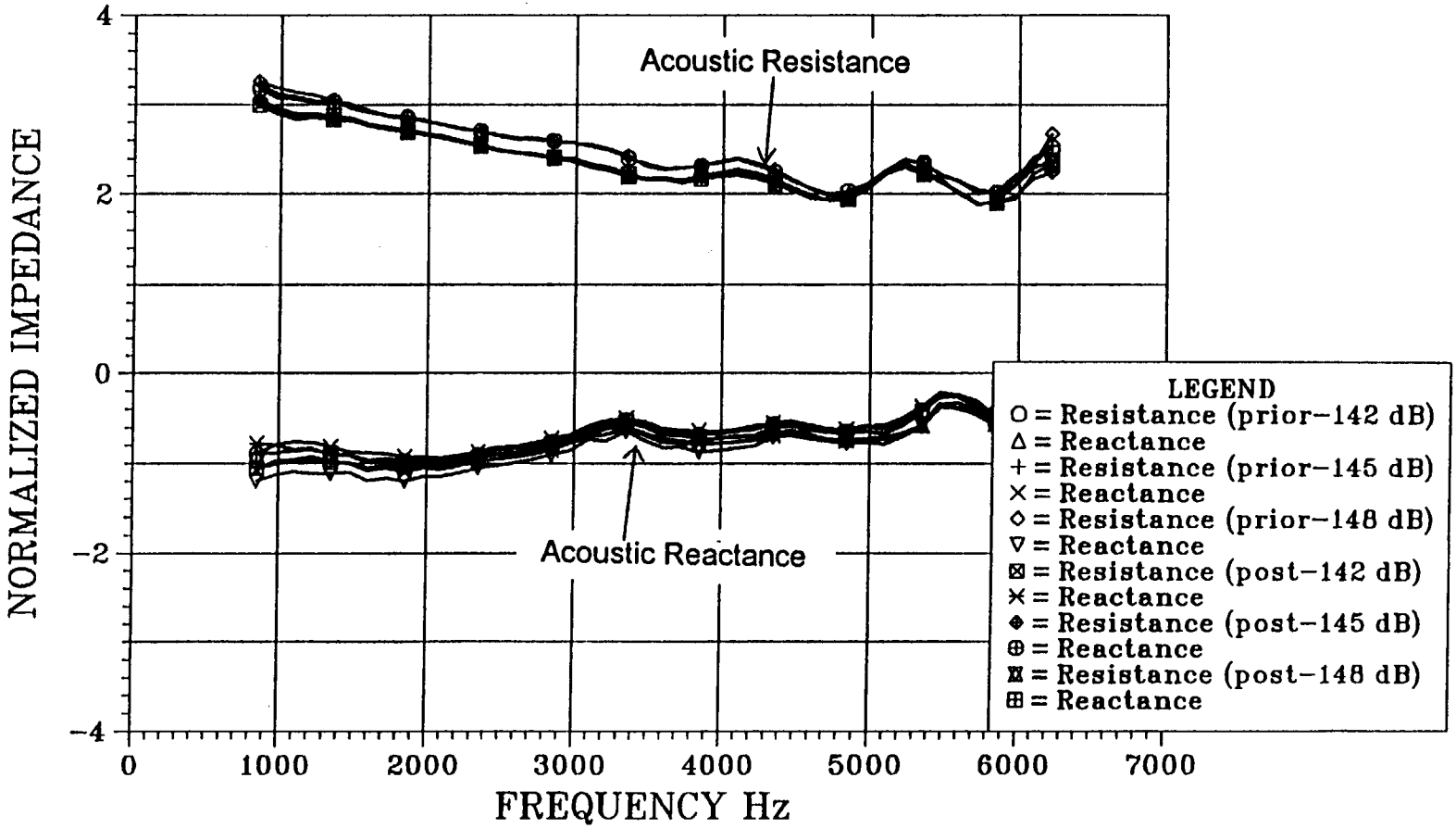

Figure 5.2-10 Acoustic Impedance of Ceramic Foam Sandwich Structures Sample #4, Location 2, Prior/Post HCF Test

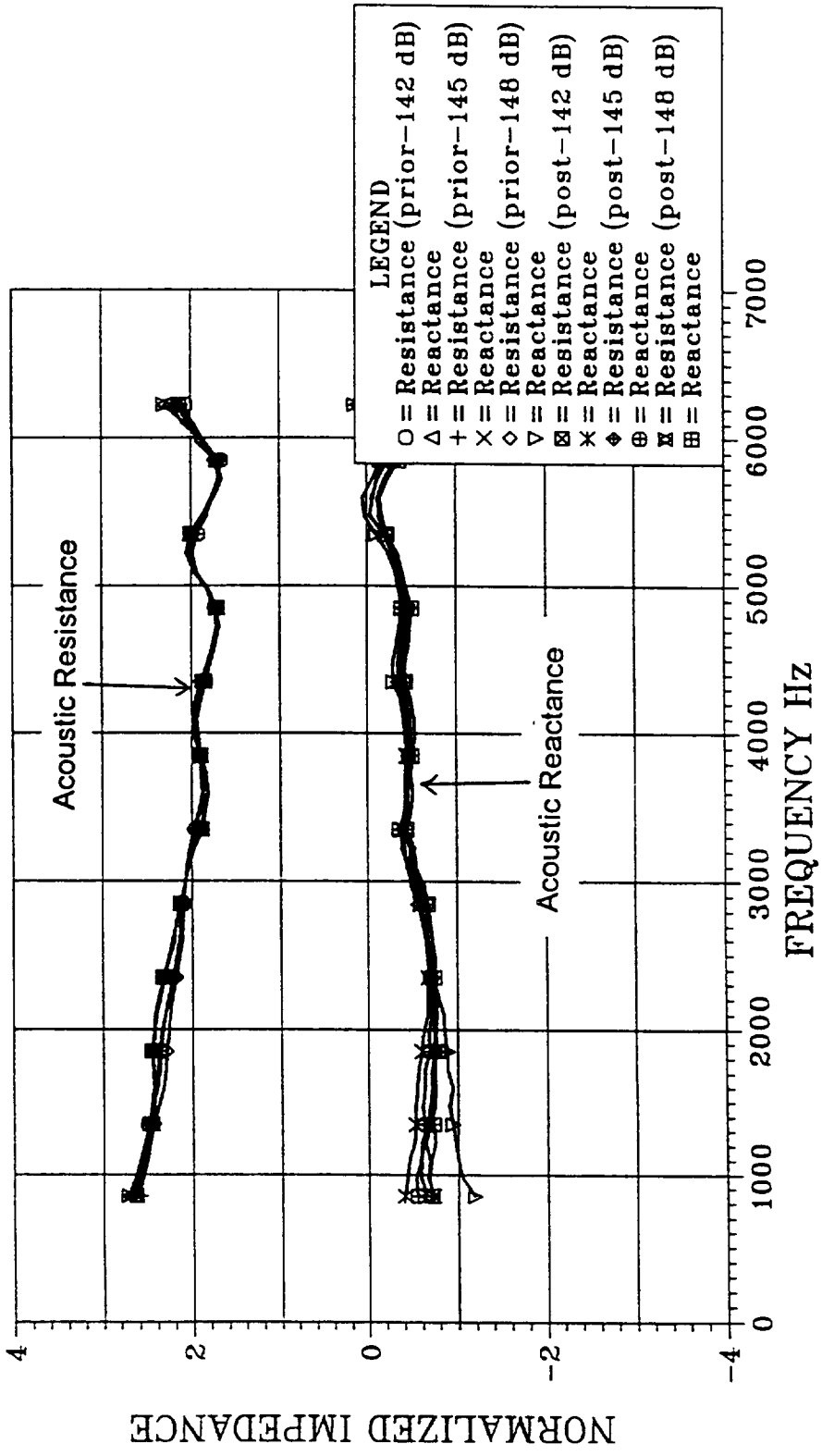

FIGURE 5.3–1 ACOUSTIC IMPEDANCE OF LMSC HTP–1437 FOAM FILLED SANDWICH STRUCTURE SAMPLE #1 AT 140 dB, PRIOR/POST HCF TEST

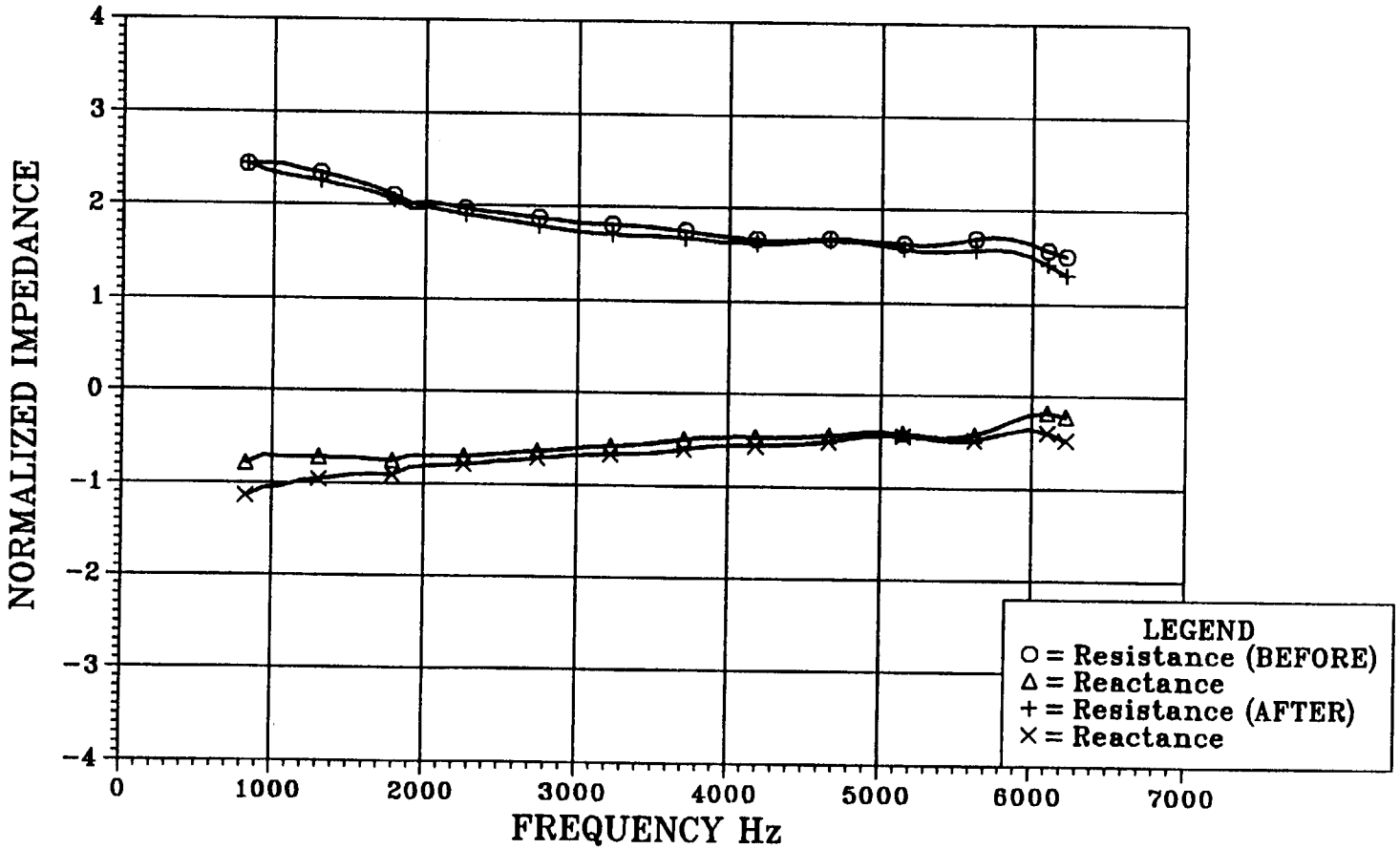

FIGURE 5.3-2 ACOUSTIC IMPEDANCE OF LMSC HTP-1437 FOAM FILLED SANDWICH STRUCTURE SAMPLE #1 AT 145 dB, PRIOR/POST HCF TEST

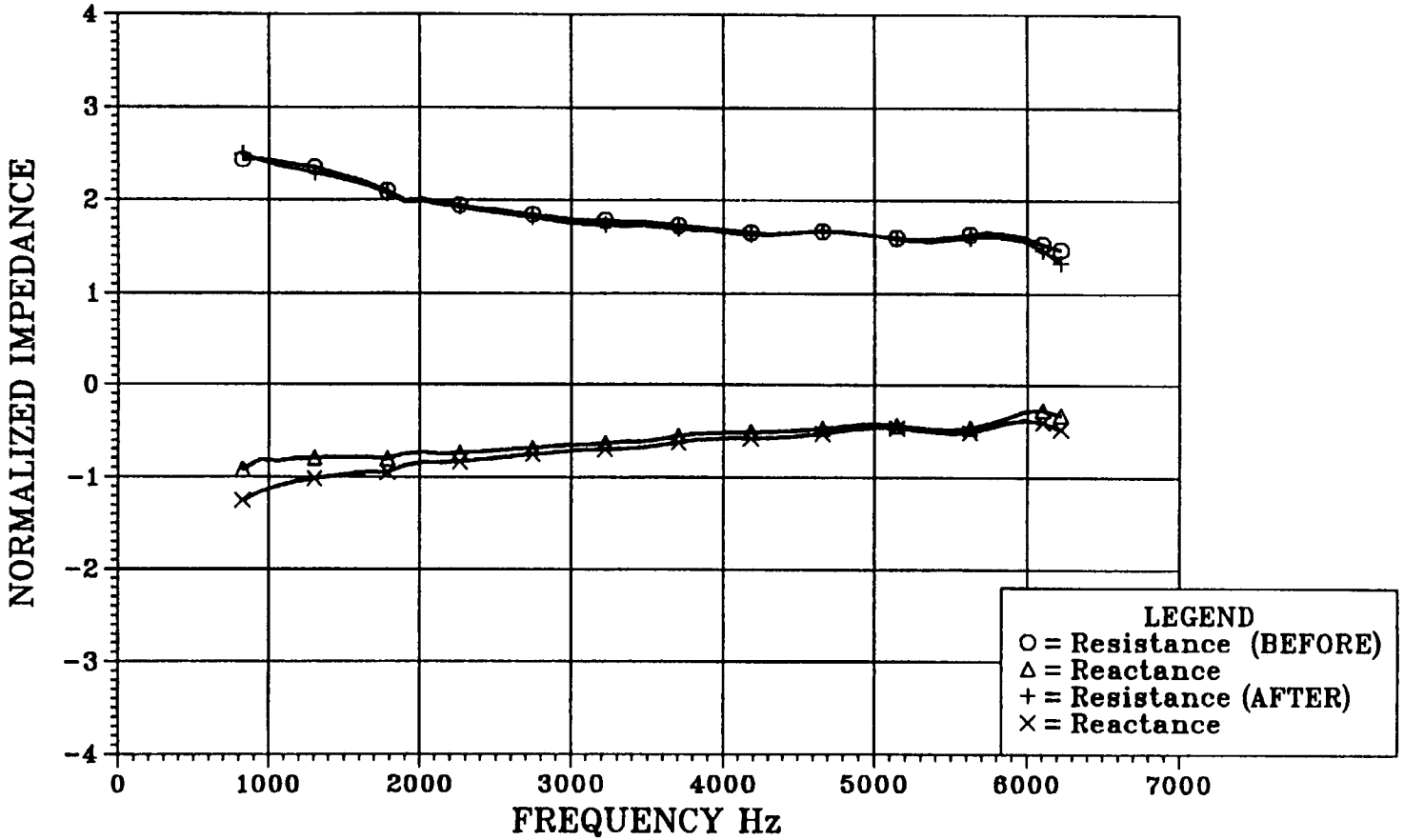

FIGURE 5.3-3 ACOUSTIC IMPEDANCE OF LMSC HTP-1437 FOAM FILLED SANDWICH STRUCTURE SAMPLE #1 AT 148 dB, PRIOR/POST HCF TEST

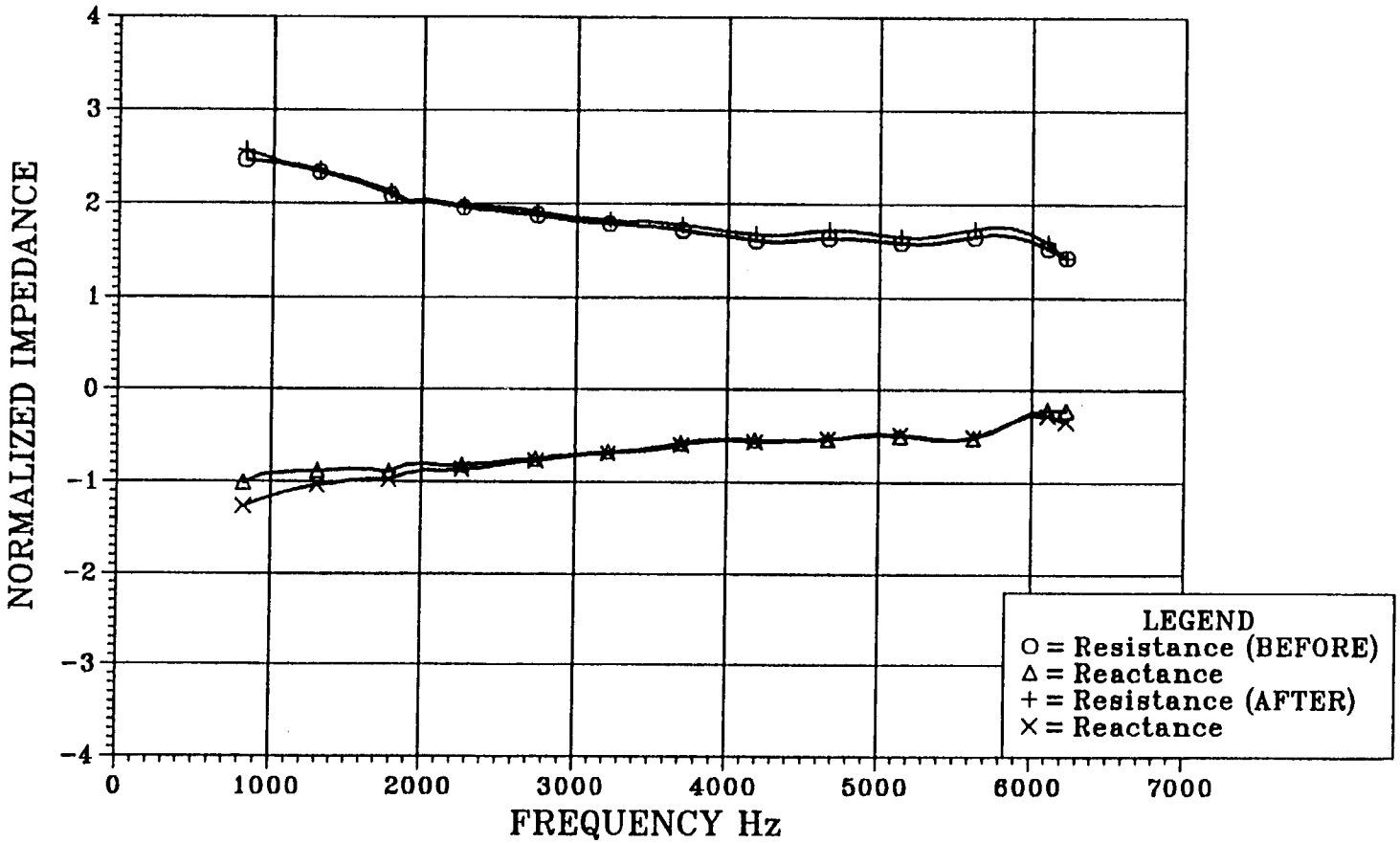

FIGURE 5.3–4 ACOUSTIC IMPEDANCE OF LMSC HTP–1437 FOAM FILLED SANDWICH STRUCTURE SAMPLE #2 AT 140 dB, PRIOR/POST HCF TEST

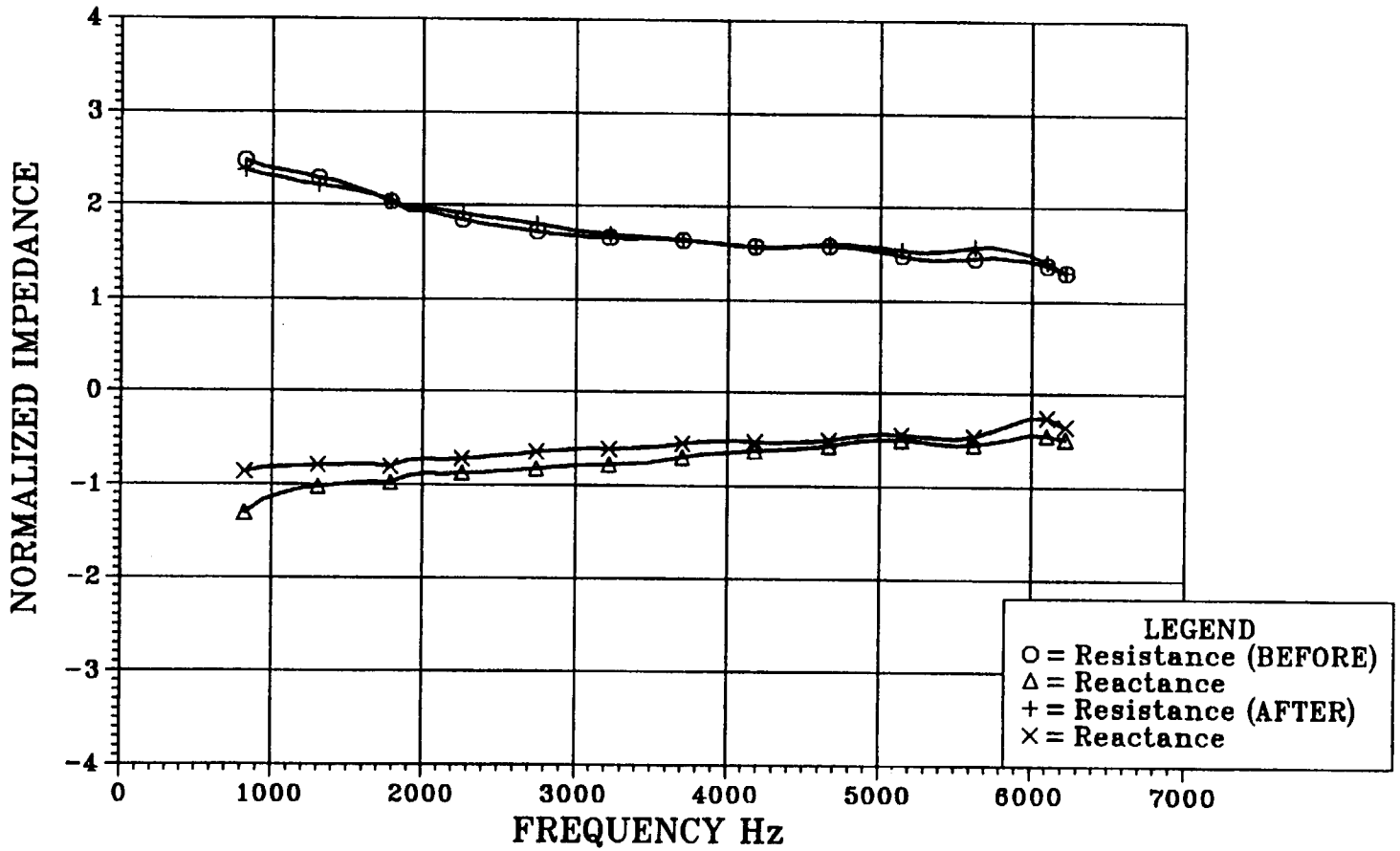

FIGURE 5.3–5 ACOUSTIC IMPEDANCE OF LMSC HTP–1437 FOAM FILLED SANDWICH STRUCTURE SAMPLE #2 AT 145 dB, PRIOR/POST HCF TEST

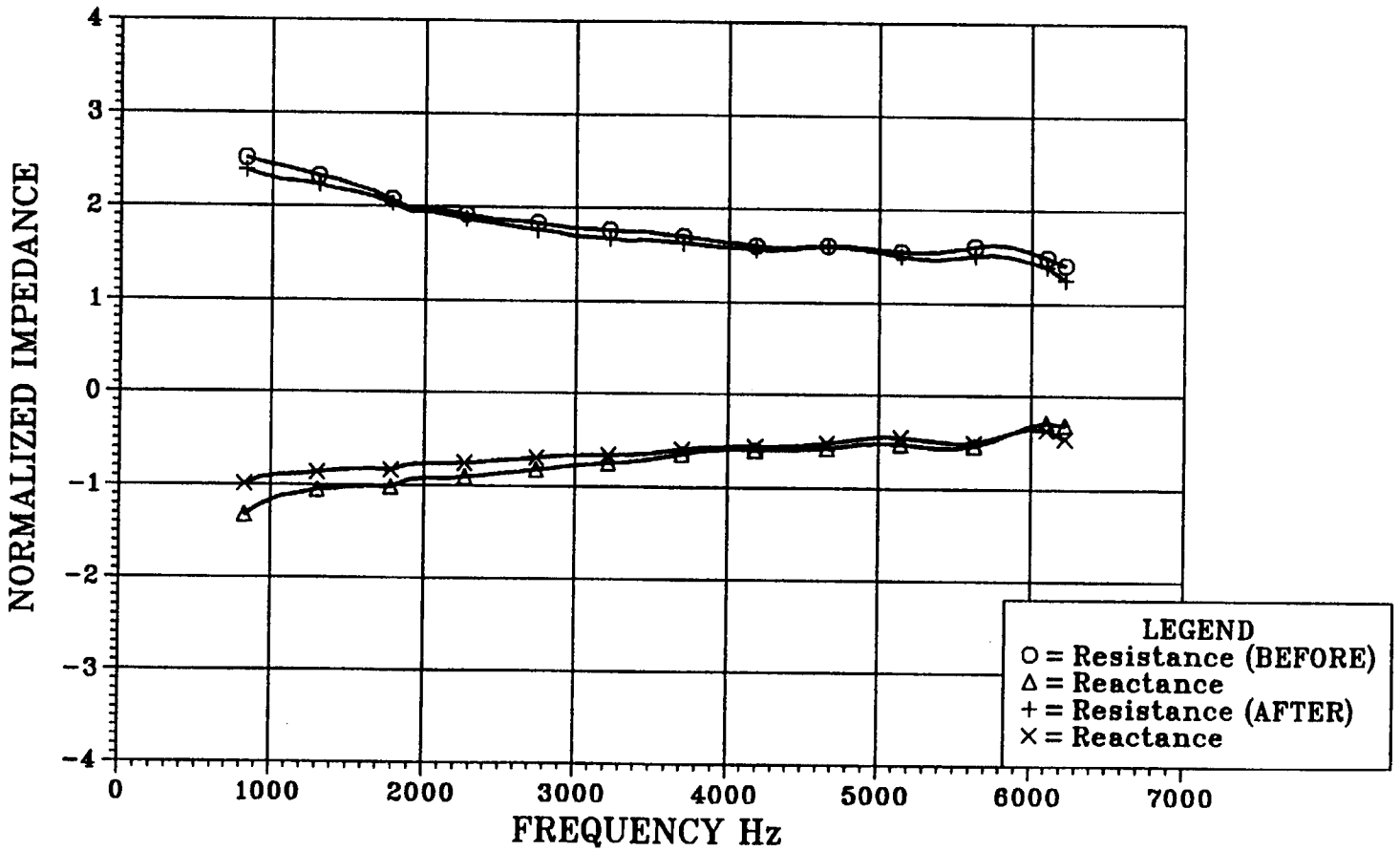

FIGURE 5.3-6 ACOUSTIC IMPEDANCE OF LMSC HTP-1437 FOAM FILLE
SANDWICH STRUCTURE SAMPLE #2 AT 148 dB, PRIOR/POST HCF TEST

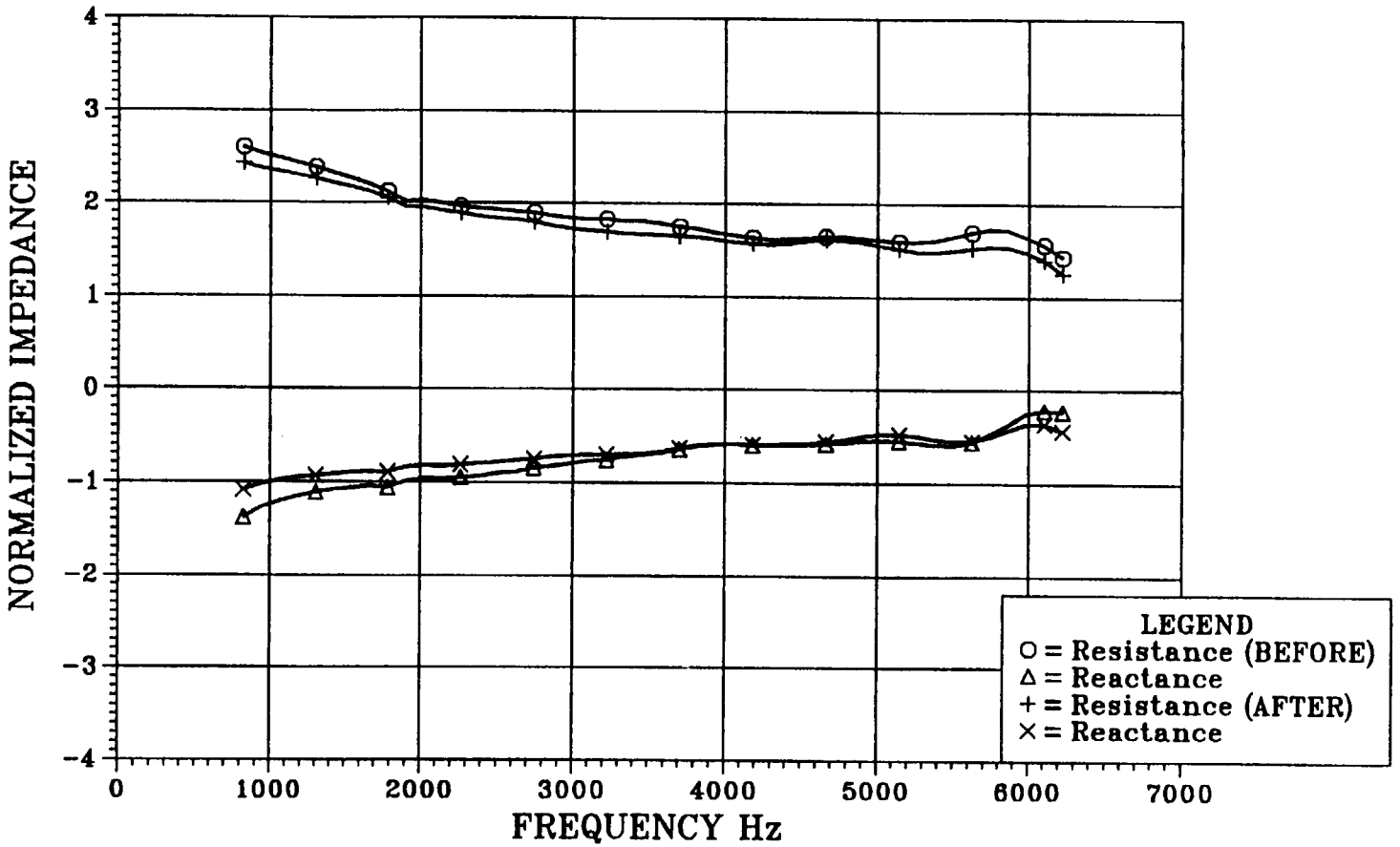

FIGURE 5.3–7 ACOUSTIC IMPEDANCE OF LMSC HTP–1437 FOAM FILLED SANDWICH STRUCTURE SAMPLE #3 AT 140 dB, PRIOR/POST HCF TEST

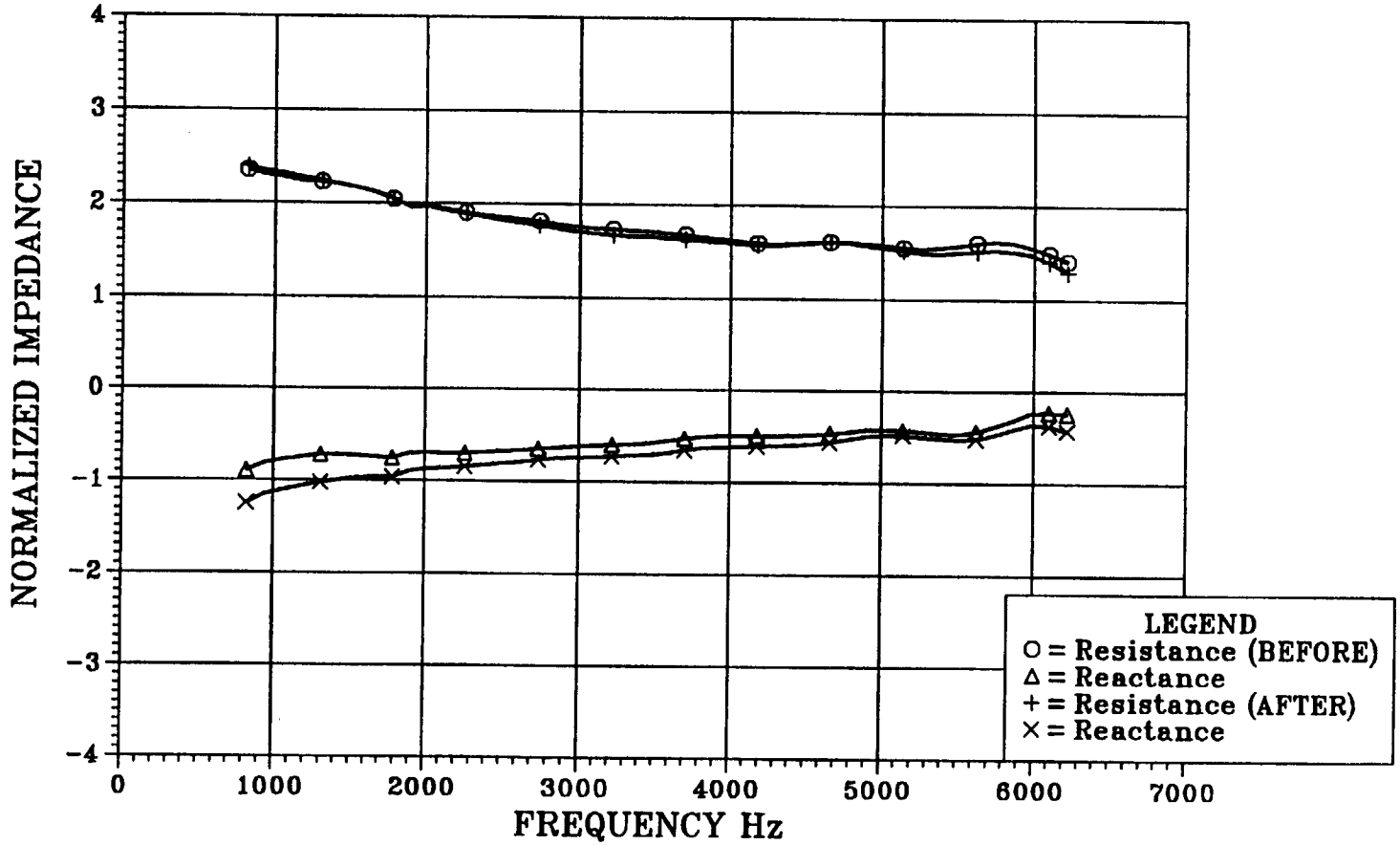

FIGURE 5.3-8 ACOUSTIC IMPEDANCE OF LMSC HTP-1437 FOAM FILLED SANDWICH STRUCTURE SAMPLE #3 AT 145 dB, PRIOR/POST HCF TEST

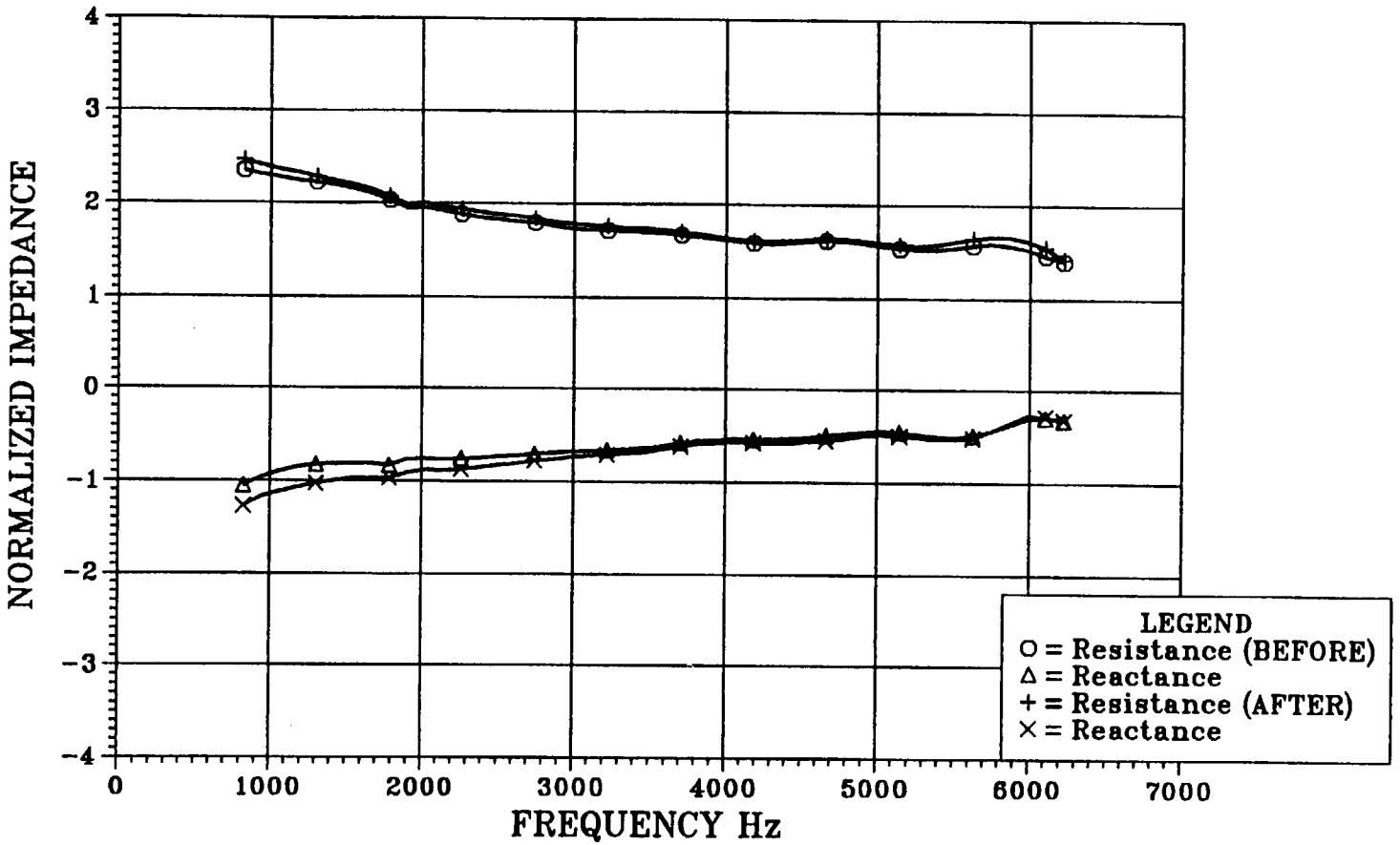

FIGURE 5.3-9 ACOUSTIC IMPEDANCE OF LMSC HTP-1437 FOAM FILLED SANDWICH STRUCTURE SAMPLE #3 AT 148 dB, PRIOR/POST HCF TEST

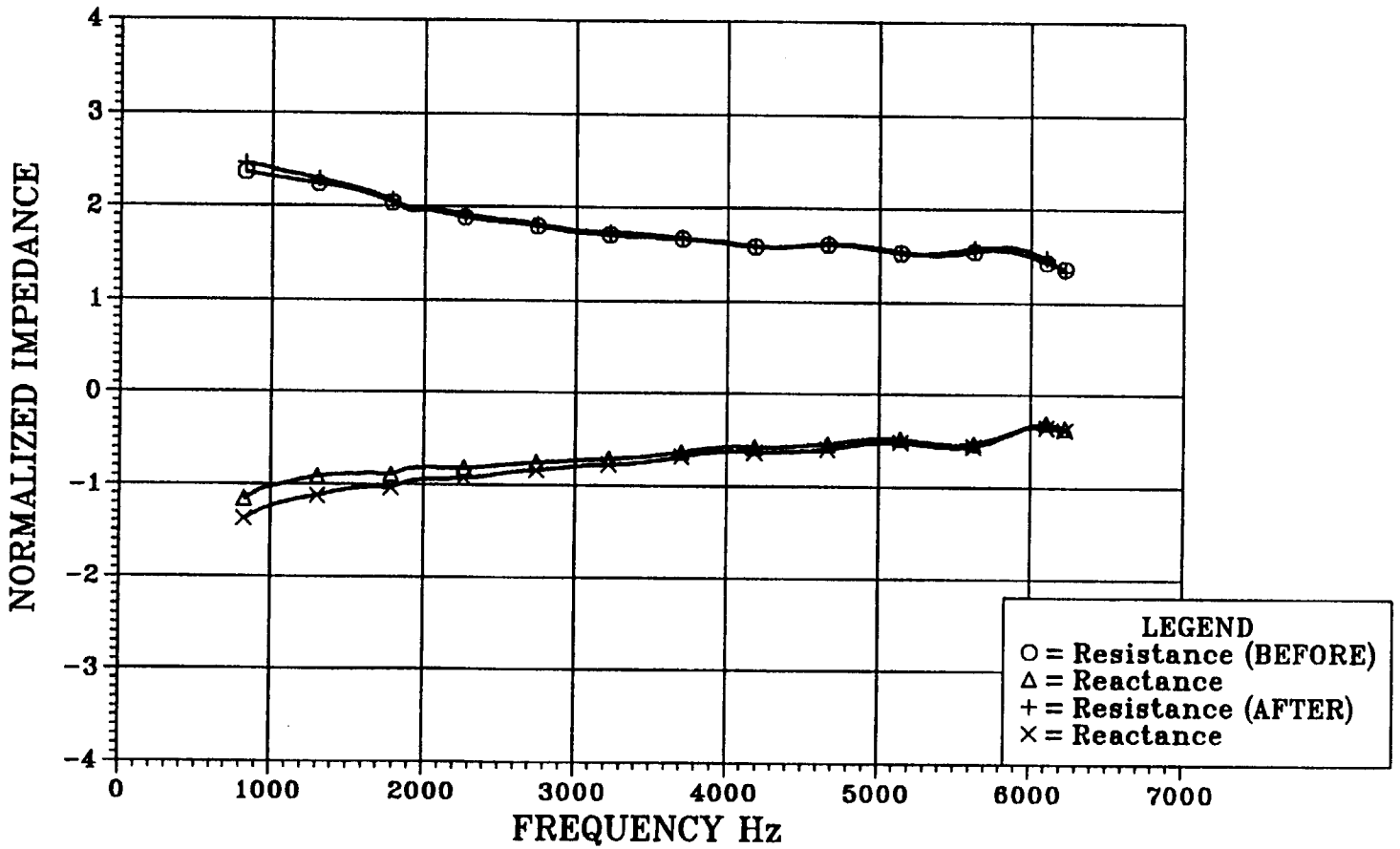

Figure 6.3-1 Sound Wave Distortion Diagram

(Reproduced from Reference 6)

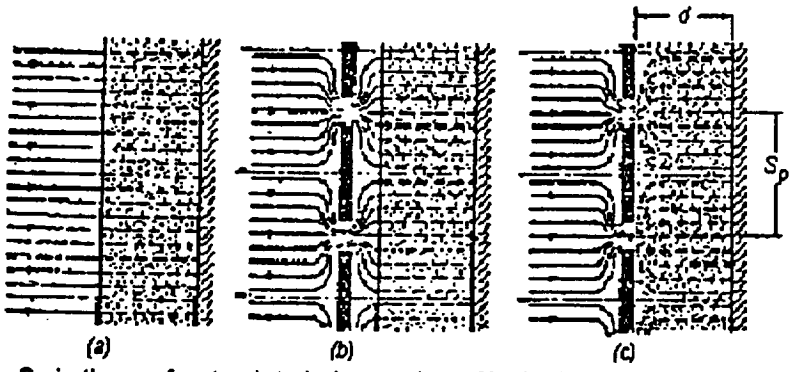

(a) No facing sheet

(b) Small gap between perforated facing and bulk material

(c) No gap between perforated facing and bulk material

S_n is the perforate plate hole spacing; *d* is the bulk thickness

Figure 6.3-2 Function $f(\delta P)$

(Reproduced from Reference 6)

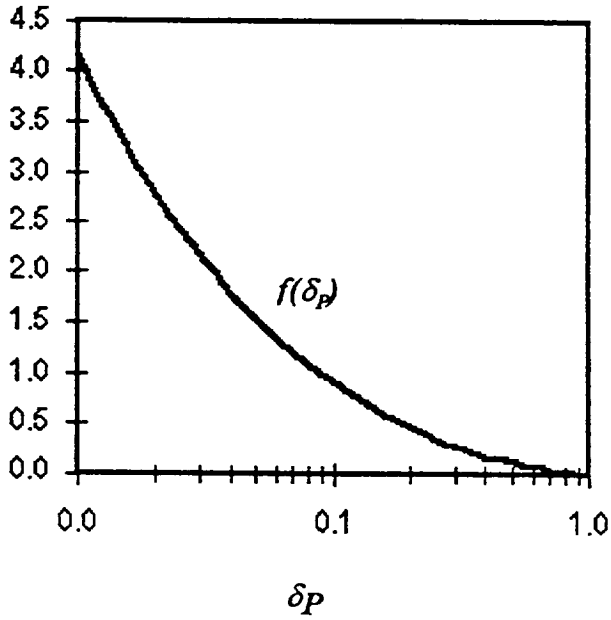

FIGURE 6.5–1 PREDICTED & MEASURED CHARACTERISTIC IMPEDANCE
HTP Foam ID# 11093, 3.3 PCF

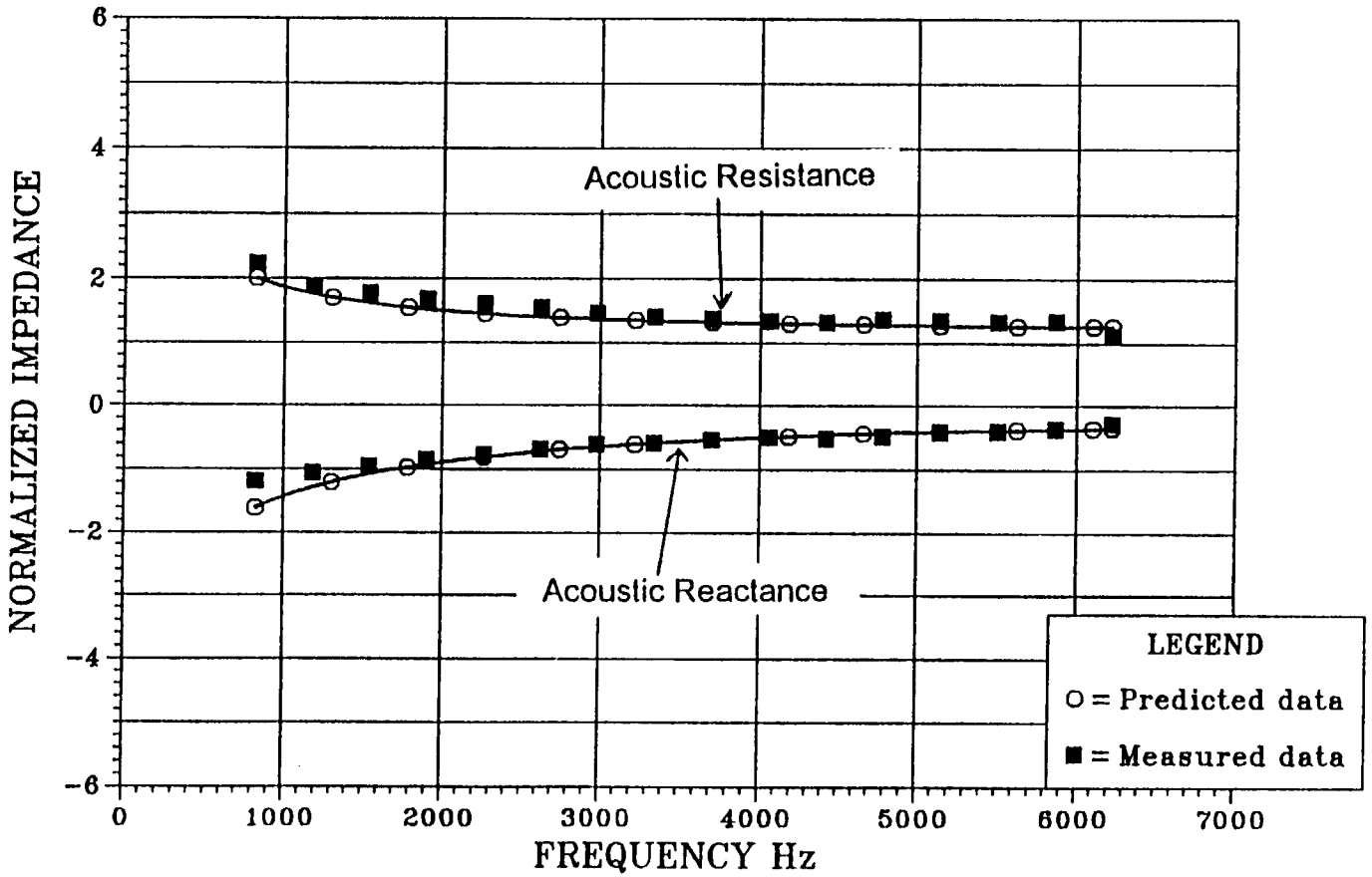

FIGURE 6.5–2 PREDICTED & MEASURED PROPAGATION CONSTANT
HTP Foam ID# 11093, 3.3 PCF

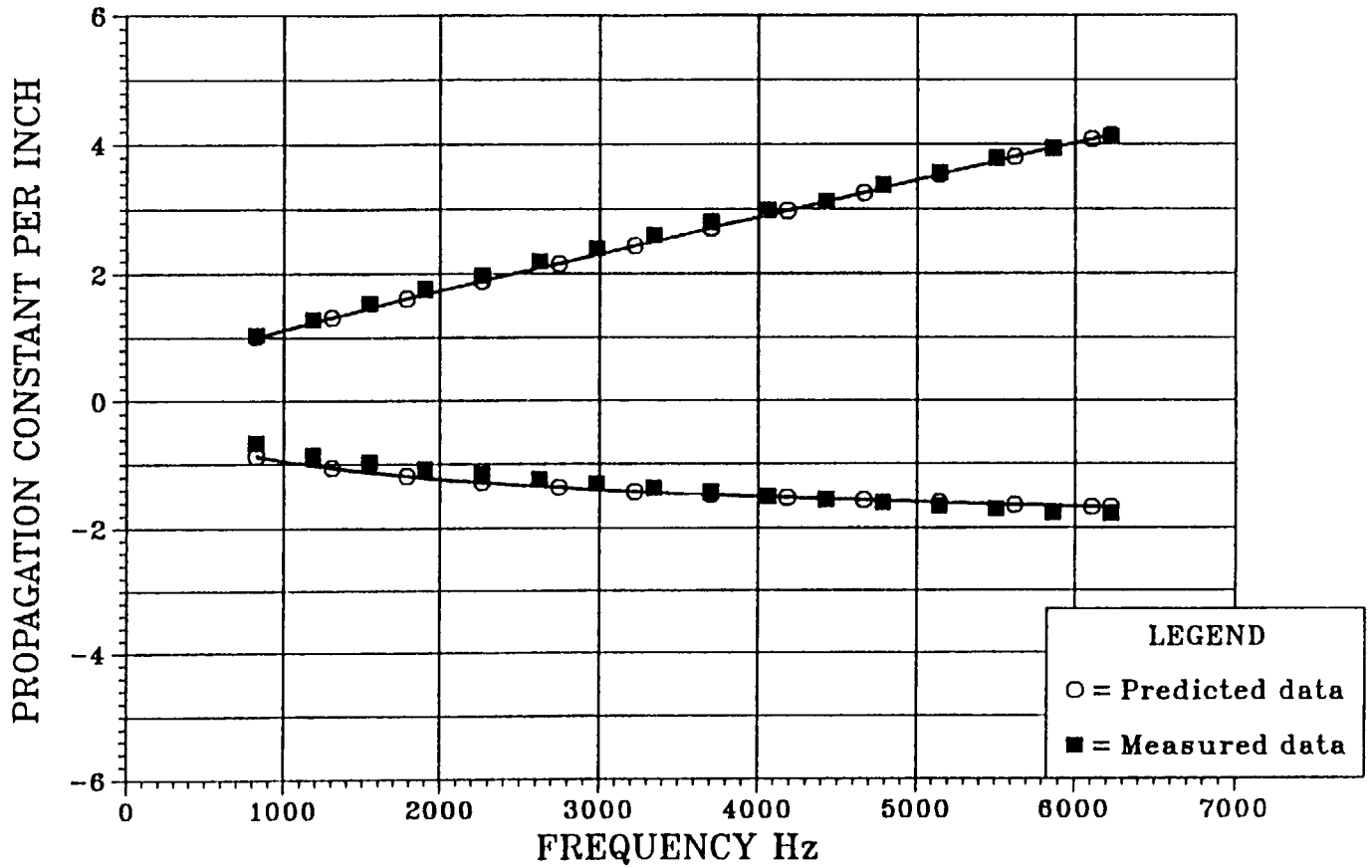

FIGURE 6.5–3 PREDICTED & MEASURED CHARACTERISTIC IMPEDANCE
HTP Foam ID# 1438, 4.91 PCF

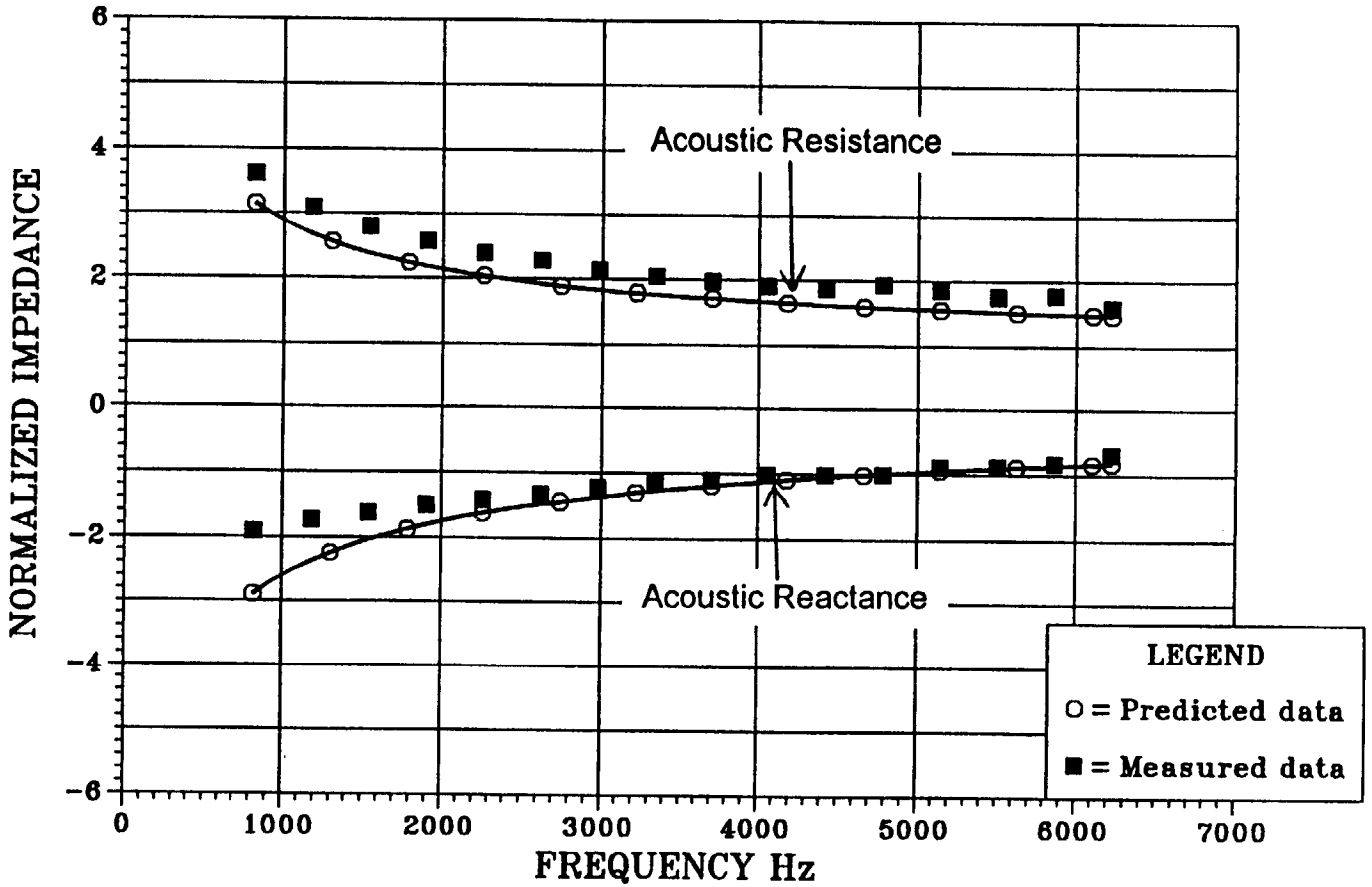

FIGURE 6.5–4 PREDICTED & MEASURED PROPAGATION CONSTANT
HTP Foam ID# 1438, 4.91 PCF

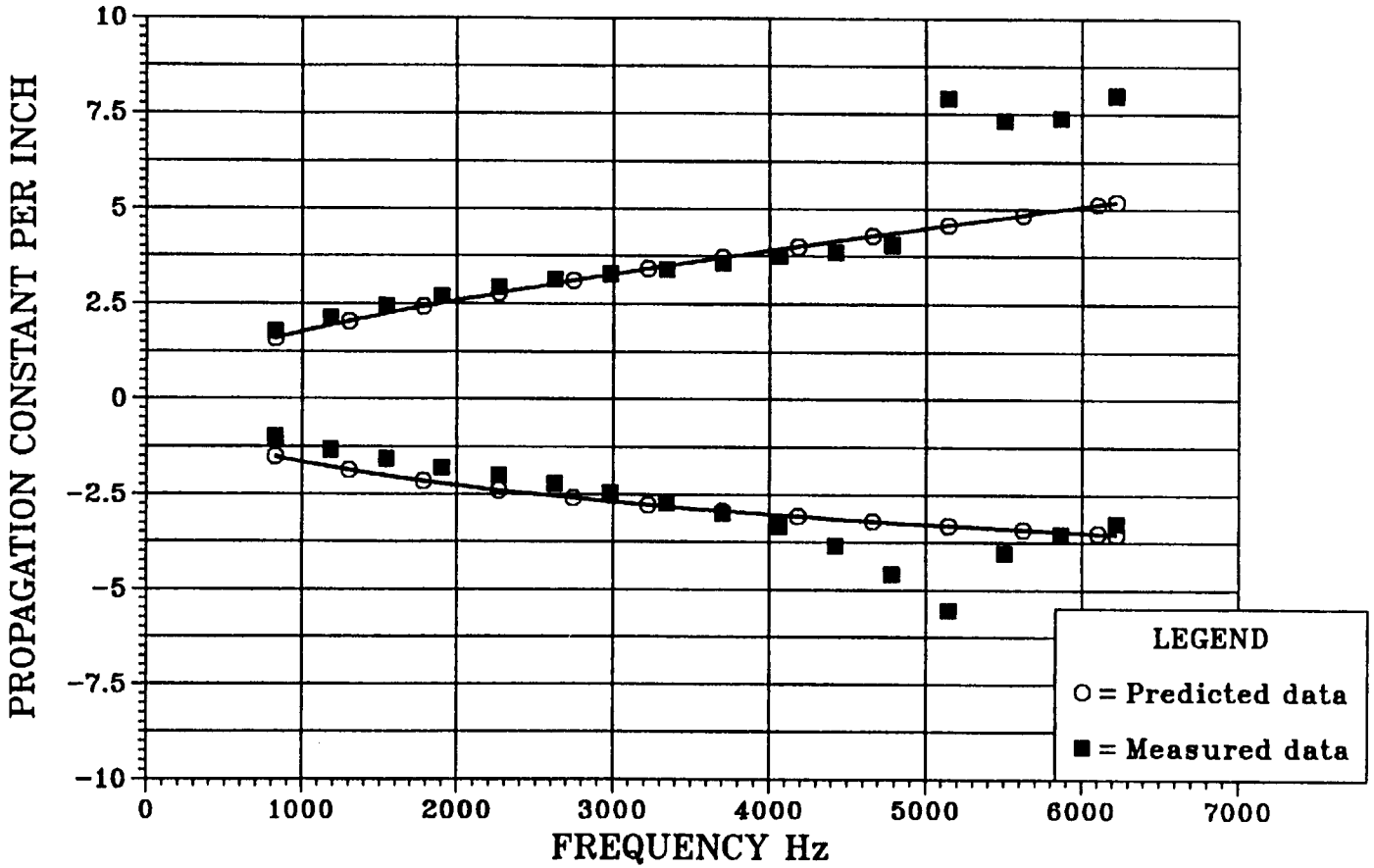

FIGURE 6.5–5 PREDICTED & MEASURED CHARACTERISTIC IMPEDANCE
HTP Foam ID# 1433A, 5.36 PCF

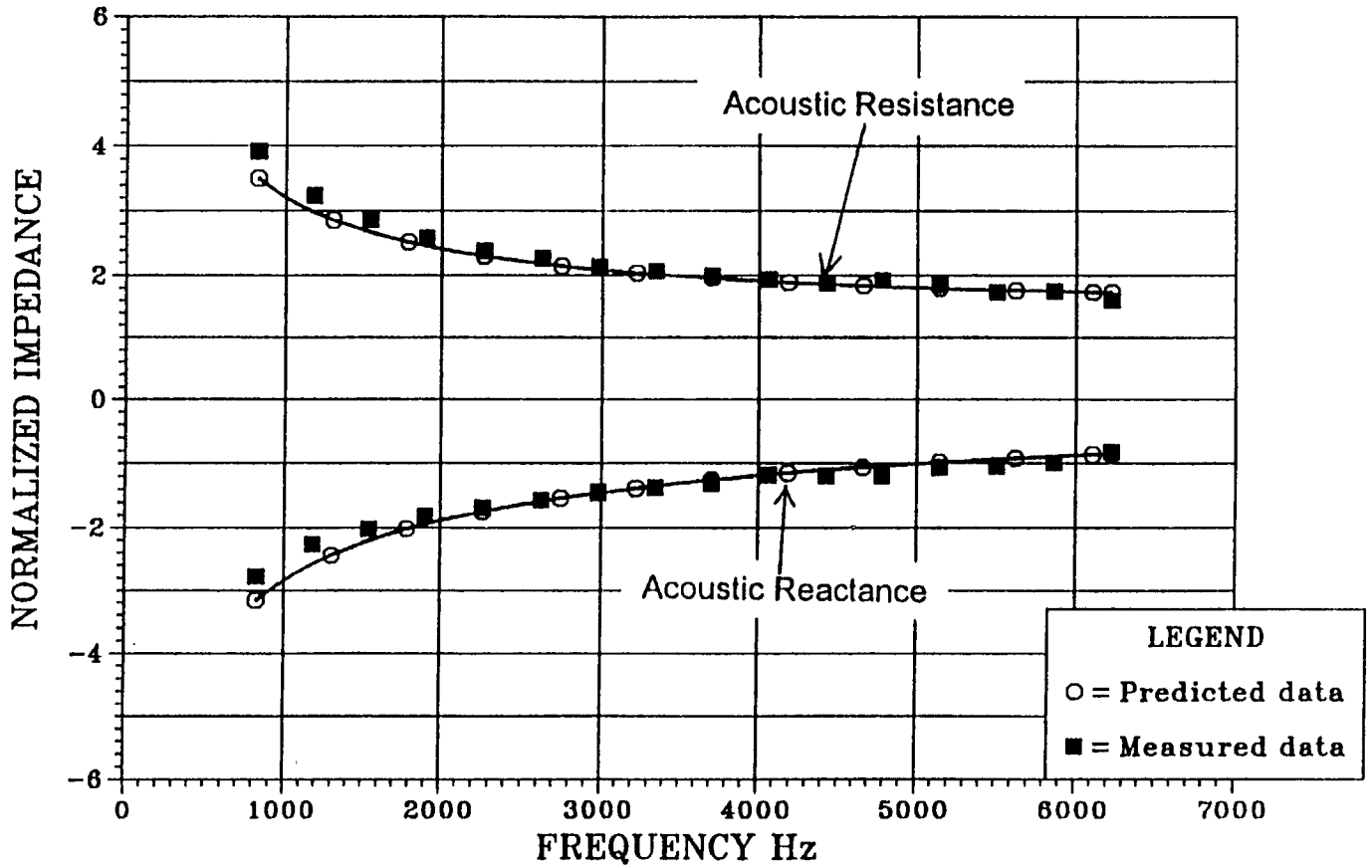

FIGURE 6.5–6 PREDICTED & MEASURED PROPAGATION CONSTANT
HTP Foam ID# 1433A, 5.36 PCF

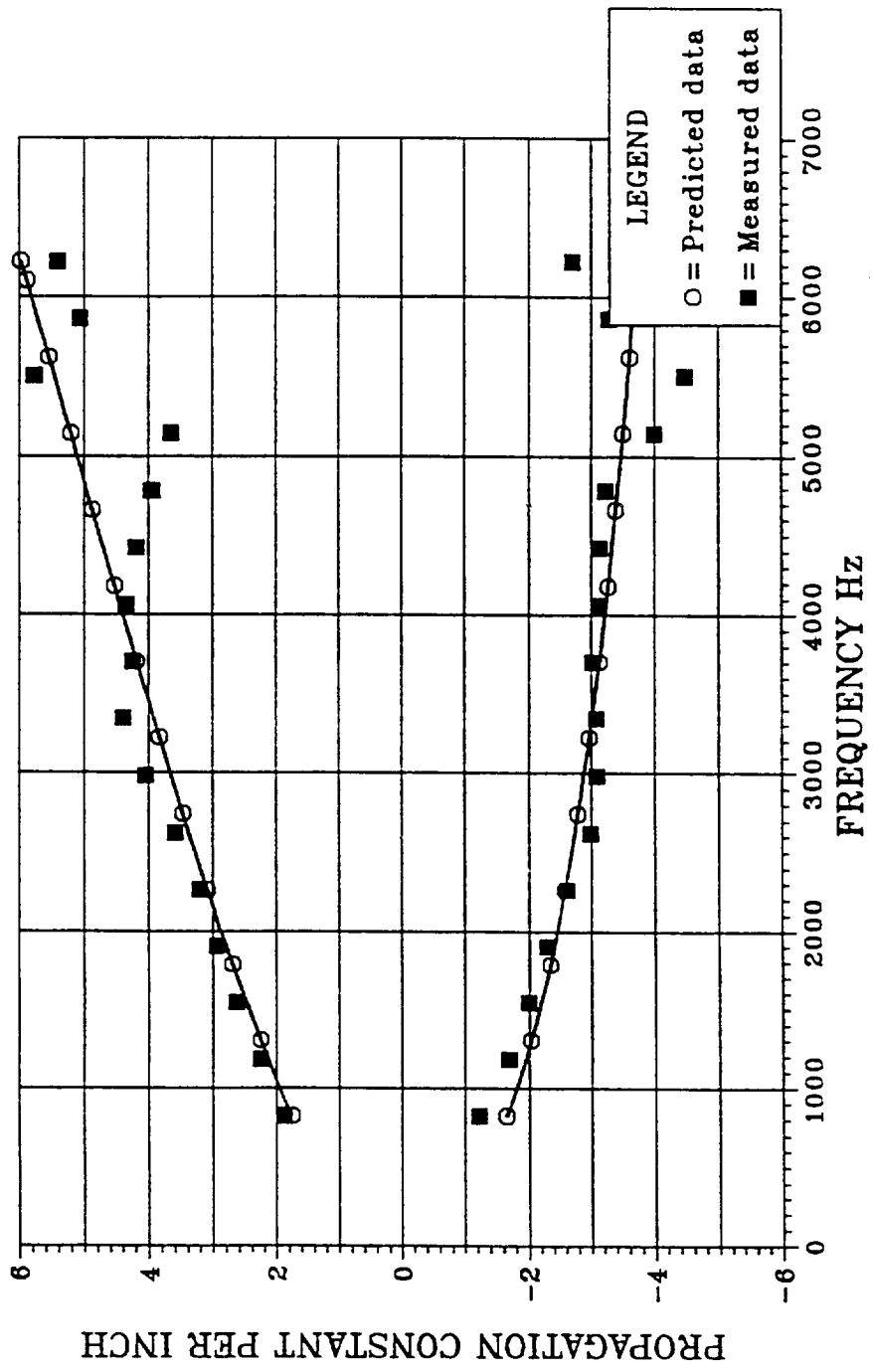

FIGURE 6.5–7 PREDICTED AND MEASURED ACOUSTIC IMPEDANCE
HTP Foam ID# 11093, 3.3 PCF, And 0.5 Inch thick

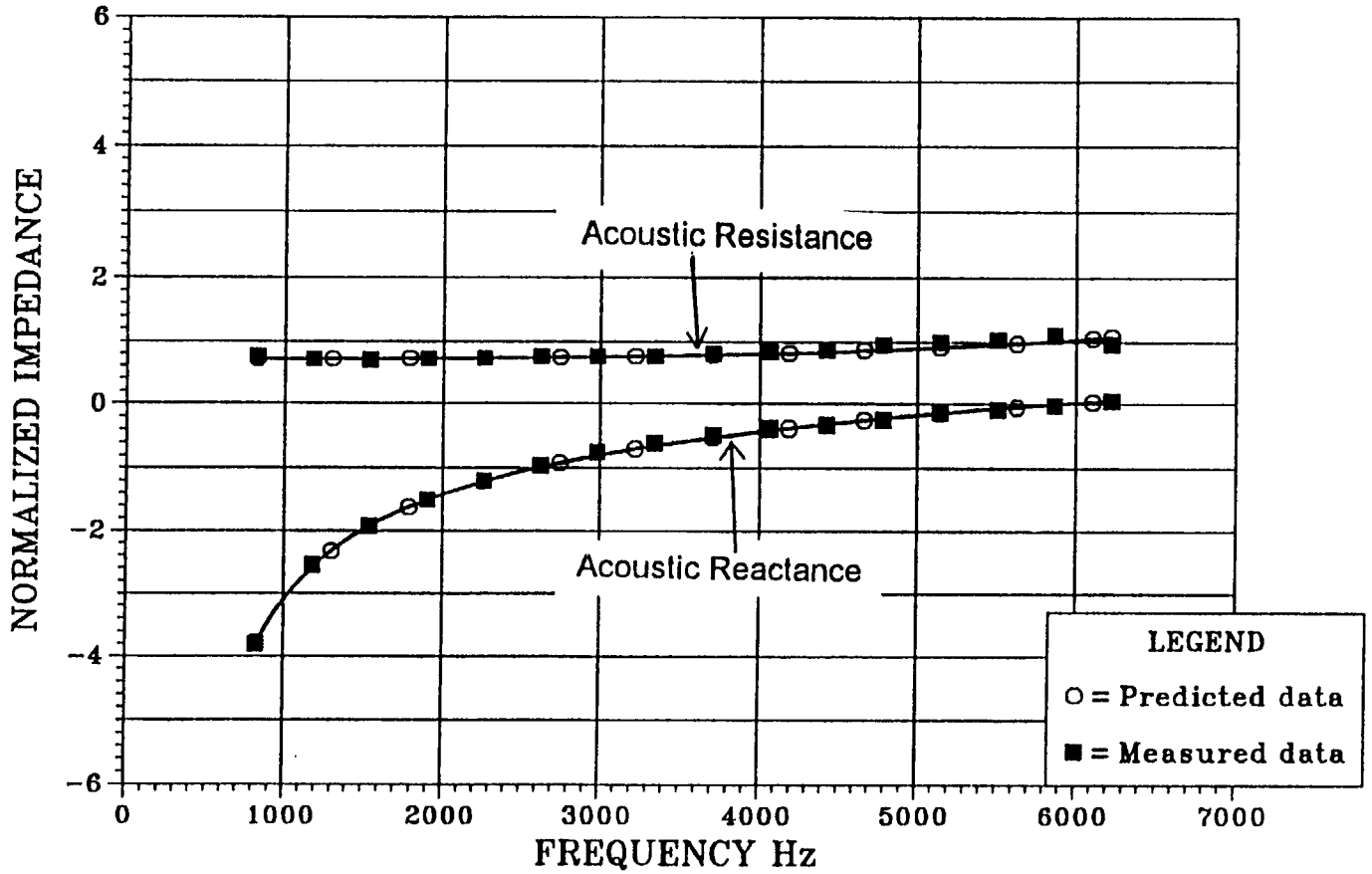

FIGURE 6.5–8 PREDICTED AND MEASURED ACOUSTIC IMPEDANCE
HTP Foam ID# 1438, 4.91 PCF, And 0.55 Inch thick

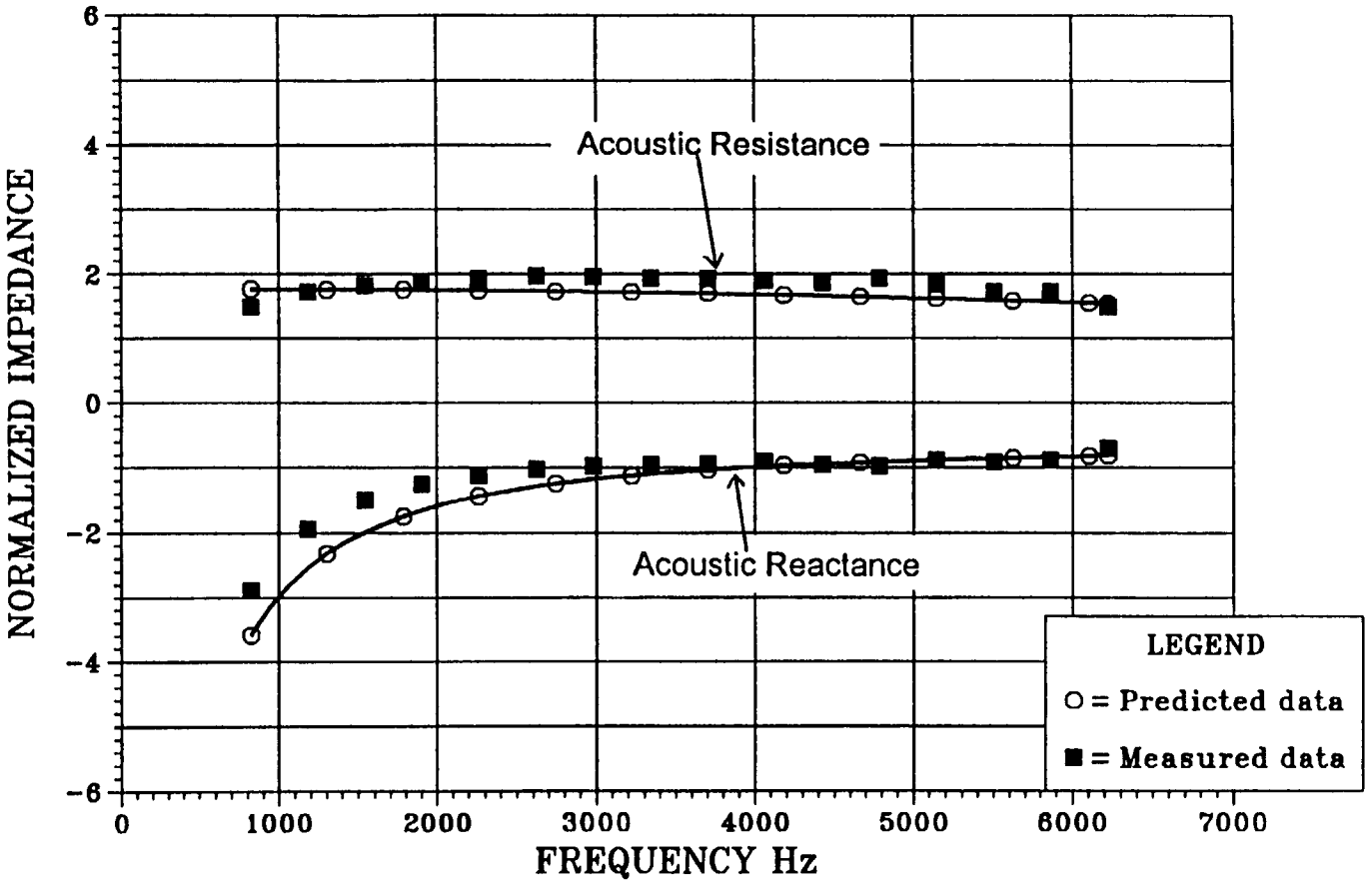

FIGURE 6.5–9 PREDICTED AND MEASURED ACOUSTIC IMPEDANCE
HTP Foam ID# 1433A, 5.36 PCF, And 0.75 Inch Thick

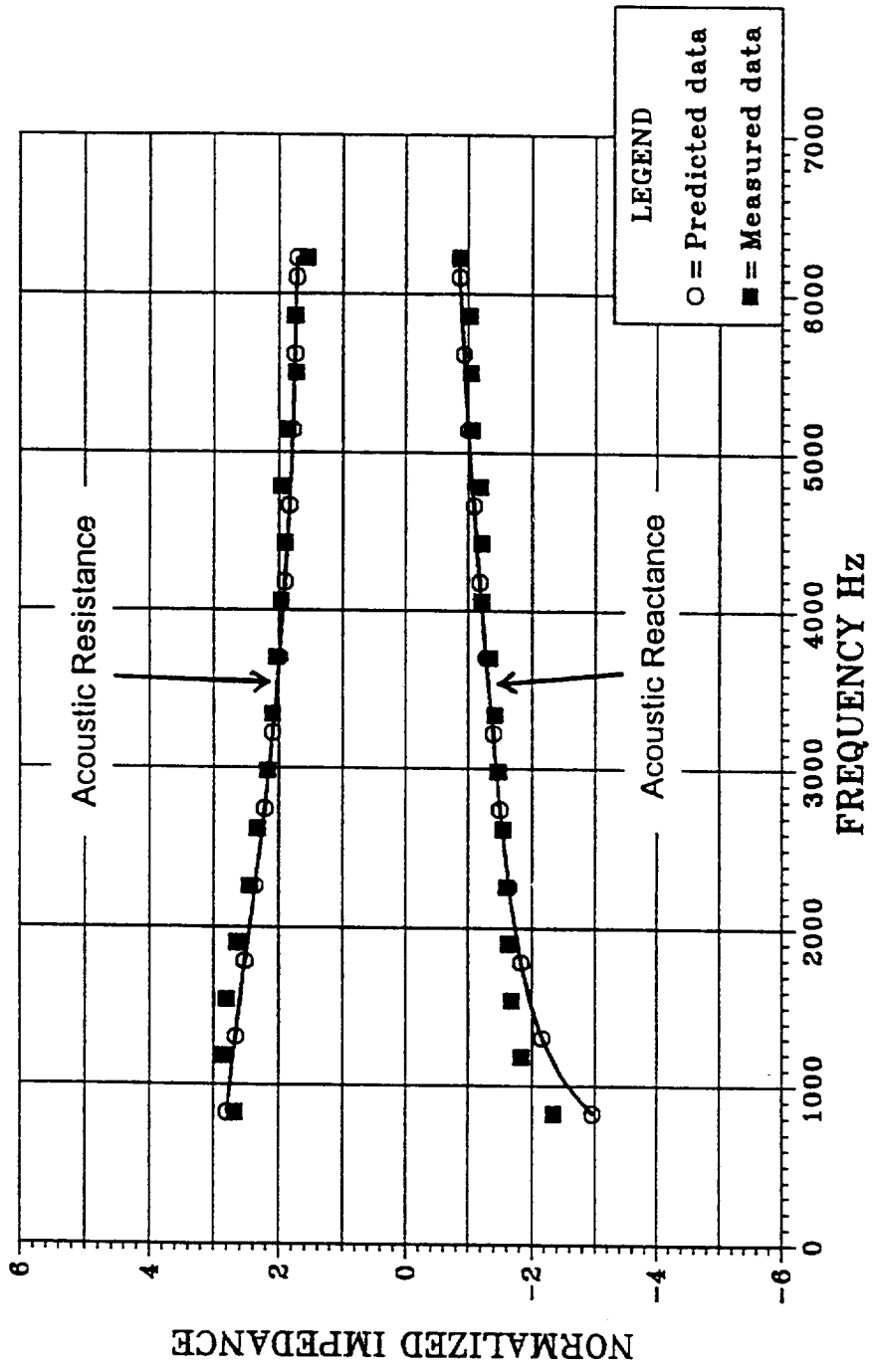

FIGURE 6.5–10 PREDICTED AND MEASURED ACOUSTIC IMPEDANCE
HTP Foam ID# 1437, 4.78 PCF, And 1.0 Inch thick

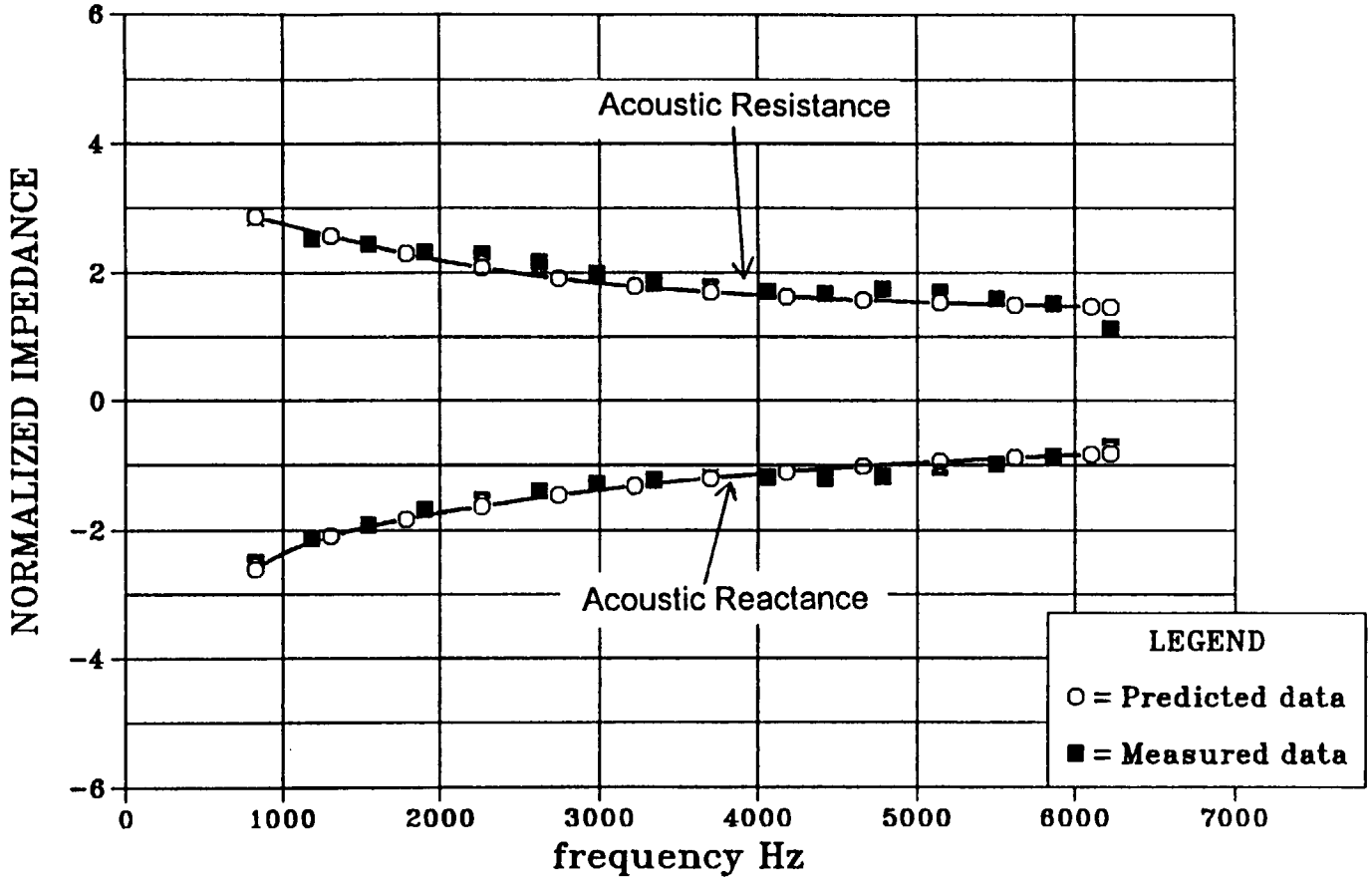

FIGURE 6.5–11 PREDICTED AND MEASURED ACOUSTIC IMPEDANCE
HTP Foam ID# 1107T, 3.94 PCF, And 1.0 Inch thick

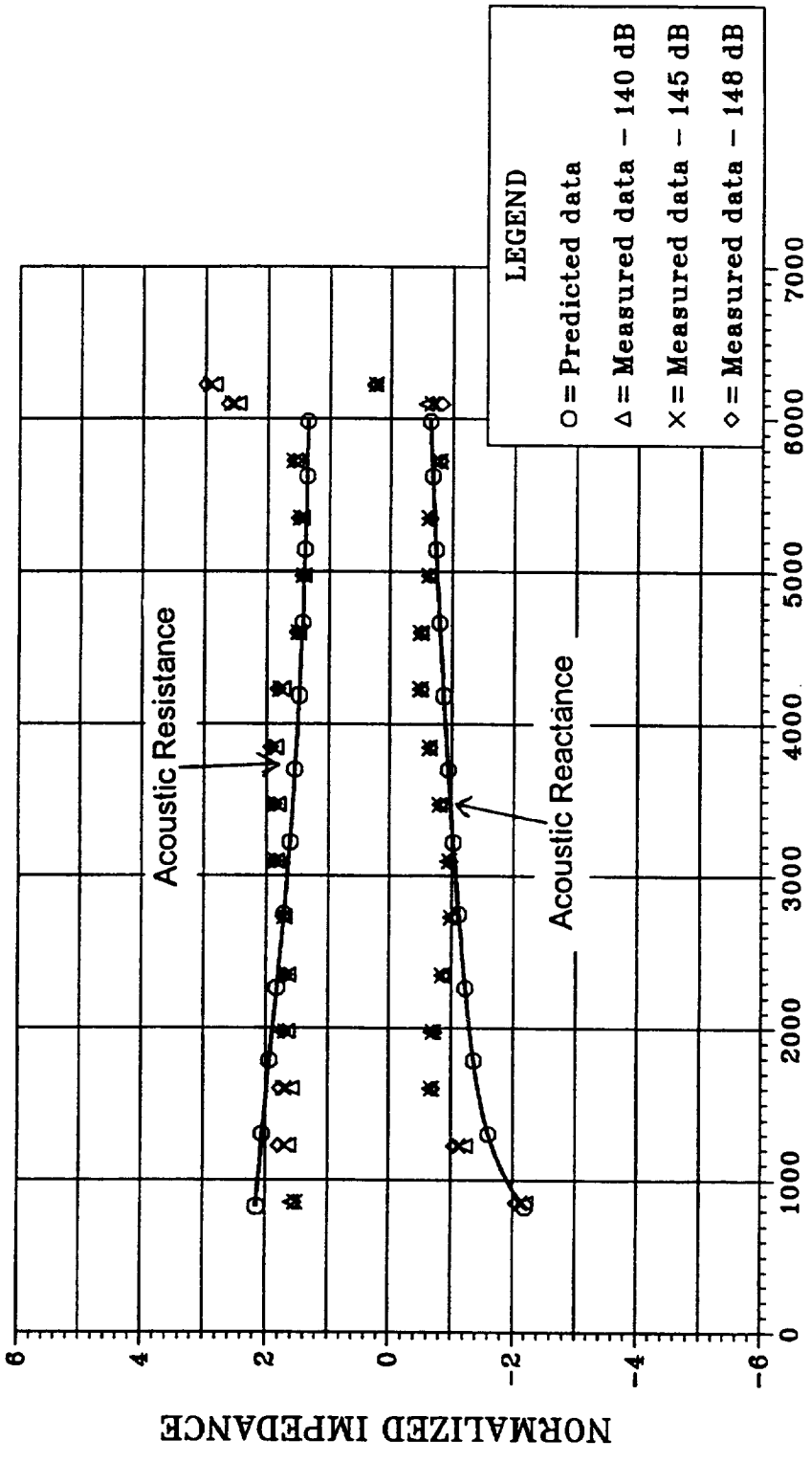

FIGURE 6.5–12 CHARACTERISTIC IMPEDANCE OF LMSC CERAMIC FOAM
HTP 04 PCF

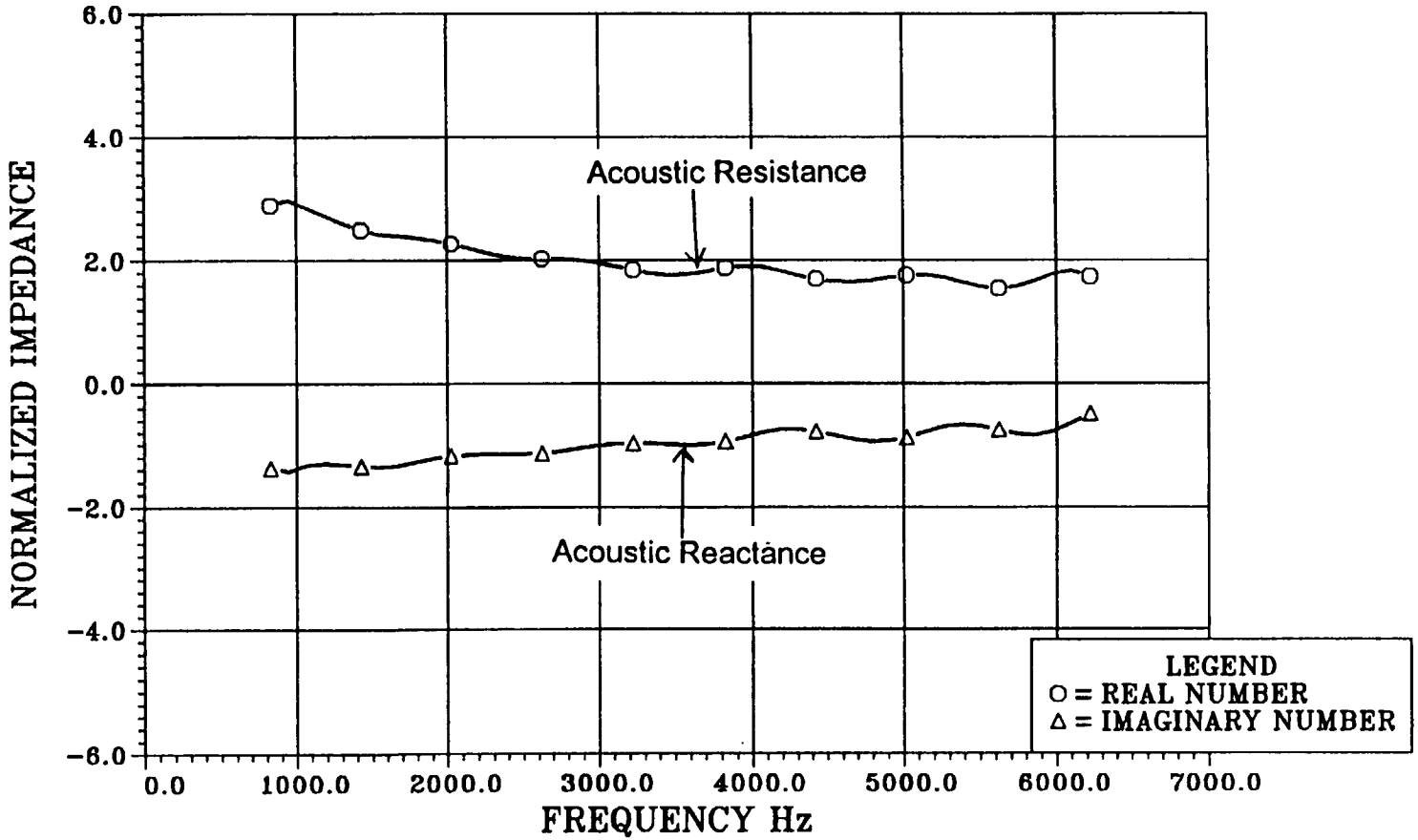

FIGURE 6.5–13 PROPAGATION CONSTANT OF LMSC CERAMIC FOAM
HTP 04 PCF

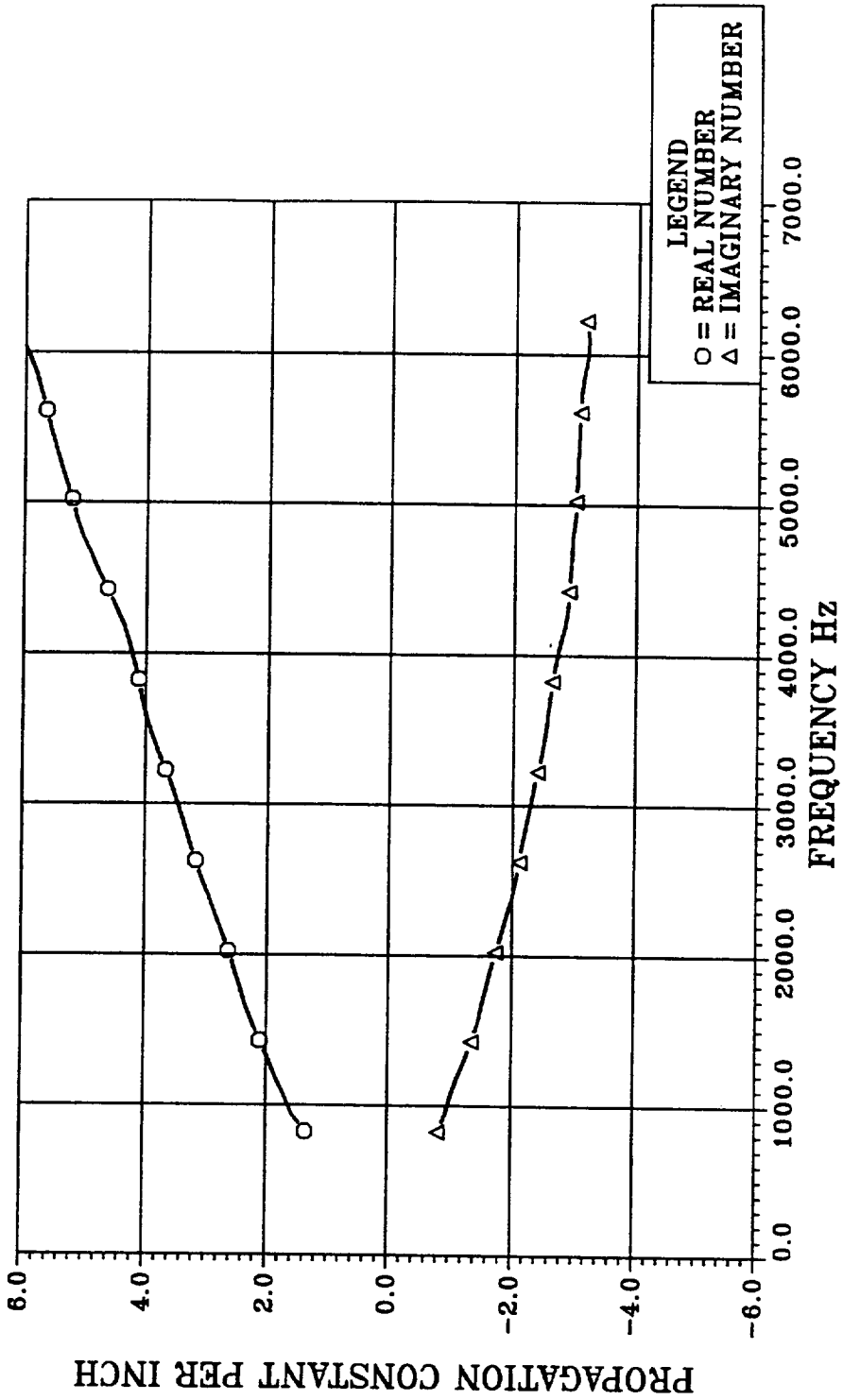

FIGURE 6.5–14 CHARACTERISTIC IMPEDANCE OF LMSC CERAMIC FOAM
HTP 06 PCF

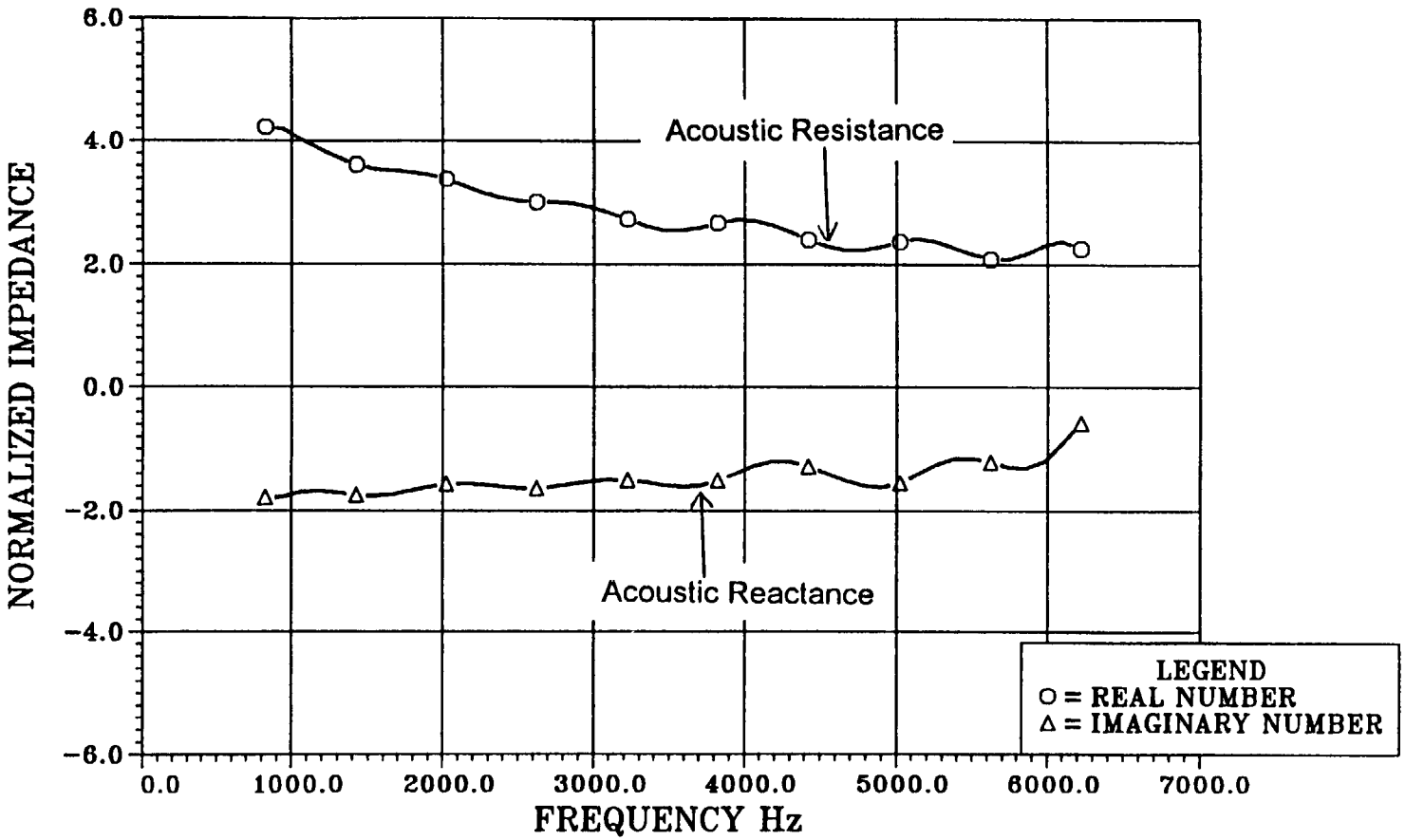

FIGURE 6.5–15 PROPAGATION CONSTANT OF LMSC CERAMIC FOAM
HTP 06 PCF

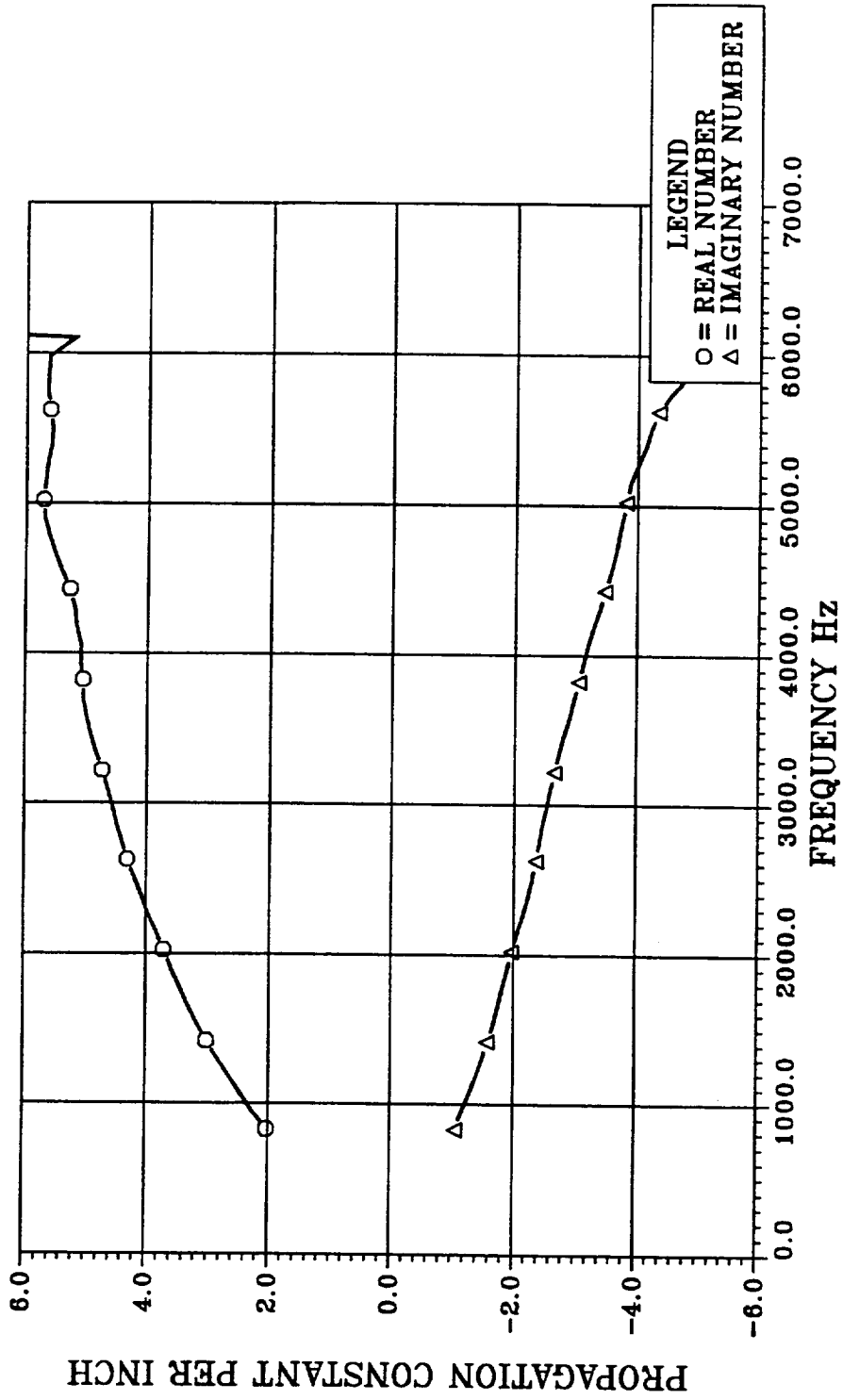

FIGURE 6.5–16 CHARACTERISTIC IMPEDANCE OF LMSC CERAMIC FOAM
HTP 10 PCF

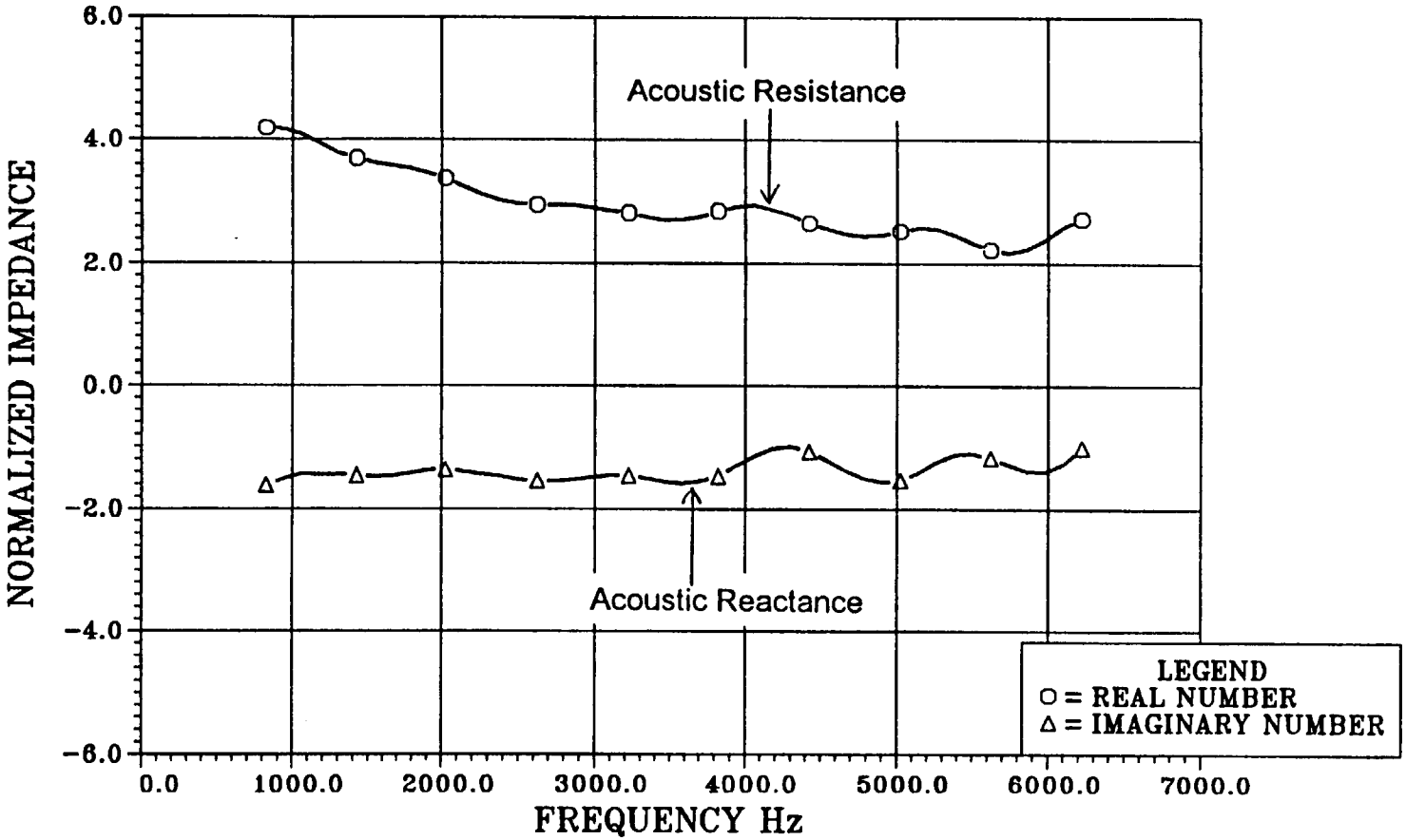

FIGURE 6.5–17 PROPAGATION CONSTANT OF LMSC CERAMIC FOAM
HTP 10 PCF

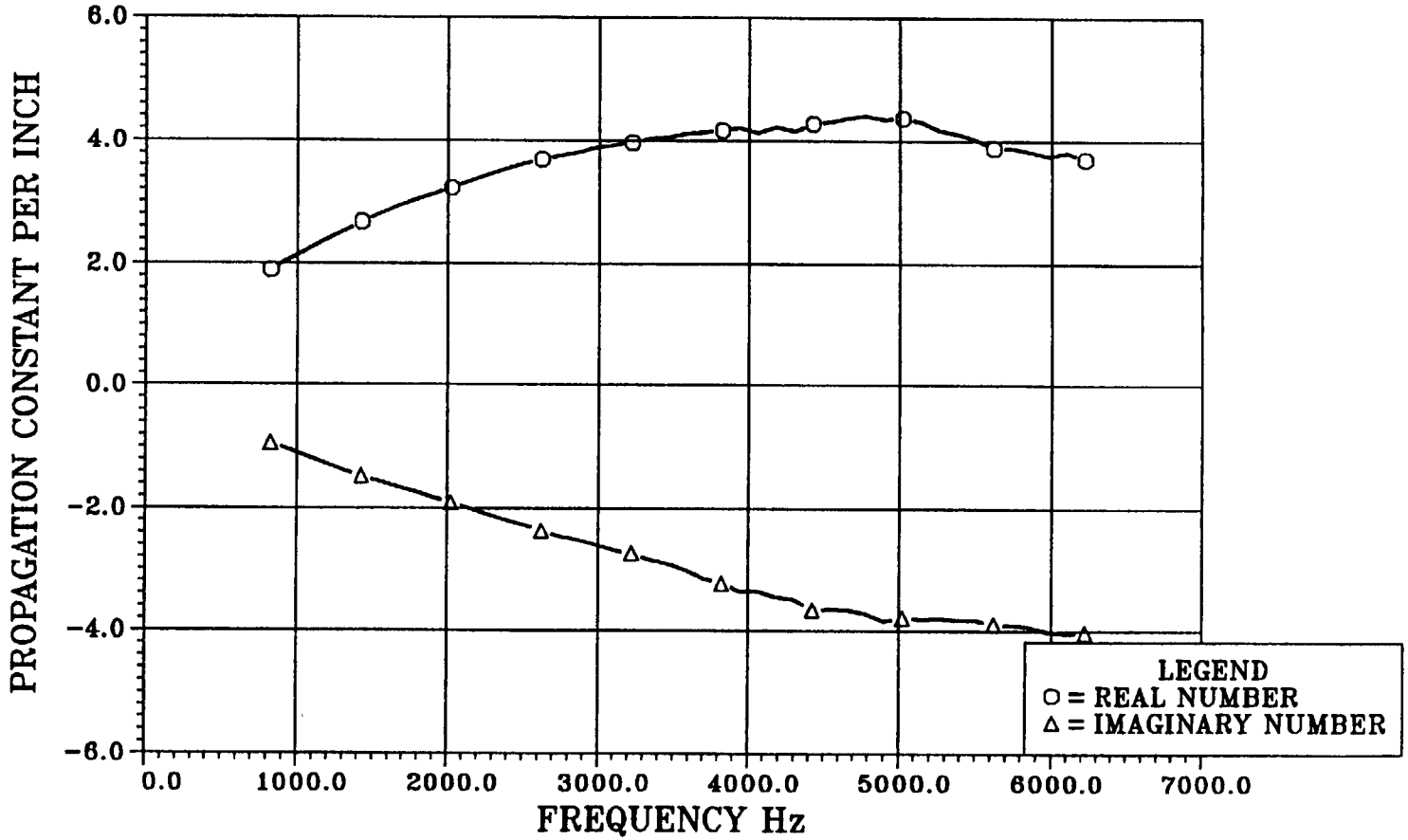

Table 1.1-1. Subsonic and Supersonic Commercial Transport Engine Operational Requirements

Operating Conditions	Subsonic Applications	Supersonic Applications
Max. Temperature Usage	1,100 ^{0}F	$\geq$ 2,000 ^{0}F
Mach Number	0.6	0.8 – 2.4
Overall Sound Pressure	160 dB	165 dB
Projected Life	> 50,000 hours	> 18,000 hours
Noise	FAR 36 Stage 3 by year 2000	FAR 36 Stage 3/no boom over populated areas
Exhaust Gas Components	CO_x, O_x, NO_x, Na (oxides), Cl, S Unburned Fuel	Unburned Fuel, Hydraulic Fluids

Table 3-1. Material and Acoustic Properties of HTP Ceramic Foams

Specimen ID	Thickness (inch)	Density (pcf)	Median Pore Size (microns)	Porosity (LMSC calculated)	Compression Strength (psi - average)	Compression Modules (psi - average)	DC Flow Resistance (rayls/cm - Rohr measured)
14360B	0.752	5.68	--	--	--	--	209
14360D	0.752	5.60	--	--	--	--	202
14360F	0.754	5.58	--	--	--	--	220
14360G	0.743	5.58	--	--	--	--	223
14360J	0.749	5.49	--	--	--	--	208
11093T	0.500	3.30	118.97	0.97062	8.7	287	58
11093B	0.503	3.30	118.97	0.97062	8.7	287	61
11095T	0.505	3.40	117.19	0.96937	14.1	502	55
11095B	0.505	3.40	117.19	0.96937	14.1	502	56
11097T	0.511	3.65	114.77	0.96750	14.6	525	59
11097B	0.504	3.65	114.77	0.96750	14.6	525	73
11105T	0.503	3.91	91.88	0.96519	14.3	563	87
11105B	0.506	3.91	91.88	0.96519	14.3	563	124
11107T	0.504	3.94	86.96	0.96492	11.6	386	102
11107B	0.500	3.94	86.96	0.96492	11.6	386	130
13031T	0.503	3.71	--	--	--	--	41
13031B	0.502	3.71	--	--	--	--	63
1438	0.557	4.91	61.73	0.96066	--	--	167
1433A	0.750"	5.36	57.27	0.95705	--	--	227
HTP-4	--	4.3	62	0.96550	--	--	--
HTP-6	--	7.2	38	0.94320	--	--	--
HTP-10	--	8.2	37	0.93430	--	--	--
HTP-12	--	12.8	26	0.89740	--	--	--
HTP-16	--	20.9	--	--	--	--	--

Table 4.1-1. Material and Acoustic Properties of Down Selected HTP Ceramic Foams

Specimen ID (Application)	Thickness (inch)	Density (pcf)	Median Pore Size (microns)	Porosity (LMMS calculated)	Compression Strength (psi - average)	Compression Modules (psi - average)	DC Flow Resistance (rayls/cm - Rohr measured)
1437 (AST Inlets)	1.0	4.78	56.09	0.96170	--	--	--
11101 (AST Bypass/Exhaust Ducts)	1.0	3.62	105.3	0.96777	--	--	--
11103 (Supersonic Nozzles)	1.0	3.58	96.13	0.97131	--	--	--

Table 5.1-1. Flatwise Tension Strength Test Results - Titanium Sandwich Structure with Ceramic Foam Inserts

Specimen type	Number of Specimens	Mean Strength (psi)	Standard Deviation (psi)
Titanium Sandwich with Uncoated Ceramic Foam*	6	1812	71
Titanium Sandwich with Coated Foam*	6	987	261

* Ti-6Al-4V Face Sheets/Ti-3Al-2.5V 3/8 inch Core

Table 5.2-1. Titanium Sandwich/Ceramic Foam Insert Specimen Dynamic Shaker Test Results

Spec #	Strain Level (RMS$\mu\varepsilon$)	Frequency (HZ)	Temp. (DEG F)	No. of Cycles	Test Results
1	305	196	RT	10^6	No Failure
2	315	196	RT	10^6	No Failure
3	301	170	1000	10^6	No Failure
4	300	181	1000	10^6	No Failure

Table 5.3-1. Titanium Sandwich/Ceramic Foam Insert Specimen (LMMS ID. 1437 with 37% POA Ti Perforate) Dynamic Shaker Test Results

Spec #	Strain Level (RMSμε)	Frequency (HZ)	Temp. (DEG F)	No. of Cycles	Test Results
1	308	281	RT	10^6	No Failure
2	300	190	1000	10^6	No Failure
4	304	278	RT	10^6	No Failure

Table 6.5-1

HTP-4 FOAM (4.3 PCF)

Characteristic Impedance Z0 and Complex wave number Calculation
Case No. = 1 Air RhoC = 41.35 th1= 0.30 th2= 0.60

Freq.	Impedance #1		Impedance #2		C-Impedance		Wave Numbers	
824.0	1.10	-6.39	1.24	-2.81	2.89	-1.37	1.36	-0.82
944.0	1.03	-5.60	1.36	-2.35	2.97	-1.42	1.59	-0.94
1064.0	1.07	-4.88	1.41	-1.98	2.85	-1.32	1.71	-1.02
1184.0	1.05	-4.28	1.45	-1.69	2.73	-1.29	1.85	-1.12
1304.0	0.99	-3.81	1.49	-1.50	2.60	-1.31	1.97	-1.24
1424.0	0.92	-3.43	1.53	-1.36	2.49	-1.34	2.11	-1.35
1544.0	0.91	-3.14	1.59	-1.25	2.42	-1.35	2.23	-1.45
1664.0	0.93	-2.92	1.65	-1.15	2.40	-1.33	2.35	-1.52
1784.0	0.98	-2.72	1.71	-1.06	2.37	-1.27	2.44	-1.59
1904.0	1.02	-2.52	1.75	-0.97	2.33	-1.21	2.53	-1.66
2024.0	1.04	-2.33	1.77	-0.91	2.27	-1.17	2.63	-1.74
2144.0	1.02	-2.15	1.79	-0.87	2.20	-1.15	2.73	-1.83
2264.0	1.00	-1.99	1.79	-0.84	2.12	-1.14	2.84	-1.91
2384.0	0.99	-1.86	1.81	-0.83	2.06	-1.14	2.95	-2.00
2504.0	0.99	-1.76	1.84	-0.83	2.03	-1.14	3.07	-2.06
2624.0	1.00	-1.67	1.88	-0.82	2.03	-1.13	3.17	-2.12
2744.0	1.03	-1.59	1.92	-0.79	2.03	-1.10	3.27	-2.16
2864.0	1.06	-1.49	1.94	-0.76	2.01	-1.05	3.36	-2.22
2984.0	1.07	-1.40	1.93	-0.73	1.97	-1.01	3.45	-2.28
3104.0	1.05	-1.30	1.90	-0.73	1.91	-0.98	3.55	-2.34
3224.0	1.03	-1.21	1.87	-0.74	1.85	-0.97	3.67	-2.40
3344.0	1.01	-1.15	1.85	-0.77	1.79	-0.97	3.79	-2.47
3464.0	1.01	-1.11	1.85	-0.81	1.77	-0.99	3.90	-2.52
3584.0	1.03	-1.08	1.88	-0.84	1.78	-1.00	4.00	-2.56
3704.0	1.08	-1.05	1.93	-0.84	1.82	-0.99	4.07	-2.60
3824.0	1.14	-1.01	1.98	-0.80	1.88	-0.94	4.12	-2.64
3944.0	1.19	-0.95	2.01	-0.75	1.90	-0.88	4.19	-2.69
4064.0	1.22	-0.86	2.00	-0.69	1.90	-0.80	4.27	-2.75
4184.0	1.21	-0.79	1.94	-0.66	1.84	-0.75	4.36	-2.83
4304.0	1.17	-0.74	1.87	-0.69	1.76	-0.75	4.49	-2.88
4424.0	1.14	-0.71	1.81	-0.75	1.70	-0.78	4.63	-2.90
4544.0	1.12	-0.71	1.77	-0.83	1.66	-0.84	4.78	-2.92
4664.0	1.13	-0.72	1.76	-0.91	1.65	-0.90	4.91	-2.94
4784.0	1.16	-0.72	1.78	-0.97	1.67	-0.94	5.05	-2.95
4904.0	1.22	-0.69	1.82	-0.98	1.72	-0.93	5.16	-2.99
5024.0	1.26	-0.63	1.86	-0.93	1.76	-0.88	5.23	-3.00
5144.0	1.29	-0.54	1.86	-0.84	1.77	-0.79	5.33	-3.02
5264.0	1.27	-0.46	1.81	-0.76	1.73	-0.70	5.42	-3.03
5384.0	1.22	-0.42	1.72	-0.73	1.65	-0.67	5.51	-3.04
5504.0	1.18	-0.42	1.64	-0.76	1.58	-0.69	5.59	-3.05
5624.0	1.18	-0.46	1.60	-0.82	1.55	-0.75	5.66	-3.07
5744.0	1.22	-0.49	1.62	-0.90	1.58	-0.82	5.74	-3.08
5864.0	1.31	-0.49	1.70	-0.92	1.67	-0.84	5.82	-3.12
5984.0	1.42	-0.42	1.81	-0.86	1.78	-0.78	5.93	-3.18
6104.0	1.48	-0.29	1.86	-0.72	1.84	-0.64	6.07	-3.20
6224.0	1.42	-0.13	1.74	-0.57	1.74	-0.49	6.30	-3.16

Impedance #1 = measured impedance at a foam thickness of 0.3 inch
Impedance #2 = measured impedance at a foam thickness of 0.6 inch
C- impedance and Wave Number = calculated characteristic impedance and propagation constant (per inch) based on the values of impedance #1 and #2.

Table 6.5-2

HTP-6 FOAM (7.2 PCF)

Characteristic Impedance Z0 and Complex wave number Calculation
Case No. = 1 Air RhoC = 41.35 th1= 0.31 th2= 0.62

Freq.	Impedance #1		Impedance #2		C-Impedance		Wave Numbers	
824.0	1.39	-5.77	2.22	-1.98	4.23	-1.79	2.03	-1.06
944.0	1.41	-5.03	2.46	-1.56	4.20	-1.78	2.26	-1.16
1064.0	1.43	-4.29	2.61	-1.24	4.02	-1.70	2.45	-1.28
1184.0	1.40	-3.75	2.76	-1.03	3.87	-1.69	2.65	-1.39
1304.0	1.38	-3.33	2.91	-0.93	3.73	-1.71	2.84	-1.49
1424.0	1.36	-3.00	3.05	-0.91	3.61	-1.75	3.02	-1.58
1544.0	1.39	-2.74	3.20	-0.92	3.54	-1.76	3.18	-1.68
1664.0	1.45	-2.53	3.34	-0.92	3.52	-1.74	3.33	-1.75
1784.0	1.52	-2.33	3.45	-0.91	3.49	-1.68	3.46	-1.82
1904.0	1.58	-2.14	3.52	-0.91	3.45	-1.62	3.59	-1.90
2024.0	1.62	-1.97	3.53	-0.96	3.38	-1.57	3.71	-1.97
2144.0	1.63	-1.83	3.49	-1.05	3.27	-1.57	3.83	-2.06
2264.0	1.63	-1.71	3.44	-1.17	3.16	-1.58	3.96	-2.15
2384.0	1.64	-1.62	3.39	-1.29	3.08	-1.61	4.08	-2.23
2504.0	1.67	-1.56	3.35	-1.39	3.03	-1.64	4.20	-2.30
2624.0	1.71	-1.49	3.35	-1.47	3.01	-1.64	4.32	-2.36
2744.0	1.76	-1.41	3.34	-1.49	3.01	-1.61	4.41	-2.41
2864.0	1.80	-1.34	3.31	-1.49	2.99	-1.57	4.50	-2.46
2984.0	1.81	-1.27	3.22	-1.48	2.93	-1.53	4.57	-2.53
3104.0	1.80	-1.21	3.10	-1.48	2.84	-1.50	4.65	-2.59
3224.0	1.77	-1.18	2.96	-1.53	2.73	-1.51	4.74	-2.66
3344.0	1.75	-1.16	2.83	-1.59	2.62	-1.54	4.84	-2.73
3464.0	1.76	-1.17	2.73	-1.66	2.55	-1.59	4.93	-2.81
3584.0	1.81	-1.18	2.70	-1.69	2.55	-1.61	5.00	-2.90
3704.0	1.88	-1.16	2.73	-1.68	2.59	-1.60	5.06	-2.97
3824.0	1.97	-1.11	2.79	-1.58	2.67	-1.51	5.06	-3.05
3944.0	2.03	-1.04	2.83	-1.47	2.72	-1.40	5.10	-3.12
4064.0	2.06	-0.95	2.82	-1.33	2.71	-1.27	5.10	-3.19
4184.0	2.05	-0.89	2.73	-1.25	2.64	-1.20	5.17	-3.28
4304.0	1.99	-0.90	2.60	-1.25	2.53	-1.20	5.20	-3.38
4424.0	1.93	-0.95	2.46	-1.33	2.40	-1.28	5.28	-3.47
4544.0	1.91	-1.03	2.34	-1.44	2.30	-1.39	5.41	-3.56
4664.0	1.90	-1.12	2.27	-1.56	2.24	-1.50	5.52	-3.64
4784.0	1.94	-1.19	2.26	-1.65	2.24	-1.59	5.62	-3.70
4904.0	2.01	-1.20	2.30	-1.67	2.29	-1.62	5.70	-3.76
5024.0	2.09	-1.15	2.38	-1.60	2.37	-1.55	5.72	-3.82
5144.0	2.12	-1.05	2.43	-1.45	2.42	-1.40	5.69	-3.88
5264.0	2.09	-0.94	2.38	-1.29	2.37	-1.25	5.66	-4.00
5384.0	2.01	-0.89	2.28	-1.18	2.27	-1.15	5.60	-4.13
5504.0	1.93	-0.92	2.18	-1.16	2.17	-1.15	5.58	-4.22
5624.0	1.88	-0.98	2.09	-1.23	2.09	-1.21	5.62	-4.34
5744.0	1.92	-1.07	2.09	-1.30	2.09	-1.29	5.66	-4.54
5864.0	2.02	-1.11	2.18	-1.31	2.18	-1.30	5.65	-4.81
5984.0	2.17	-1.05	2.31	-1.20	2.31	-1.19	5.63	-5.26
6104.0	2.29	-0.86	2.38	-0.90	2.38	-0.90	5.22	-5.27
6224.0	2.28	-0.65	2.25	-0.58	2.26	-0.58	11.80	-6.77

Impedance #1 = measured impedance at a foam thickness of 0.31 inch
Impedance #2 = measured impedance at a foam thickness of 0.62 inch
C- impedance and Wave Number = calculated characteristic impedance and propagation constant (per inch) based on the values of impedance #1 and #2.

Table 6.5-3

HTP-10 FOAM (8.2 PCF)

Characteristic Impedance Z0 and Complex wave number Calculation
Case No. = 1 Air RhoC = 40.97 thi= 0.43 th2= 0.87

Freq.	Impedance #1		Impedance #2		C-Impedance		Wave Numbers	
824.0	1.52	-3.95	2.89	-0.91	4.19	-1.62	1.90	-0.94
944.0	1.70	-3.40	3.23	-0.66	4.18	-1.51	2.07	-1.04
1064.0	1.82	-2.91	3.49	-0.55	4.09	-1.43	2.22	-1.15
1184.0	1.85	-2.51	3.66	-0.60	3.93	-1.44	2.38	-1.26
1304.0	1.89	-2.20	3.75	-0.72	3.78	-1.44	2.52	-1.38
1424.0	1.93	-1.97	3.82	-0.88	3.69	-1.46	2.67	-1.48
1544.0	1.99	-1.79	3.85	-1.02	3.62	-1.48	2.80	-1.57
1664.0	2.07	-1.63	3.85	-1.12	3.58	-1.46	2.92	-1.66
1784.0	2.14	-1.48	3.83	-1.17	3.54	-1.42	3.03	-1.74
1904.0	2.19	-1.35	3.75	-1.21	3.47	-1.37	3.12	-1.83
2024.0	2.21	-1.25	3.63	-1.28	3.38	-1.36	3.22	-1.92
2144.0	2.21	-1.19	3.47	-1.36	3.25	-1.39	3.33	-2.00
2264.0	2.21	-1.15	3.31	-1.44	3.13	-1.43	3.43	-2.10
2384.0	2.22	-1.14	3.18	-1.52	3.03	-1.47	3.53	-2.19
2504.0	2.25	-1.16	3.10	-1.59	2.98	-1.53	3.62	-2.27
2624.0	2.31	-1.16	3.06	-1.62	2.96	-1.55	3.69	-2.37
2744.0	2.37	-1.16	3.03	-1.61	2.96	-1.55	3.75	-2.46
2864.0	2.41	-1.14	3.02	-1.58	2.96	-1.53	3.80	-2.52
2984.0	2.43	-1.10	2.96	-1.54	2.92	-1.49	3.88	-2.60
3104.0	2.44	-1.08	2.91	-1.50	2.87	-1.45	3.92	-2.69
3224.0	2.44	-1.09	2.85	-1.51	2.83	-1.46	3.97	-2.75
3344.0	2.43	-1.14	2.78	-1.55	2.76	-1.51	4.04	-2.85
3464.0	2.42	-1.20	2.72	-1.60	2.71	-1.56	4.06	-2.92
3584.0	2.47	-1.25	2.73	-1.62	2.72	-1.59	4.12	-3.02
3704.0	2.54	-1.24	2.77	-1.58	2.76	-1.55	4.14	-3.16
3824.0	2.65	-1.18	2.87	-1.49	2.86	-1.47	4.17	-3.24
3944.0	2.73	-1.04	2.93	-1.31	2.93	-1.30	4.21	-3.36
4064.0	2.73	-0.91	2.97	-1.15	2.96	-1.14	4.13	-3.36
4184.0	2.69	-0.80	2.88	-1.04	2.88	-1.02	4.23	-3.45
4304.0	2.60	-0.79	2.80	-1.00	2.80	-0.99	4.16	-3.49
4424.0	2.53	-0.88	2.66	-1.08	2.66	-1.07	4.28	-3.67
4544.0	2.45	-1.02	2.57	-1.22	2.57	-1.21	4.31	-3.66
4664.0	2.39	-1.16	2.49	-1.38	2.49	-1.37	4.37	-3.67
4784.0	2.37	-1.30	2.45	-1.51	2.45	-1.50	4.41	-3.73
4904.0	2.39	-1.37	2.47	-1.57	2.47	-1.56	4.35	-3.85
5024.0	2.44	-1.34	2.52	-1.55	2.53	-1.54	4.37	-3.80
5144.0	2.48	-1.23	2.58	-1.42	2.58	-1.41	4.31	-3.82
5264.0	2.45	-1.08	2.57	-1.24	2.57	-1.24	4.18	-3.81
5384.0	2.34	-0.98	2.47	-1.13	2.47	-1.12	4.12	-3.83
5504.0	2.22	-0.97	2.35	-1.11	2.34	-1.10	4.03	-3.63
5624.0	2.11	-1.06	2.24	-1.17	2.23	-1.17	3.88	-3.90
5744.0	2.06	-1.17	2.19	-1.29	2.18	-1.28	3.88	-3.91
5864.0	2.11	-1.27	2.24	-1.39	2.24	-1.38	3.82	-3.94
5984.0	2.26	-1.30	2.40	-1.40	2.39	-1.39	3.75	-4.02
6104.0	2.46	-1.17	2.60	-1.27	2.60	-1.27	3.81	-4.04
6224.0	2.58	-0.94	2.74	-1.01	2.73	-1.01	3.70	-4.03

Impedance #1 = measured impedance at a foam thickness of 0.43 inch
Impedance #2 = measured impedance at a foam thickness of 0.87 inch
C- impedance and Wave Number = calculated characteristic impedance and propagation constant (per inch) based on the values of impedance #1 and #2.

REPORT DOCUMENTATION PAGE

Form Approved
OMB No. 0704-0188

1. AGENCY USE ONLY (*Leave blank*)	2. REPORT DATE	3. REPORT TYPE AND DATES COVERED
	July 1997	Contractor Report

4. TITLE AND SUBTITLE
Lightweight Ceramics for Aeroacoustic Applications

5. FUNDING NUMBERS
C NAS1-20102
TA 4
WU 538-03-12-02

6. AUTHOR(S)
H. W. Kwan, G. T. Spamer, J. Yu, and B. Yasukawa

7. PERFORMING ORGANIZATION NAME(S) AND ADDRESS(ES)
Rohr, Inc.; Chula Vista, California *and*

Lockheed Martin Missiles and Space; Sunnyvale, California

8. PERFORMING ORGANIZATION REPORT NUMBER

9. SPONSORING / MONITORING AGENCY NAME(S) AND ADDRESS(ES)
National Aeronautics and Space Administration
Langley Research Center
Hampton, VA 23681-0001

10. SPONSORING / MONITORING AGENCY REPORT NUMBER
NASA CR-201709

11. SUPPLEMENTARY NOTES
Langley Technical Monitor: Tony L. Parrott; Final Report
Kwan, Spamer, Yu: Rohr, Inc.; Yasukawa: Lockheed Martin

12a. DISTRIBUTION / AVAILABILITY STATEMENT
Unclassified - Unlimited

Subject Category 71

12b. DISTRIBUTION CODE

13. ABSTRACT (*Maximum 200 words*)

Rohr, Inc., in cooperation with Lockheed Martin Missiles and Space (LMMS) Division, has investigated the use of a HTP (High Temperature Performance) ceramic foam for aeroacoustic applications under NASA Contract NAS1-20102, Task 4. HTP ceramic foam is a composition of silica and alumina fibers developed by LMMS. This foam is a lightweight high-temperature fibrous bulk material with small pore size, ultra high porosity, and good strength. It can be used as a broadband noise absorber at both room and high temperature (up to 1800 °F). The investigation included an acoustic assessment as well as material development, and environmental and structural evaluations. The results show that the HTP ceramic foam provides good broadband noise absorbing capability and adequate strength when incorporating the HTP ceramic foam system into a honeycomb sandwich structure. On the other hand, the material is sensitive to Skydrol and requires further improvements. Good progress has been made in the impedance model development. A relationship between HTP foam density, flow resistance, and tortuosity will be established in the near future. Additional effort is needed to investigate the coupling effects between face sheet and HTP foam material.

14. SUBJECT TERMS
acoustic treatment; engine noise suppression; high-temperature bulk liner; lightweight ceramic foam

15. NUMBER OF PAGES
130

16. PRICE CODE
A07

17. SECURITY CLASSIFICATION OF REPORT	18. SECURITY CLASSIFICATION OF THIS PAGE	19. SECURITY CLASSIFICATION OF ABSTRACT	20. LIMITATION OF ABSTRACT
Unclassified	Unclassified		